

Institut für Technische Chemie II der Technischen Universität München

Surface modification of HZSM-5 zeolites

Shourong Zheng

Vollständiger Abdruck der von der Fakultät für Chemie der Technischen Universität München zur Erlangung des akademischen Grades eines

Doktors der Naturwissenschaften

genehmigten Dissertation.

Vorsitzender: Univ.-Prof. Komm. Dr. Walter Nitsch, em.

Prüfer der Dissertation:

1. Univ.-Prof. Dr. Johannes A. Lercher
2. Univ.-Prof. Dr. Klaus Köhler

Die Dissertation wurde am 27. November 2002 bei der Technischen Universität München eingereicht und durch die Fakultät für Chemie am 11. December 2002 angenommen.

Abstract:

HZSM-5 zeolites were modified using solid state reaction with antimony oxide or chemical liquid deposition of *tetra*-ethoxysilane (TEOS). The modification led to marked decrease in the concentration of externally accessible acid sites and to blocking of the pore mouth of the zeolites. This suppressed the secondary isomerization on the outside of the zeolite crystals and lowered the diffusivities of *o*- and *m*-xylenes. Using frequency response method to assess the individual transport rates of aromatic molecules it was shown that two different processes of the transport existed. The modification increased selectively the slower rate of transport. These modification effects enhanced the shape selectivity in toluene disproportionation.

HZSM-5 Zeolithe wurden durch die Festphasenreaktion mit Antimontrioxid oder durch die chemische flüssige Abscheidung von Tetraethoxysilan (TEOS) modifiziert. Die Modifikation führte zu einer starken Verringerung der Konzentration an sauren Zentren auf der äusseren Oberfläche und zur Blockierung der Porenöffnungen der Zeolithe. Dadurch wurde die sekundäre Isomerisierung unterdrückt und die Diffusion der *o*- und *m*-Xylole verlangsamt. Mit Hilfe der Frequency-Response-Methode, welche zur Bestimmung der Diffusionsgeschwindigkeiten von aromatischen Molekülen eingesetzt wurde, konnte gezeigt werden, dass zwei verschiedene Transportprozesse ablaufen. Durch die Modifizierung wurde die langsamere Transportart bevorzugt. Diese Modifizierungseffekte verstärkten die Formselektivität der Toluol-Disproportionierung.

To my mother,

to Ying

Acknowledgements

I would like to thank Prof. Dr. Johannes A. Lercher for giving me the opportunity to finish my PhD work in his laboratory. His scientific insights and supports in my work and life are especially valuable for the implementation of this work. I am grateful to Andy not only for his patience in correcting my papers and thesis, but also for fruitful discussions throughout my PhD study.

Very special thanks are given to Prof. Dr. K. Köhler for the help with ICWYS conference in Beijing; Hilton for his instructions to all setups and helpful scientific discussions; Hiroaki for fixing the FR setup and suggestions; Thomas and Josef for scientific suggestions; Dr. Peter Röger from Süd-Chemie for zeolite samples and scientific discussions; Xuebing for discussion and Limei for nice food; Ruqing for valuable help with German documents; Martin S for excellent computer techniques; Alex H for helping me go through German documents; Andreas F for useful discussions and information; Jan-Olaf for setting nice office atmosphere and skillful MAS NMR techniques; Adam for helping me with BET measurements; Renate and Christian for the help with IR experiments; Maria for the help with Raman spectroscopy; other members from TCII catalysis and reaction engineering group, Fred, Stefen G., Jochen, Florencia, Anil, Linda, Van Nhu, Krishna, Stefen F., Gabriela, Iker, Toshi, Alex G., Oriol, Jan K., Sven, Hendrik and Jenö for all sorts of help inside the lab; the Bayerischer Forschungsverbund Katalyse for financial support. I would like to thank Frau Schüler and Frau Hermann for their help. Technical supports from Xaver, Andreas M, Martin N are highly appreciated.

The encouragements from my family and friends are especially helpful to my PhD study. I would like to thank my wife, Ying, for her love, supports and understanding during my stay in München.

Shourong
November 2002

Table of contents

Chapter 1. Introduction	1
1.1. General introduction	2
1.2. Structure and acidity of zeolites	3
1.3. Mechanisms of the shape selectivity	7
1.3.1. Reactant shape selectivity	
1.3.2. Product shape selectivity	
1.3.3. Transition shape selectivity	
1.4. Diffusion in zeolites	10
1.5. Post synthesis modification of zeolites	13
1.6. Several shape selective reactions catalyzed by HZSM-5 zeolites	18
1.6.1. Xylene isomerization	
1.6.2. Toluene disproportionation	
1.6.3. Toluene methylation	
1.7. Scope and structure of this thesis	21
Chapter 2. Influence of surface modification on the acid site distribution of HZSM-5	27
2.1. Introduction	28
2.2. Experimental	30
2.3. Results	33
2.3.1. ²⁷ Al MAS NMR	
2.3.2. IR spectra of the zeolites	
2.3.3. NH ₃ adsorption and temperature programmed desorption	
2.3.4. Adsorption of pyridine	
2.3.5. Adsorption of di- <i>tert</i> -butyl-pyridine	
2.4. Discussion	41
2.4.1. Surface hydroxyl groups	
2.4.2. Acid sites on the external surface and in the pore mouth of the zeolites	
2.4.3. Silylation mechanism of CLD	
2.5. Conclusions	46
Chapter 3. On the influence of modification by chemical liquid deposition on toluene diffusion in HZSM-5	50
3.1. Introduction	51
3.2. Experimental	52

3.3. Results	54
3.4. Discussion	59
3.4.1. Toluene adsorption in the zeolites	
3.4.2. Toluene diffusion in the zeolites	
3.5. Conclusions	65
Chapter 4. On the enhanced selectivity of HZSM-5 modified by chemical liquid	
Deposition	69
4.1. Introduction	70
4.2. Experimental	71
4.3. Results and discussion	73
4.3.1. Pore volume	
4.3.2. Toluene isotherm	
4.3.3. Structural IR	
4.3.4. DTBPy adsorption	
4.3.5. Diffusivities of aromatic molecules	
4.3.6. Toluene disproportionation	
4.3.7. Influence of pre-dealumination on the modification effects	
4.3.8. Influence of unselective acid sites	
4.4. Conclusions	83
Chapter 5. On the enhanced <i>para</i>-selectivity of HZSM-5 modified by antimony oxide	85
5.1. Introduction	86
5.2. Experimental	87
5.3. Results	90
5.4. Discussion	101
5.4.1. Dispersion of antimony oxide on the zeolite	
5.4.2. Influences of modification on the properties of the zeolite	
5.4.3. Influences of modification on the activity and selectivity of the zeolites for toluene disproportionation	
5.5. Conclusions	107
Chapter 6. Summary and conclusions	111
6.1. Summary	
6.2. Conclusion	

Curriculum vitae	116
List of publications	117

Chapter 1

Introduction

1.1. General introduction

Aromatic compounds, especially benzene, toluene and xylenes (BTX), are valuable raw materials in the chemical industries. BTX are basic resources of most of aromatic derivatives and xylenes are used to produce polymers, plasticizers and engineering plastics. In particular, *p*-xylene in high purity is highly required in the production of terephthalic acid by oxidation. The worldwide supplied amount of xylenes consists of 24% of *p*-xylene, 23% of *o*-xylene and 53% of *m*-xylene, which is approximately the composition in the thermodynamic equilibrium of xylene mixture. The market requirement of xylenes, however, consists of 60% of *p*-xylene, 18% of *m*-xylene and 20% of *o*-xylene. Obviously, the surplus amount of *o*-xylene and *m*-xylene has to be converted into more valuable *p*-xylene. At the same time, worldwide BTX production provides a markedly higher amount of toluene and a lower amount of benzene compared to that of market requirement. Industrial processes, including super-fractionation, crystallization and adsorption methods were developed to obtain *p*-xylene in high purity. Based on the issues of the raw material sources and operating cost, the exploration and development of the industrial processes using toluene, *o*-xylene and *m*-xylene to selectively produce *para*-xylene is desirable¹.

Toluene alkylation with methanol, toluene disproportionation and *o*-xylene isomerization are industrially used to selectively produce *para*-xylene, which plays an important role in redistribution of BTX. A large number of catalysts have been applied in these processes². Among of these catalysts, zeolites, in particular middle-porous ZSM-5 zeolites, show marked advantages in the selectivity and coke resistance. The high selectivity of HZSM-5 zeolites is ascribed to their similar dimension of the pore openings to these of aromatic molecules and can be further enhanced by delicately adjusting the pore openings, i.e. pore size engineering. In principle, the selectivity, activity and lifetime of zeolite are related to the structure and composition of zeolite,

the diffusivities of the reactants and products and post-synthesis modification.

1.2. Structure and acidity of zeolites

Zeolites are crystalline and micro-porous aluminosilicates consisting of AlO_4 and SiO_4 tetrahedral units connected via oxygen atom bridges. Approximately 40 natural zeolites have been found and more than 150 zeolites were synthesized^{3,4}. Typically, zeolites can be classified into five categories: 8-, 10-, 12-membered oxygen ring, dual pore and mesoporous systems⁵. The characteristics of typical zeolites are listed in Table 1¹.

Table 1. Characteristics of some typical porous materials

Zeolite	Number of rings	Pore size (Å)	Pore/channel structure
<i>8-membered oxygen ring</i>			
Erionite	8	3.6×5.1	Intersecting
<i>10-membered oxygen ring</i>			
ZSM-5	10	5.1×5.6	Intersecting
ZSM-11	10	5.3×5.4	Intersecting
<i>Dual pore system</i>			
Ferrierite	10, 8	4.2×5.4 3.5×4.8	One dimensional 10:8 intersecting
Mordenite	12 8	6.5×7.0 2.6×5.7	One dimensional 12:8 intersecting
<i>12-membered oxygen ring</i>			
ZSM-12	12	5.5×5.9	One dimensional
Faujasite	12	7.4 7.4×6.5	intersecting 12:12 intersecting
<i>Mesoporous system</i>			
VPI-5	18	12.1	One dimensional
MCM41-S	-	16-100	One dimensional

As extensively used porous materials, zeolites show marked advantages over other solid materials:

- (1) Well defined structure which could be clearly related to the activity and selectivity;
- (2) Well defined inner pores in which active species can be hosted;
- (3) Adjustable frame-work composition and cations associated with different stability, hydrophilicity/hydrophobicity and acid-base properties;
- (4) A large amount of structures which can be chosen as shape-selective catalysts for different reactions.

The presence of AlO_4 in the framework introduces negative charges into the structure of the zeolites, which are usually compensated by protons, metal cations, or NH_4^+ . The presence of different compensation cations can render zeolites the redox or acidic and basic properties, which can be used as potential catalytic materials for oxidation, reduction or acid (base)-catalyzed reactions.

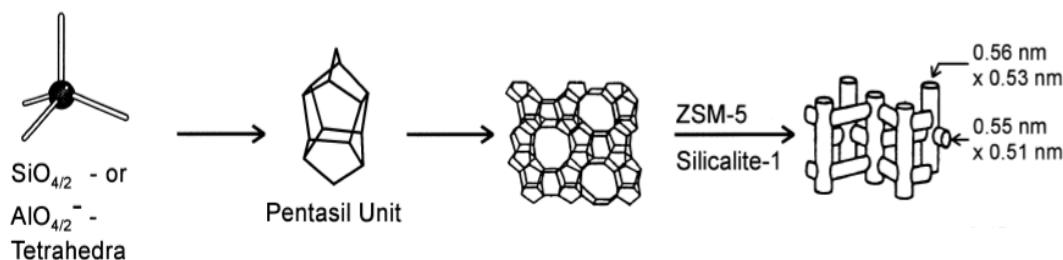


Figure 1. Structure of ZSM-5 zeolite

ZSM-5 zeolite is one of the most important zeolites used in petrochemical industry. The structure of ZSM-5 zeolite and its analogue silicalite-1, shown in Figure 1, has 10-membered oxygen ring and two types of channel systems with similar size: straight channels ($5.3 \times 5.6 \text{ \AA}$) and sinusoidal channels ($5.1 \times 5.5 \text{ \AA}$). These two different channels are perpendicular to each other and generate intersections with diameters of 8.9 \AA . This 10-membered oxygen-ring-sized pore system with uniform dimension as well as the absence of large cages with small windows leads to the special coke-resistant properties of HZSM-5 zeolites⁶.

ZSM-5 zeolites in protonic type (HZSM-5) have been extensively used in acid catalyzed reactions⁷. HZSM-5 zeolites can be synthesized with a broad range of Si-Al ratio from 6 to ∞ . The protonic form of ZSM-5 zeolites can be typically obtained from

as-synthesis zeolites by following steps: (i) calcination of as-synthesis ZSM-5 zeolites to decompose the organic amine template (ii) ion exchange of zeolites in sodium form with NH_4NO_3 solution to give NH_4^+ form and (iii) subsequent calcination of NH_4^+ form of zeolites into their protonic form.

In principle, the acid strength and acid types are the key properties of zeolites, which play a crucial role in the activity and selectivity of the zeolites.

The acid properties of the zeolites can be characterized using indicator⁸, alkane cracking, temperature programmed desorption⁹, micro-calorimetry¹⁰, IR spectroscopy^{11,12} and MAS NMR observations¹³, which were well summarized by Farneth and Gort¹⁴ and Jentys and Lercher¹⁵. Two different types of acid sites are usually observed in HZSM-5 zeolites: Brønsted and Lewis acid sites. Brønsted acid sites are related to aluminum located in the framework of the zeolites. Lewis acid sites, however, are related to the extra-framework aluminum (EFAL) or distorted aluminum in the framework. EFAL is usually generated during the synthesis, calcination or/and ion exchange process. Typically, Brønsted and Lewis acid sites can be differentiated and qualified using IR spectroscopy of pyridine adsorption. The characteristic IR bands of pyridine interacting with Brønsted and Lewis acid sites can be observed at around 1540 cm^{-1} and 1450 cm^{-1} , respectively^{16,17}.

The acid strength of zeolite is mainly dependent on the Si-Al ratio. The strongest Brønsted acid sites can be obtained upon completely isolated Al in framework due to the higher electro-negativity of Si compared to Al. If Si/Al ratio higher than 10, the strength of the acid sites keeps almost constant¹⁸. However, the acid strength can be enhanced by the presence of extra-framework Al (EFAL), which is ascribed to the inductive effects relative to Lewis acid sites on the neighboring Brønsted acid sites^{19,20}. Narayanan *et al.*²¹ observed high heats of adsorption with increased Al content using micro-calorimetric method. In addition, the synthesis methods also influence the acid strength. ZSM-5 zeolite synthesized by non-template method showed high heats of adsorption compared to that obtained using template due to the easy generation of EFAL.

The locations of Brønsted acid sites can markedly influence the activity and selectivity of zeolites. Reactions on the acid sites located in the pore mouth region have higher turn-over frequency (TOV) compared to these in the interior pores as the diffusion hindrance for reactants or products from the pores of zeolites can be avoided. Therefore, the influence of the acid sites located on the external surface and pore mouth region of zeolites can not be ignored although the concentration of these acid sites is assumed to be minor, generally 3-5% of the total amount of acid sites^{22,23}. The locations of the acid sites, however, are still in a debate mainly focusing on whether a portion of Brønsted acid sites are located on the external surface of HZSM-5 zeolites. Simulation results²⁴ indicated a minor energy difference between different locations of Al atoms in the intersection and channels of HZSM-5 zeolites. The results from IR spectroscopy study²⁵ showed an inhomogeneous distribution of Al atoms in the zeolite crystals. Marschmeyer *et al.*²⁶ used XPS and x-ray Auger electron spectroscopy to determine the Al distribution in the zeolite and concluded that Al was heterogeneously distributed in the framework and a large portion of Al on the surface was not in the framework position. Dedecek *et al.*²⁷ also suggested that Al was not randomly distributed in ZSM-5 zeolites, and the Al distribution was dependent on the chemical composition and synthesis procedure. It is generally accepted that some of Brønsted acid sites are located in the pore mouth region of HZSM-5 zeolites, which are blamed for the unselective behavior of zeolites^{28,29,30}. However, Thamm *et al.*³¹ studied the sorption of aromatics in HZSM-5 zeolites using micro-calorimetry and deduced that most of Brønsted acid sites were located in the intersections of HZSM-5 zeolites. Armaroli *et al.*^{32,33} also concluded that Brønsted acid sites were constrained in the interior pores of HZSM-5 zeolites using a variety of probe sorbates.

The concentration of the acid sites located on the external surface and in the pore mouth region of zeolites can be determined using probe molecules with larger kinetic diameters compared to the entrance of the zeolites and thus these molecules are believed to interact only with the acid sites located on the external surface and in the pore mouth region. Corma *et al.*³⁴ used quinoline as a probe molecule to

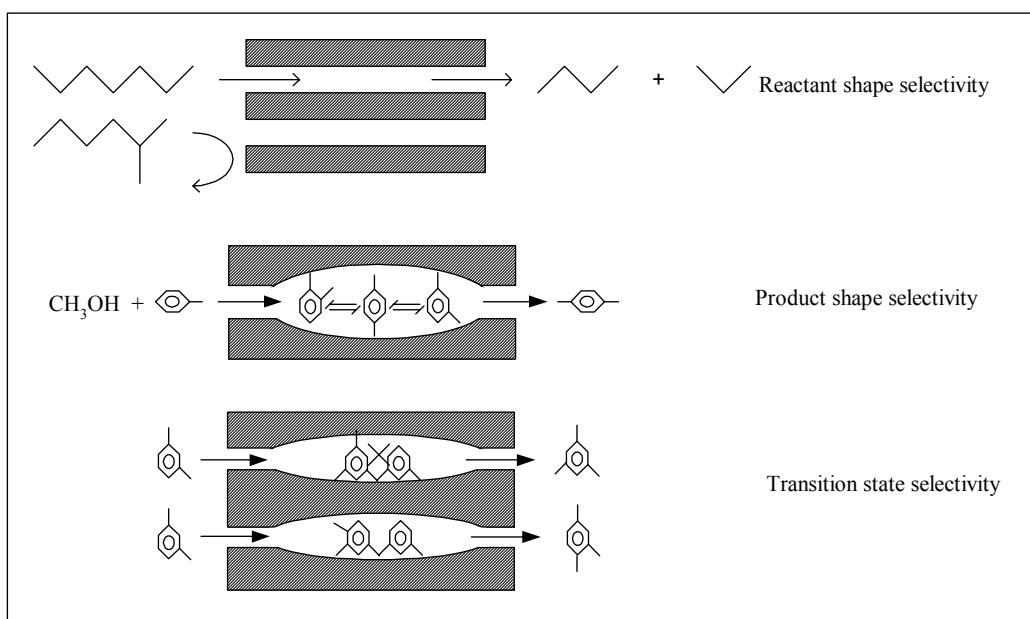
determine the acid sites located on the external surface and in the pore mouth region of the zeolite. O'Connor *et al.*^{35,36,37} measured the concentration of the acid sites of silylated HZSM-5 zeolites using temperature programmed desorption (TPD) of 4-methyl-quinoline. As the kinetic diameter of 4-methyl-quinoline (7.3 Å) is larger than the pore openings of HZSM-5 zeolites (5.6 × 5.3 Å), this molecule is incapable of completely entering into the pores and, therefore, the acid sites on the external surface of HZSM-5 can be quantitatively determined. Recently, Melson *et al.*³⁸ used 2,4-dimethylpyridine adsorption to gravimetrically determine the concentration of acid sites on the external surface of HZSM-5. Drago *et al.*³⁹ determined the locations and strength of acid sites by calorimetric titration using pyridine, 2,6-lutidine and 2,6-di-*tert*-butylpyridine and concluded that all strong acid sites were located in the channels of HZSM-5 zeolites and only a small amount of weak acid sites were located on the external surface. Corma *et al.*⁴⁰ studied the adsorption of di-*tert*-butyl-pyridine (DTBPy) by IR spectroscopy to quantitatively monitor externally accessible acid sites of different zeolites, such as Mordenite, ZSM-5, ZSM-11 and SSZ-26. Pieterse *et al.*⁴¹ used IR spectroscopy to determine the concentration of the externally accessible acid sites of FER and TON zeolites using adsorption of 2,4,6-trimethylpyridine.

Generally, the determination of the locations and concentration of the unselective acid sites is difficult due to the unknown geometry and ill definition of the external surface of zeolites. Therefore, the unambiguous description of the surface geometry and straightforward characterization methods to quantify the unselective acid sites is of great help to understand the selectivity of zeolites.

1.3. Mechanisms of the shape selectivity

Shape selectivity of catalyst has been well documented since it was first described by Weize and Friette 40 years ago⁴². In particular, zeolites usually show specific selectivity in some reactions due to their microporous properties. It is generally believed that the majority of the active sites is located in the pores of zeolite.

Typically, five fundamental steps are involved in an overall reaction using zeolite as catalyst: (i) diffusion of molecules from gas phase into the pores of the zeolite; (ii) adsorption of molecules on active sites; (iii) conversion of reactants molecules into product molecules; (iv) desorption of product molecules from active sites and eventually (v) diffusion of product molecules into gas phase from the pores of the zeolite. The shape selectivity of the zeolite for a specific reaction may be possibly involved in step (i), (iii) or/and (v). Based on different controlling steps, the shape selectivity of zeolites usually observed can be classified into three different types, including reactant shape selectivity, product shape selectivity and transition state selectivity⁴³, which are described in scheme 1.



Scheme 1. Shape-selectivity of zeolite

1.3.1 Reactant shape selectivity

Reactant shape selectivity can be observed in the case of different participating reactant molecules with smaller and bulkier diameters compared to the pore entrance of zeolite. Reactants with smaller kinetic diameters can penetrate into the interior pores of zeolite and access the active sites located in the pores of the zeolite. Reactants with larger kinetic diameters, however, can not diffuse into the pores of

zeolite and the reaction with bulky reactant molecules involved can be encumbered.

An example is the hydrogenation of olefins over Pt loaded CaA zeolite⁴⁴, in which propylene and 1-butene showed high hydrogenation activity, low activity, however, was observed for *iso*-butylene.

1.3.2. Product shape selectivity

Molecules with different kinetic diameters show marked difference in the diffusivities in zeolite if their kinetic diameters are in the similar dimension as the pore openings. Deviation of product distribution from the equilibrium composition can be usually observed if products with large difference in their diffusivities are involved in the reaction. Principally, product with higher diffusivity is preferentially produced compared to those with low diffusivities. This selectivity may play a more crucial role if product has comparative kinetic diameter to the pore openings as a minor variation in the molecule kinetic diameter results in a marked difference in the diffusivity.

Product shape selectivity is usually used to explain the *p*-selectivity of HZSM-5 zeolites for toluene disproportionation. The diffusivity of *p*-xylene in HZSM-5 zeolite is approximately 100-1000 times higher than these of *o*- and *m*-xylene which leads to the fast diffusion of *p*-xylene out of the pores of HZSM-5 zeolite⁵.

1.3.3. Transition state selectivity

Transition state selectivity is usually used to explain the preferential production of products in the pores of zeolite. The pore system of zeolite renders different steric hindrances to the transition states leading to different products. Dominant product can be expected if the resource transition state is sterically preferred in the pores of the zeolite.

The trans-alkylation reaction of methylethylbenzene on H-Mordenite was well explained by transition state selectivity⁴⁵. A marked lower concentration of symmetrical tri-alkyl-benzene was found in the products compared to that on HY zeolite, which was ascribed to the smaller pore space of H-Mordenite available for a bi-molecular reaction compared to that of HY zeolite.

Other types of shape selectivity are also proposed to explain the specific reaction selectivity, e.g. molecular traffic controlled shape selectivity⁴⁶.

1.4. Diffusion in zeolites

For a reaction occurring in the porous materials, most of the active sites are located in the interior channels of the porous materials and, therefore, reactant molecules have to diffuse into the channels in prior to the adsorption and eventual reaction on these sites. Simultaneously, product molecules also have to diffuse out of the channels after desorption from the active sites. During the diffusion processes, hindrance to a different extent is based on the relative kinetic diameters of the reactant and product molecules to that of the channels of the catalytic materials. The hindrance effects may become marked if the diameters of the reactant and product molecules are comparable to the pores or channels of these porous materials. Therefore, the diffusivities of reactants and products play a crucial role in the selectivity and activity of the catalysts.

A variety of studies have addressed the measurements of the diffusivities of different molecules in porous materials. Typically, diffusion of gas molecules in the porous materials can be divided into three different regimes⁴⁷: (i) gaseous or molecular diffusion; (ii) Knudsen diffusion and (iii) configurational diffusion. When the average free distance of molecules is smaller than the pore diameter of the porous materials, collision between molecules is dominant and the diffusion behaves as molecular diffusion. If the average free distance of diffusion molecules is larger than the diameter of pores, collision between molecules and the wall of the channels is dominant and the diffusion behaves as Knudsen diffusion. When the diameter of diffusion molecules is comparable to that of the channels of the porous materials, diffusion converts from Knudsen diffusion to configurational diffusion. The diffusion regimes are shown in Figure 2.

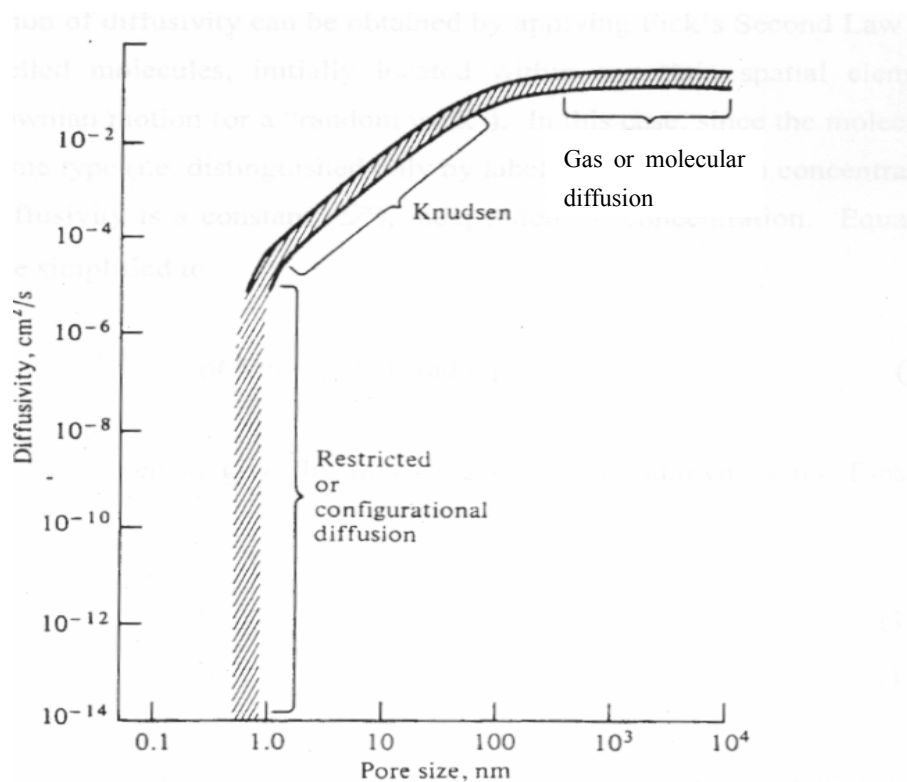


Figure 2. The dependence of the diffusivity on the relative pore diameter

For most shape selective reactions catalyzed by zeolite based materials, configurational diffusion is of crucial importance due to the similar kinetic diameters of reactants and products to the pore size of the zeolites. Particular interests have been focused on the measurements of the diffusivities of aromatic molecules, such as benzene, toluene and xylenes, in ZSM-5 zeolites, as the diameters of these molecules are in the same dimension of the pore diameter of ZSM-5 type zeolites and, moreover, these molecules are usually involved in some selective reactions with HZSM-5 as catalyst, for instance, toluene disproportionation, xylene isomerization and toluene alkylation. In parallel, diversifies of measurement methods have been developed to precisely assess the diffusivities of these molecules in different zeolites, including pulsed-field gradient NMR (PFG NMR)^{48,49}, neutron diffraction^{50,51}, zero-length column^{52,53}, uptake-rate measurement including FT-IR^{54,55,56,57}, tracer exchange⁵⁸, and frequency response (FR) method^{59,60}. Typically, PFG NMR and neutron diffraction are

typically used to determine the self-diffusivity. However, uptake rate measurements are usually used to observe the transport diffusivity. The transport diffusivity can be relative to the intracrystalline diffusivity by using Darken equation⁶¹. For the determinations of diffusivity by the uptake methods, the adsorption system is under non-equilibrium or near-equilibrium, therefore, multi-factors may influence the determination, such as heats of adsorption (desorption)^{62, 63}, external transport resistance^{64, 65, 66} or atmosphere⁶⁷. Generally, diffusion coefficients determined by PFG NMR are larger than these by normal uptake methods. Some discrepancies, therefore, have been usually observed between same systems determined by different techniques.

The properties of the zeolite may influence the determination of the diffusivity. Mirth and Lercher⁶⁸ observed two magnitudes lower diffusion coefficient of *p*-xylene in HZSM-5 zeolites with small crystals compared to the zeolite with large crystals. Gavalcante *et al.*⁶⁹ also observed 10 times lower diffusivity of cyclohexane in silicalite with small crystals compared to that with large crystals. Kärger *et al.*⁷⁰ observed lower diffusivity of methane in chabazites and the dependence of the diffusivity on the crystal size using sorption method. This lower diffusivity in the zeolite with small crystal is usually ascribed to the surface barrier^{64, 65}. Vasenkov⁷¹ *et al.* observed a decreased self-diffusion coefficient of methane and butane molecules in ZSM-5 zeolite with increased root-mean-square displacement using PFG NMR, which was ascribed to an inter-crystalline surface barrier resulted from the intersections between the elementary building blocks of the crystals and intergrowth sections of zeolite crystals. Furthermore, different treatments of the zeolite, e.g. hydrothermal treatment, led to additional transport resistance⁷².

The acidic properties of the zeolites also influence the diffusivities of the molecules. Choddhary *et al.*⁷³ observed that the diffusivity of benzene in HZSM-5 zeolite was lower than in silicalite and concluded that the change in the Si/Al ratio and ion exchange degree had influence on the diffusivity of benzene. Hashimoto *et al.*⁷⁴ observed lower diffusivities of aromatic molecules in HZSM-5 zeolite compared to

these in silicalite. Shen *et al.*⁷⁵ observed the diffusivity of benzene decreased by 2-3 times in HZSM-5 zeolite compared in silicalite using the FR method. Similar results were also obtained by other authors^{57,76}.

The appearance of the strong adsorption sites in the silicalite resulted in a marked decrease in the diffusivity of hydrocarbons at very low concentration⁷⁷. Furthermore, the activation energy of the diffusion of hydrocarbons was markedly higher at very low concentration compared to that at high concentration. The presence of sodium ion in ZSM-5 zeolite led to a lower diffusivity^{73,78}.

The diffusivity sometimes is dependent on the concentration of sorbate. Typically, five different dependences of the diffusivity on the concentration of sorbate were usually observed^{67,79}.

For the diffusion of aromatic molecules in ZSM-5 zeolites, the dependence of the diffusivity on the molecule loading is still under controversy. Choddhary and Tsikoyiannis^{73,80} observed a markedly increased diffusivity of benzene with the increase of molecule loading. Zikanova *et al.*⁸¹ claimed an independence of the diffusivity of benzene in silicalite on the concentration of benzene. L. V Rees *et al.*⁸² observed a decreased dependence of the diffusivities of aromatic molecules on the concentration.

After modification of the zeolite, the properties of the zeolites, including the pore openings, the concentration of acid sites and silanol groups also changed, which may influence the diffusivities of sorbates. For HZSM-5 zeolite, significant diffusion hindrance occurs for sorbates with larger kinetic diameter as the pore openings, such as *o*-xylene and *m*-xylene, after the narrowing of pore openings⁸³. However, the diffusivity of sorbates with slightly smaller kinetic diameter, such as benzene, alkyl-benzene or *p*-xylene, was seldom discussed⁸⁴.

1.5. Post synthesis modification of zeolites

As-synthesized HZSM-5 zeolites always show low selectivity due to the

presence of the unselective acid sites, which are believed to be located on the external surface and in the pore mouth regions of zeolites. In addition, the small difference in the diffusivities between the desired products and undesired products in as-synthesized zeolites attributes to the low selectivity of zeolites. Therefore, post-synthesis modification methods, described as pore size engineering⁸⁵, are proposed to tailor the properties of zeolites to achieve high selectivity.

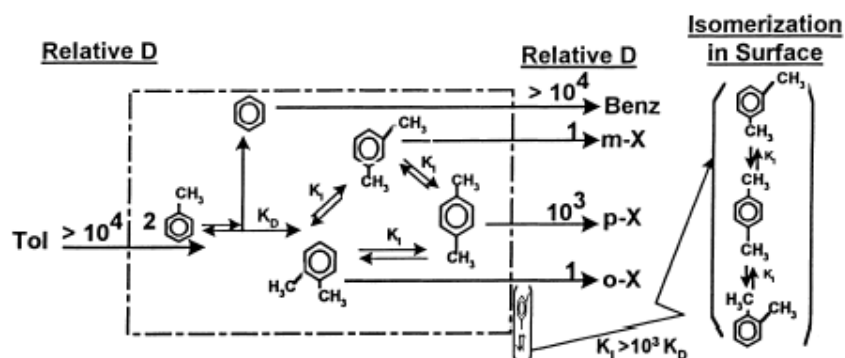


Figure 3: Selective toluene disproportionation in HZSM-5 zeolite

A typical shape-selective example, i.e. toluene disproportionation over HZSM-5 zeolite, is presented in Figure 3¹. Toluene disproportionation occurs in the pores of HZSM-5 zeolites to generate xylenes and benzene and simultaneously xylenes are isomerized. The products diffuse out of the pores of the zeolite in different rate (see Figure 3). At the same time, xylenes are isomerized in the pores and on the external surface of the zeolite although it has not been generally accepted. The *para*-selectivity can be achieved if following conditions are satisfied⁸³:

$$D_p \gg D_{m,o}$$

$$K_I \geq D_{m,o}/r^2$$

$$K_D \leq D_T/r^2$$

$$(K_I/K_D)_{observed} \leq 1$$

Where K_I and K_D the rate constants of isomerization and disproportionation, respectively. D_p and $D_{m,o}$ the diffusion coefficients of *p*-xylene and *m*-xylene or

o-xylene, r the radius of zeolite crystals.

Generally, modification of zeolites aims at passivating the unselective acid sites, by which isomerization of xylenes in the external surface of the zeolite (see Figure 3) can be suppressed. At the same time, narrowing the pore mouth openings of zeolites can be achieved, which decreases the diffusivities of *o*- and *m*-xylene ($D_{m,o}$). These combined effects from post-synthesis modification can effectively enhance the *p*-selectivity of the zeolite. Indeed, the enhanced selectivity has been observed by adopting a variety of modification methods for HZSM-5 zeolites.

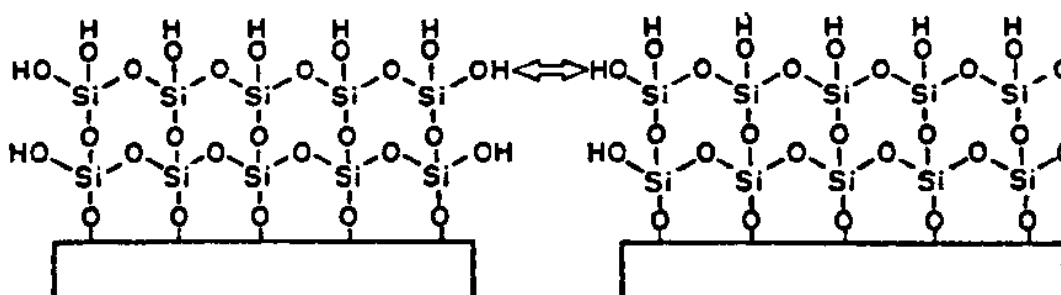


Figure 4. Pore narrowing of modified zeolite by chemical vapor deposition

Keading *et al.*^{86,87,88,89} prepared P, Si, B, Mg or Mn oxides modified zeolites using impregnation methods and observed an enhanced *para*-selectivity for alkylation of toluene, toluene disproportionation and isomerization, which was attributed to the narrowing of the pore openings or/and the blocking of the acid sites on the external surface of the zeolites. Niwa *et al.*^{90, 91} used chemical vapor deposition (CVD) of TEOS or TMOS to modify the external surface of the zeolites and observed a substantially enhanced *para*-selectivity for *o*-xylene isomerization, toluene disproportionation and toluene alkylation by methanol. It was concluded that inert SiO₂ layers were deposited on the external surface of the zeolite and led to a narrowing of the pore entrance of zeolite by 1-2 Å⁹², which contributed to the enhanced *para*-selectivity. Moreover, a marked lower cracking activity of 1,3,5-triisopropylbenzene after CVD modification was also observed, which

suggested the passivation of the unselective sites, although Niwa *et al.*⁹³ excluded the relation of the enhanced selectivity to the passivation of the unselective sites. Shikh *et al.*⁹⁴ proposed a mechanism to describe the process of CVD, which was plotted in Figure 4. The generation of inert SiO₂ layers led to the narrowing of the pore mouth of the zeolite. The modification effects of SiO₂ deposition on zeolites can be controlled using different operating parameters. Manstein *et al.*⁹⁵ recommended using low deposition temperature and multi-cycle modification to achieve higher modification effects. Si/Al ratio of zeolite is also a crucial factor for the control of the modification effects. Effective pore mouth narrowing for silicalite could be achieved only if higher reaction and longer reaction time were used compared to HZSM-5 zeolites⁹⁶.

Gao *et al.*^{97,98,99} studied the influence of chemical liquid deposition (CLD) on the *para*-selectivity of HZSM-5 zeolites using different deposition agents. It was found that the pore openings could be finely controlled by inert SiO₂ layers. Gao *et al.* suggested that the enhanced *para*-selectivity was only attributed to the modulation of the pore openings of the zeolites. Zheng *et al.*¹⁰⁰ studied the influence of CLD on the distribution of acid sites and concluded that the concentration of Brønsted and Lewis acid sites was markedly decreased and the enhanced modification effects could be achieved using multi-cycle silylation for zeolite with small crystals¹⁰¹.

Kürschner *et al.*¹⁰² obtained the modified HZSM-5 zeolites by hydrothermal treatment at high temperature, which led to the dealumination of HZSM-5 zeolites and an enrichment of extra-framework Al on the external surface of the zeolite was observed. The model proposed suggested that EFAL was enriched on the external surface of the zeolites and blocked the unselective acid sites, which inhibited the secondary isomerization of *p*-xylene to other isomers. Thus, Kürschner *et al.* attributed the enhanced *para*-selectivity only to the blocking of the unselective acid sites.

SiO₂ deposition on the external surface of the zeolite can be also achieved using secondary synthesis, which was carried out by a hydrothermal synthesis with pure

silica source¹⁰³. A successful introduction of SiO₂ layer on the external surface of the zeolite also led to a decrease in the concentration of the unselective acid sites and an enhanced *para*-selectivity for toluene disproportionation and toluene alkylation.

Deposition of antimony oxide onto HZSM-5 zeolite could enhance the *para*-selectivity¹⁰⁴. The passivation of the acid sites located on the external surface and in the pore mouth region was observed at high antimony oxide loading. Li *et al.*¹⁰⁴ concluded that the passivation of the unselective acid sites was the crucial reason for the enhanced *para*-selectivity. However, Zhu *et al.*¹⁰⁵ attributed the enhanced *para*-selectivity for toluene alkylation to the narrowing of the pore openings resulted from the partial decomposition of HZSM-5 zeolites.

Tynjala *et al.*¹⁰⁶ found that the deposition of SiO₂ and Ge₂O₃ on the surface of the zeolite effectively enhanced the selectivity of the modified zeolite for the conversion of methanol to hydrocarbons, which was ascribed to the blocking of acid sites and the pore openings.

Selective deposition of coke onto the surface of HZSM-5 zeolites was studied in details by Olson *et al.*⁸³. The coke was only detained on the external surface of the crystals and the acid sites located in the pores of the zeolites were preserved, additionally, the diffusion of other isomers with large kinetic diameters out of the pores was suppressed. Fang *et al.*¹⁰⁷ used five-stage on-stream treatment to manipulate coke located on the external surface and obtained 50% *para*-selectivity for toluene disproportionation.

Ohayon *et al.*^{108,109} used a desilication-reinsertion-stabilization method to tune the pore size of HZSM-5 zeolites. The modified zeolite with small crystals showed high selectivity to aromatic molecules for methanol conversion to hydrocarbons.

In summary, it is generally accepted that the pore mouth narrowing of HZSM-5 zeolites results in the significant diffusion hindrance for *o*- and *m*-xylenes and thus the enhanced *para*-selectivity can be achieved. Typical influence of the narrowing of the pore openings on the *para*-selectivity is summarized in Figure 5⁸³, which shows that the diffusivity of *o*-xylene as well as the *para*-selectivity of the zeolites can be

regulated by varying the crystal size of the zeolites and the modification methods. The functions of the unselective acid sites, however, are still under controversy. Therefore, the influence of the passivation of the unselective sites on the enhanced *para*-selectivity of the silylated zeolites is still unclear. The main reason is that most modification methods tailor the surface of the zeolites and, therefore, lead to simultaneous changes in the pore openings and the concentration of the unselective acid sites. Consequently, the influences from the pore mouth narrowing and the passivation of the unselective acid sites on the enhanced *para*-selectivity are difficult to be differentiated and more straightforward methods have to be developed to elucidate the influences of the passivation of the unselective acid sites on the *para*-selectivity.

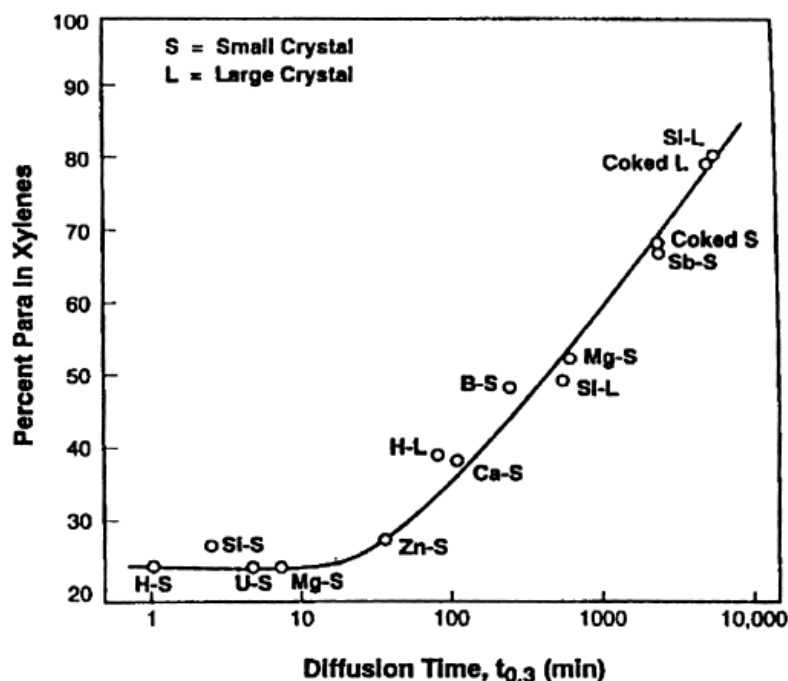


Figure 5. The dependence of the *p*-selectivity on the diffusion rate of *o*-xylene in different zeolites

1.6. Several shape-selective reactions catalyzed by HZSM-5 zeolites

HZSM-5 zeolite is one of the most used zeolites in the chemical and

petrochemical industry. Typical industrial catalytic processes using HZSM-5 zeolites include cracking of waxy components, the conversion of methanol to gasoline, xylene isomerization, alkylation, trans-alkylation, and disproportionation, etc.. Among of these applications, xylene isomerization, toluene disproportionation and toluene methylation are typical shape selective reactions catalyzed by HZSM-5 zeolites to produce *p*-xylene¹¹⁰.

1.6.1. Xylene isomerization

Xylene isomerization is often used as a test reaction to characterize the acidity and porosity of solid acid materials^{111,112}. In addition, xylene isomerization acts as the secondary reaction in toluene disproportionation and toluene methylation. In principle, xylene isomerization occurs via an intermolecular or/and an intra-molecular mechanism dependent on the pore structure, the concentration of reactant, the density of acid sites and the type of acid sites. A high density of acid sites, the presence of Lewis acid sites, a high reactant concentration and a large pore space favour the bimolecular mechanism^{113,114,115}. For xylene isomerization in HZSM-5 zeolites, xylene isomerization usually occurs via intra-molecular mechanism due to the high Si-Al ratio and the same dimension of the pores of HZSM-5 zeolite to the diameters of xylene molecules.

As the diffusivity of *para*-xylene is about 100-1000 times higher than that of *m*-xylene and *o*-xylene, *m*-xylene isomerization over HZSM-5 zeolite is observed as a reactant controlled reaction¹¹⁶. A higher *para*-selectivity is observed due to a transition state shape-selectivity, by which the transition state leading to *o*-xylene is statically suppressed and the transition state leading to *p*-xylene is preferred.

For *o*-xylene isomerization, the direct generation of *p*-xylene from *o*-xylene is not preferred due to a 1,2-methyl shift mechanism. *p*-Xylene is only generated from *m*-xylene. At low reaction temperature, low *p*-selectivity is obtained due to a low secondary isomerization rate of *m*-xylene. Increasing isomerization temperature leads to a high concentration of *m*-xylene accumulated in the pores of the zeolite and, therefore, a high *p*-selectivity can be achieved.⁵⁵

1.6.2. Toluene disproportionation

Toluene disproportionation is an industrial process to selectively produce *p*-xylene. Two different reaction mechanisms for toluene disproportionation were proposed by Xiong *et al.*^{117,110}: methyl transfer and diphenyl methane mechanisms. The *para*-selectivity is generally believed to be controlled by product diffusion or/and transition state shape selectivity. For transition state shape selectivity, the transition state leading to *o*-xylene and *m*-xylene is suppressed and the transition state leading to *p*-xylene is favoured in the channels of HZSM-5 zeolites. For product diffusion selectivity, *p*-xylene has higher diffusivity compared to these of *o*-xylene and *m*-xylene and thus the diffusion of *o*-xylene and *m*-xylene is suppressed which leads to the *p*-selectivity. The *para*-selectivity can be effectively enhanced by using zeolites with large crystals or modification of the external surface of zeolite, by which the difference of the diffusivities between *p*-xylene and *o*- or *m*-xylene is enlarged and the acid sites located on the external surface and in the pore mouth region of the zeolites are passivated.

1.6.3. Toluene methylation

Due to the fast adsorption and occupation of methanol in the acid sites of the zeolite, direct adsorption of toluene molecules in the acid sites is suppressed. Methanol molecules absorbed in the acid sites via a methoxonium¹¹⁸ at low temperature or methoxy species¹¹⁹ at high temperature, at the same time, toluene molecules weakly interacts with these species. Either the methoxonium species or methoxy groups alkylate toluene molecules to generate xylenes at reaction temperature. Blaszkowshi *et al.*¹²⁰ concluded that *o*-xylene is the prevailed primary product compared to other isomers, however, a high primary concentration of *p*-xylene was suggested due to the transition state shape selectivity^{121,6}. Usually, a low *para*-selectivity can be observed at low methylation temperature. Increasing reaction temperature leads to an increase in the *para*-selectivity, which is generally attributed to the marked increase in the isomerization rate compared to the methylation reaction¹²². Due to the significant influence of diffusion of the products, the

modification of the zeolite in order to enlarge the difference in the diffusivities amongst xylenes can also enhance the *para*-selectivity of toluene methylation.

1.7. Scope and structure of this thesis

Modification of HZSM-5 zeolites to obtain stable and selective catalysts attracts academic and industrial interest. Modification of zeolites by chemical liquid deposition provides the most feasible way to prepare industrial catalysts in large scale. The modification mechanism of CLD and influences of modification on the selectivity of zeolites, however, are less clear. Therefore, this work aims at elucidating the mechanism of CLD modification and the factors controlling the selectivity of zeolite.

The influences of CLD modification on the acidic properties of the zeolites with different crystals were described in **Chapter 2**. The influence of modification on toluene diffusion and the properties of the zeolites controlling the selectivity of the zeolites were studied in **Chapter 3** and **4**. A feasible method to modify the zeolite by solid state reaction was proposed in **Chapter 5**. Finally, the results of this thesis were summarized in **Chapter 6**.

References

1. Tsai, T.; Liu, S.; Wang, I. *Appl. Catal. A: General* **181**, 355 (1999).
2. Wells, G. M. *Handbook of petrochemicals and processes*, Gower Press, Vermont, 1991
3. Meier, W. M.; Olson, D. M. *Atlas of Zeolite Structure Types*, 3th Ed., Butterworth-Heinemann, London (1992).
4. Vaughan, D. E. W., *Natural Zeolites: Occurrence, Properties and Use*, Sand, L. B. and Mumpton, F. A. Eds., London Pergamon, 1978.
5. Chen, N. Y.; Garwood, W. E.; Dwyer, F. G. *Shape selective Catalysis in Industrial Application*, 2nd ed., revised and expanded, Marcel Dekker, New York, 1996.
6. Chen, N. Y.; Kaeding, W. W.; Dwyer, F. G. *J. Am. Chem. Soc.* **101**, 6783 (1979).
7. Tanabe, K.; Hölderich, W. *Appl. Catal. A: General* **181**, 399 (1999).

8. Bennesi, H. A. *J. Phys. Chem.* **61**, 970 (1957).
9. Niwa, M.; Katada, N. *Catal. Surv. Jpn.* **1**, 215 (1997).
10. Cardona-Martinez, N.; Dumesic, J. A. *Adv. Catal.* **38**, 149 (1992).
11. Lercher, J. A.; Gründling, C.; Eder-Mirth, G. *Catal. Today* **27**, 353 (1996).
12. Sato, H. *Catal. Rev.* **39**, 395 (1997).
13. Klinowski, J. *Chem. Rev.* **91**, 1459 (1991).
14. Farneth, W. E.; Gorte, R. J. *Chem. Rev.* **95**, 615 (1995).
15. Jentys A.; Lercher, J. A. *Stud. Surf. Sci. Catal.* **137**, 345 (2001).
16. Emeis, C. A. *J. Catal.* **141**, 371 (1993).
17. Zholobenko, V. L.; Makarova, M. A.; Dwyer, J. J. *Phys. Chem.* **97**, 5962 (1993).
18. Rabo, J. A.; Gajda, G. J. In: *Guidelines for Mastering the properties of Molecular Sieves*, Barthomeuf, D.; Derouane, E. G.; Hölderich, W. Eds., Nato ASI Series B, Vol. 221, Plenum Press, New York, 1990, p. 273.
19. Rhodes, N. P.; Rudham, R. *J. Chem. Soc. Faraday Trans.* **89**, 2551 (1993).
20. Wang, Q. L.; Gianneto, G.; Guisnet, M. *J. Catal.* **130**, 471 (1991).
21. Narayanan, S.; Sultana, A.; Le, Q. T.; Auroux, A. *Appl. Catal. A: General* **168**, 193 (1998).
22. Fraenkel, D. *Ind. Eng. Chem. Res.*, **29**, 1814 (1990).
23. Paparatto, G.; de Alberti, G.; Leofanto, G.; Padovan, M. *Stud. Surf. Sci. Catal.*, **44**, 225 (1989).
24. Schroeder, K.; Sauer, J. *Zeolites*, **12**, 20 (1992).
25. Schueth, F.; Althoff, R. *J. Catal.* **143**, 388 (1993).
26. Marschmeyer, S.; Papp, H. *Surf. Inter. Annal.* **25**, 660 (1997).
27. Dedecek, J.; Kaucky, D.; Wichterlova, B. *Chem. Commun.* 970 (2001).
28. Bhat, Y. S.; Rao, K. V.; Halgeri, A. B. *J. Catal.* **159**, 368 (1996).
29. Fraenkel, D. *Ind. Eng. Chem. Res.* **29**, 1814 (1990).
30. Wang, I.; Ay, C. L.; Lee, B. J.; Chen, M. H. *Appl. Catal.* **54**, 257 (1989).
31. Thamm, H. *J. Phys. Chem.* **91**, 8 (1987).
32. Armaroli, T.; Trombetta, M.; Alejandre, A. G.; Solis, J. R.; Busca, G. *Phys. Chem. Chem. Phys.* **2**, 3341 (2000).
33. Trombetta, M.; Armaroli, T.; Alejandre, A. G.; Solis, J. R.; Busca, G. *Appl. Catal. A: General* **192**, 125 (2000).

34. Coma, A.; Fornes, V.; Rey, F. *Zeolites* **13**, 56 (1993).
35. Weber, R. W.; Möller, K. P.; Unger, M.; O'Conner, C. T. *Micropor. Mesopor. Mater.* **23**, 179 (1998).
36. Weber, R. W.; Möller, K. P.; O'Conner, C. T. *Micropor. Mesopor. Mater.* **35**, 533 (2000).
37. Weber, R. W.; Fletcher, J. C. Q.; Möller, K. P.; O'Conner, C. T. *Micropor. Mater.* **7**, 15 (1996).
38. Melson, S.; Schüth, F. *J. Catal.* **170**, 46 (1997).
39. Drago, R. S.; Dias, S. C.; Torrealba, M.; de Lima, L. *J. Am. Chem. Soc.* **119**, 4444 (1997).
40. Coma, A.; Fornes, V.; Forni, L.; Marquez, F.; Martinez-Triguero, J.; Moscotti, D. *J. Catal.* **179**, 451 (1998).
41. Pieterse, J. A. Z.; Veeffkind-Reyes, S.; Seshan, K.; Lercher, J. A. *J. Phys. Chem. B* **104**, 5715 (2000).
42. Weisz, P. B.; Frilette, V. J. *J. Phys. Chem.* **64**, 382 (1960).
43. Csicsery, S. M. *zeolites*, **4**, 203 (1984).
44. Weisz, P. Z.; Frilette, V. J. *J. Phys. Chem.* **64**, 382 (1960).
45. Csicsery, S. M. *J. Chem. Eng. Data* **12**, 118 (1967).
46. Derouane, E. G.; Gabelica, Z.; Jacobs, P. A. *J. Catal.* **70**, 238 (1981).
47. Xiao, J.; Wei, J. *Chem. Eng. Sci.* **47**, 1123 (1992).
48. Kärger, J.; Ruthven, D. M. *Zeolites* **9**, 267 (1989).
49. Kärger, J.; Ruthven, D. M. *Diffusion in Zeolites and Other Microporous Solids*, Wiley, New York, 1992.
50. Cohen, L. E.; Kahn, R.; Mezei, F. *J. Chem. Soc., Faraday Trans. I* **79**, 1911 (1983).
Jobic, H.; Bée, M. and Pouget, S. *J. Phys. Chem. B* **104**, 7130 (2000).
51. Jobic, H.; Bee, M.; Caro, J.; Bülow, M.; Kärger, J.; Pfeifer, H. *Stud. Surf. Sci. Catal.*, **65**, 445 (1991).
52. Brandani, S.; Jama, M.; Ruthven, D. M. *Micropor. Mesopor. Mater.* **35**, 283 (2000).
53. Ruthven, D. M.; Brandani, S. *Membr. Sci.* **6**, 187 (2000).
54. Karge, H. G.; Nießen, W. *Catalysis Today* **8**, 451 (1991).

55. Mirth, G.; Lercher, J. A. *J. Catal.* **139**, 24 (1993).
56. Schumacher, R.; Karge, H. G. *J. Phys. Chem.* **103**, 1477 (1999).
57. Zikanova, A.; Bulow, M.; Schlodder, H. *Zeolites* **7**, 115 (1987).
58. Förste, C.; Kärger, J.; Pfeifer, H.; Riekert, L.; Bülow, M. *J. Chem. Soc. Faraday Trans.*, **86**, 881 (1990).
59. Yasuda, Y. *Heter. Chem. Rev.* **1**, 103 (1994).
60. Rees, L. V. C. *Stud. Surf. Sci. Catal.* **84**, 1133 (1994).
61. Ash, R.; Barrer, R. M. *Surf. Sci.* **8**, 461 (1967).
62. Chihara, K.; Suzuki, M.; Kawazoe, K. *Chem. Eng. Sci.* **31**, 505 (1976).
63. Lee, L. K.; Ruthven, D. M. *J. Chem. Soc. Faraday Trans. 1* **75**, 2406 (1979).
64. Bülow, M. *Z. Z. Chem.* **25**, 81 (1985).
65. Käger, J.; Bülow, M.; Millward, G. R.; Thomas, J. M. *Zeolites*, **6**, 146 (1986).
66. Vasenkov, S.; Böhlmann, W.; Galvosas, P.; Geier, O.; Liu, H.; Kärger, J. *J. Phys. Chem. B* **105**, 5922 (2001).
67. Kärger, J.; Pfeifer, H. *Zeolites*, **7**, 90 (1987).
68. Mirth, G.; Lercher, J. A. *J. Phys. Chem.*, **95**, 3736 (1991).
69. Cavalcante, C. L.; Ruthven, D. M. *Ind. Eng. Chem. Res.* **34**, 185 (1995).
70. Kärger, J.; Caro, J. *J. Chem. Soc. Faraday 1*, **73**, 1363 (1977).
71. Vasenkov, S.; Boehlmann, W.; Galvosas, P.; Geier, O.; Liu, H.; Käger, J. *J. Phys. Chem. B* **105**, 5922 (2001).
72. Kärger, J.; Bülow, M.; Millward, G. R.; Thomas, J. M. *Zeolites*, **6**, 146 (1986).
73. Choudhary, V. R.; Srinivasan, K. R. *J. Catal.* **102**, 316 (1986); **102**, 329 (1986).
74. Masuda, T.; Fujikata, Y.; Nishida, K.; Hashimoto, K. *Micropor. Mesopor. Mater.* **23**, 157 (1998).
75. Shen, D.; Rees, L. V. C. *Zeolites* **11**, 666 (1991).
76. Qureshi, W. R.; Wei, J. *J. Catal.* **126**, 147 (1990).
77. Hufton, J. R.; Ruthven, D. M.; Danner, R. P. *Micropor. Mater.*, **5**, 39 (1995).
78. Forni, L.; Viscardi, C. F.; Oliva, C. *J. Catal.* **97**, 469 (1986).
79. Kärger, J.; Ruthven, D. M. *Stud. Surf. Sci. Catal.* **105**, 1843 (1997).
80. Tsikoyiannis, J. G., 1986, Ph.D. thesis, Department of Chemical Engineering, MIT, Cambridge, MA.
81. Zikanova, A.; Bulow, M.; Schlodder, H. *Zeolites* **7**, 115 (1987).

82. Song, L.; Rees, L. V. C. *Micropor. Mesopor. Mater.* **35-36**, 301 (2000).
83. Olson, D. H.; Haag, W. O. *Catalytic materials relationship between structure and reactivity*, ACS Symp. Ser. **248**, 275 (1984).
84. Karge, H. G.; Niessen, W.; Bludau, H. *Appl. Catal. A: General* **146**, 339 (1996).
85. Vansant, E. F., in: *Pore Size Engineering in Zeolite*, Wiley, Chichester, UK, 1990
86. Kaeding, W. W.; Chu, C.; Young, L. B.; Butter, S. A. *J. Catal.* **69**, 392 (1981).
87. Kaeding, W. W.; Chu, C.; Young, L. B.; Weinstein, B.; Butter, S. A. *J. Catal.* **67**, 159 (1981).
88. Young, Y. B.; Butter, S. A.; Kaeding, W. W. *J. Catal.* **76**, 418 (1982).
89. Kaeding W. W.; Young, L. B.; Chu, C. *J. Catal.* **89**, 267 (1984).
90. Niwa, M.; Katada, N.; Murakami, T. *J. Phys. Chem.* **94**, 6441 (1990).
91. Niwa, M.; Katada, N.; Murakami, Y. *J. Catal.* **134**, 340 (1992).
92. Niwa, M.; Kato, S.; Hattori, T.; Murakami, Y. *J. Chem. Soc., Faraday Trans. 1* **80**, 3135 (1984).
93. Kim, J.; Kunieda, T; Niwa, M. *J. Catal.* **173**, 433 (1998).
94. Shaikh, R. A.; Hegde, S. G.; Behlekar, A. A.; Rao, B. S. *Catal. Today* **49**, 201 (1999).
95. Manstein, H.; Moeller, K. P.; Boehringer, W.; Oconnor, C. T. *Micropor. Mecropor. Mater.* **51**, 35 (2002).
96. Begum, H. A.; Katada, N.; Niwa, M. *Micropor. Mesopor. Mater.* **46**, 13 (2001).
97. Yue, Y.; Tang, Y.; Liu, Y.; Gao, Z. *Ind. Eng. Chen. Res.* **35**, 430 (1996).
98. Yue, Y.; Tang, Y.; Kan, Y.; Gao, Z. *Acta Chimica Sinica* **54**, 591 (1996).
99. Qing, X.; Yue, Y.; Gao, Z. *Chinese J. Catal.* **19**, 349 (1998).
100. Zheng, S.; Heydenrych, H. R.; Jentys, A.; Lercher, J. A. *J. Phys. Chem. B* **106**, 9552 (2002).
101. Zheng, S.; Heydenrych, H. R.; Röger, P.; Jentys, A.; Lercher, J. A. *Stud. Surf. Sci. Catal.*, **135**, 214 (2001).
102. Kürschner, U.; Jerschke, H. G.; Schreier, E; Völter, J. *Appl. Catal.* **57**, 167 (1990).
103. Lee, C. S.; Park, T.; Lee, W. Y. *Stud. Surf. Sci. Catal.* **105**, 1349 (1997)
104. Li, G.; Zhao, J. *Petro-chemical Engineering (Chinese)* **16**, 276 (1987).
105. Zhu, S.; Meng, X.; Wang, Y.; Zhang, W.; Lin, B. *Chem. J. Chin. Uni.* **20**,

- 616 (1999).
106. Tynjala, P.; Pakkanen, T. T. *J. Mol. Catal. A: Chem.* **122**, 159 (1997).
107. Fang, L. Y.; Liu, S. B.; Wang, I. *J. Catal.* **185**, 33 (1999).
108. Ohayon, D.; Mao, R. L. V.; Ciaravino, D.; Hazel, H.; Cochenec, A.; Rolland, N. *Appl. Catal. A: General* **217**, 241 (2001).
109. Le Van Mao, R.; Le, S. T.; Ohayon, D.; Caillibot, F.; Gelebart, L.; Denes, G. *Zeolites*, **19**, 270 (1997).
110. Cejka, J.; Wichterlova, B. *Catal Rev.* **44**, 375 (2002).
111. Guisnet, M. *Acc. Chem. Res.* **23**, 392 (1990).
112. Guisnet, M.; Gnep, N. S.; Morin, S. *Micropor. Mesopor. Mater.* **35**, 47 (2000).
113. Csicsery, S. M.; *J. Org. Chem.* **34**, 3338 (1969).
114. Csicsery, S. M.; Hickson, D. A. *J. Catal.* **19**, 386 (1970).
115. Wang, K. M.; Lunsford, J. H. *J. Catal.* **262** (1972)
116. Müller, G.; Narbeshuber, T.; Mirth, G.; Lercher, J. A. *J. Phys. Chem.*, **98**, 7436 (1994).
117. Xiong, Y.; Rodewald, P. G.; Chang, C. D. *J. Am. Chem. Soc.* **117**, 9427 (1995).
118. Mirth, G.; Lercher, J. A. *J. Phys. Chem.*, **125**, 351 (1991).
119. Rakoczy, J.; Sulikowski, B. *React. Kinet. Catal. Lett.* **36**, 241 (1988).
120. Blaszkowski, S. R.; Van Santen, R. A. *J. Phys. Chem.* **99**, 11728 (1995)
121. Sayed, M. B.; Vadrine, J. C. *J. Catal.* **101**, 43 (1986).
122. Mirth, G.; Cejka, J.; Nusterer, E.; Lercher, J. A. *Stud. Surf. Sci. Catal.* **83**, 287 (1994).

Chapter 2

Influence of surface modification on the acid site distribution of HZSM-5

Abstract

The hydroxyl groups on the external surface and in the pore mouth region of HZSM-5 zeolites with different crystal sizes were modified by chemical liquid deposition (CLD) of tetra-ethoxysilane (TEOS). The effects of silylation on the acid sites of the zeolites were monitored using NH_3 sorption, IR spectroscopy of the hydroxyl groups of the zeolites, as well as of adsorbed pyridine and di-*tert*-butyl-pyridine (DTBPy). Silylation reduced the concentration of Brønsted acid sites of samples with a crystal size of 3 μm and 0.5 μm by 5.1% and 21%, respectively. Blocking of Lewis acid sites of the zeolites was additionally observed. Silylation preferentially occurred in the pore mouth region of the zeolites. The deactivation of Lewis acid sites was found to occur prior to the reaction with the bridging hydroxyl groups and the silanol groups. The extent of silylation reached was found to depend on the particle size of the sample. A multi-cycle procedure can be used to increase the effects of the modification.

2.1. Introduction

HZSM-5 zeolite has been extensively applied in many petrochemical processes^{1,2} as its well-defined ten-membered ring channel system allows to achieve a high selectivity to *p*-isomers during disproportionation of alkyl-benzene, isomerization of *di*-alkyl-benzene and alkylation of toluene.³⁻¹⁰ However, acid sites present on the external surface and in the pore mouth region of HZSM-5 zeolites usually lower the selectivity.¹¹⁻¹⁵

Various modification methods have been applied to enhance the shape selectivity of HZSM-5 zeolites.^{4,10-12,16-18} In general, the modifications aim at suppressing secondary reactions occurring on the external surface and/or at hindering the diffusion of undesired products out of the pores of the zeolites. Thus, the deactivation of the acid sites on the external surface (blocking active sites for secondary reactions) and/or the narrowing the pore openings of HZSM-5 (enlarging differences in the diffusivities of isomers) improves the shape-selectivity of HZSM-5 zeolites.

Post synthesis modification by chemical vapor deposition (CVD) of silicon alkoxides, such as tetra-ethoxysilane (TEOS) and tetra-methoxysilane (TMOS), is one of the most effective methods to enhance the shape selectivity of HZSM-5 zeolites. The silylation mechanism by means of CVD has been well documented by Niwa *et al.*¹⁹⁻²¹ Because the minimum kinetic diameters of the silicon alkoxides typically used are larger than the pore diameter of HZSM-5, only hydroxyl groups on the outer surface and close to the pore openings react with the silylating agents and form Si-O-Si or Si-O-Al bonds, which leads to a passivation of these unselective acid sites. In addition, an inert silica layer is deposited on the outer surface and in the pore mouth region of the zeolites and, therefore, the pore openings are simultaneously narrowed or partially blocked.

Alternatively, chemical liquid deposition (CLD) can be used to modify the external surface of zeolites²²⁻²⁵. The main advantage of the reaction in liquid phase (CLD) compared to the reaction in gas-phase (CVD) is that the liquid reaction can be easier transferred to an industrial preparation in large-scale quantities. However,

systematic studies on the CLD mechanism, which allows a quantitative description of the modification effects, are lacking.

The concentration of acid sites in the parent and modified zeolites has been extensively studied before and after silylation by CVD or CLD methods by pyridine adsorption and NH_3 -TPD, as well as test reactions, such as cracking of 1,3,4-triisopropylbenzene and n-hexane.^{6,17,26} It should be emphasized, however, that these reports mostly address the qualitative changes induced by the surface modification. In a series of papers O'Connor *et al.*^{24-25,27} described the concentration of acid sites of silylated HZSM-5 zeolites by using TPD of 4-methyl-quinoline. As the kinetic diameter of 4-methyl-quinoline (7.3 Å) is larger than the pore openings of HZSM-5 zeolites (5.6×5.3 Å), this molecule is incapable of completely entering into the pores and, therefore, the passivation of the acid sites on the external surface of HZSM-5 by silylation can be quantitatively described. Recently, Melson *et al.*²⁸ used 2,4-dimethylpyridine adsorption to determine gravimetrically the concentration of acid sites on the external surface of HZSM-5, Corma *et al.*²⁹ studied the adsorption of di-*tert*-butyl-pyridine (DTBPy) by IR spectroscopy to quantitatively monitor externally accessible acid sites of different zeolites, such as Mordenite, ZSM-5, ZSM-11 and SSZ-26 and Pieterse *et al.*³⁰ used IR spectroscopy to determine the concentration of the externally accessible acid sites of FER and TON zeolites by adsorption of 2,4,6-trimethylpyridine.

In this chapter, IR spectroscopy, NH_3 -TPD and pyridine as well as DTBPy adsorption were used to quantitatively determine the changes in the concentration of externally accessible acid sites of HZSM-5 zeolites before and after CLD modification using TEOS. The quantitative results from different characterization methods are compared and the mechanism of the modification is discussed on a molecular basis.

2.2. Experimental

2.2.1. Materials

Two samples of HZSM-5 with a Si/Al ratio of 45 (determined by X-ray fluorescence) and an average particle diameter of 0.5 and 3 μm (determined by SEM), designated HZS and HZL, were used as parent zeolites. X-ray diffraction (XRD) showed that HZL and HZS were well-crystalline materials and that the crystallinity of HZS was slightly lower compared to HZL. Pyridine and DTBPy were obtained from Sigma Aldrich. Hexane and tetra-ethoxysilane (TEOS) ($\geq 99\%$) were obtained from Fluka. All chemicals were used as received.

2.2.2. Silylation

Typically, 2 g of zeolite were suspended in 50ml of hexane and the mixture was heated under stirring until reflux. 0.3 ml of TEOS, corresponding to a loading of 4 wt% SiO_2 , was introduced into the mixture and the silylation was carried out for 1 h under reflux and stirring. Subsequently, hexane was removed by evacuation. The samples were dried at 393 K for 2 h and calcined at 773 K for 4 h in dry air. Samples prepared by single cycle silylation are referred to as HZ \times -4% (\times denoting the zeolite with large or small crystals, 4% the concentration of SiO_2 deposited by wt %). Three-cycle silylation for HZS was carried out by repeating the above described procedure including the intermediate calcinations steps for three times (the sample is referred to as HZS-3 \times 4%).

2.2.3. ^{27}Al MAS NMR

^{27}Al MAS NMR spectra of the zeolites were recorded on a Bruker AVANCE MSL-300 NMR spectrometer at a field strength of 7.5 T and 15 kHz spinning speed using 4 mm ZrO_2 -rotors. Spectra were collected at a frequency of 78.205 MHz with 1.0 μs excitation pulses and 0.1 s recycle times. The ^{27}Al chemical shifts were referenced to 1 molar aqueous solution of $\text{Al}(\text{NO}_3)_3$.

2.2.4. NH₃ sorption and temperature programmed desorption

The NH₃ sorption and temperature programmed desorption (TPD) on the parent and silylated zeolites was studied using a modified SETARM TG-DSC 111 instrument. Around 15 mg of sample was pressed into wafers, broken into small platelets and charged into the crucible of the TG-DSC system. The sample was activated by heating at 823 K for 1 h and after cooling to 373 K NH₃ adsorption was carried out.

Physically adsorbed NH₃ was removed by degassing at 373 K until further weight loss was not observed (~3 h). NH₃-TPD of the sample was carried out by heating the sample with 10 K/min from 373 to 1073 K. The amount of NH₃ desorbed was quantitatively monitored by the weight loss and the partial pressure in the gas phase using a mass spectrometer.

2.2.5. IR spectroscopy

The IR spectra were recorded at 4 cm⁻¹ resolution using a Bruker IFS 88 FTIR spectrometer. The samples were pressed into self-supporting wafers and placed in a gold sample holder in the center of a furnace, which was mounted in an *in situ* cell connected to a vacuum system. The sample was activated in vacuum (<10⁻⁶ mbar) by heating to 823 K with a rate of 10 K/min and holding at this temperature for 1 h. All IR spectra were collected at 423 K. The adsorption of pyridine and DTBPy was carried out at a partial pressure of 2×10⁻² mbar using an equilibration time of 15 min. After removing physically adsorbed molecules by degassing at 423 K for 1 h the IR spectra were collected at 423 K. In order to allow quantitative comparisons of the peak intensities, all IR spectra were normalized using the area of the overtone lattice vibration bands of the zeolites at 1990 cm⁻¹ and 1870 cm⁻¹.

Note, that the determination of the concentration of Brønsted acid sites accessible for DTBPy using the characteristic band at 3367 cm⁻¹ was not possible for HZL and HZL-4% due to the low transmittance of these samples in the region of the hydroxyl groups. Therefore, the intensity of the characteristic band at 1616 cm⁻¹ (characteristic of DTBPy adsorbed on Brønsted acid sites) and the results obtained from pyridine

adsorption were used to quantitatively determine the concentration of accessible Brønsted acid sites. The intensity of the bridging hydroxyl groups of HZL and HZL-4% were obtained by equation 1:

$$A_{\text{OH,L}} = A_{\text{OH,S}} \times B_{\text{Py,L}}/B_{\text{Py,S}} \quad [1]$$

where $A_{\text{OH,L}}$ is the peak area of the bridging hydroxyl groups of the zeolite with the large crystal size, $A_{\text{OH,S}}$, the peak area of the bridging hydroxyl groups of the zeolite with the small crystal size, $B_{\text{Py,L}}$ and $B_{\text{Py,S}}$ are the concentrations of Brønsted acid sites determined by pyridine adsorption on the zeolites with the large and small crystal sizes, respectively. The fraction of the bridging hydroxyl groups of HZL and HZL-4% interacting with DTBPy were obtained by:

$$A'_{\text{OH,L}} = A_{1616,L}/S_{1616,S} \quad [2]$$

where $A'_{\text{OH,L}}$ is the peak area of the bridging hydroxyl groups interacting with DTBPy for the sample with the large crystal size, $A_{1616,L}$ the peak area of the band at 1616cm^{-1} and $S_{1616,S}$ the slope of the linear relation between the area of the band at 1616cm^{-1} and the amount of bridging hydroxyl groups interacting with DTBPy for the sample with the small crystal size.

2.2.6. Deuteration

Deuterium exchange of the zeolite was carried out under static conditions at 423 K and a D_2O partial pressure of 1mbar in the *in situ* IR cell. After activation at 823 K for 1 h, the zeolite was exchanged with D_2O for 40 min. The deuterium-exchanged zeolite was activated at 823 K to remove physically adsorbed D_2O and the IR spectra were collected at 423 K.

2.3. Results

2.3.1. ^{27}Al MAS NMR

The ^{27}Al MAS NMR spectra of the zeolites before and after silylation are compared in Figure 1. The ratios of extra-framework Al species (EFAl) to framework Al species (FAI) calculated from the intensities of the peaks at a chemical shift of 0 ppm (octahedral Al) and 53 ppm (tetrahedral Al) were 0.024 and 0.028 for HZS and HZL, respectively, which indicates that for both samples the majority of Al is present in the framework of the zeolite. After silylation, the ratios of FAI to EFAl did not change for the zeolites with different particle sizes.

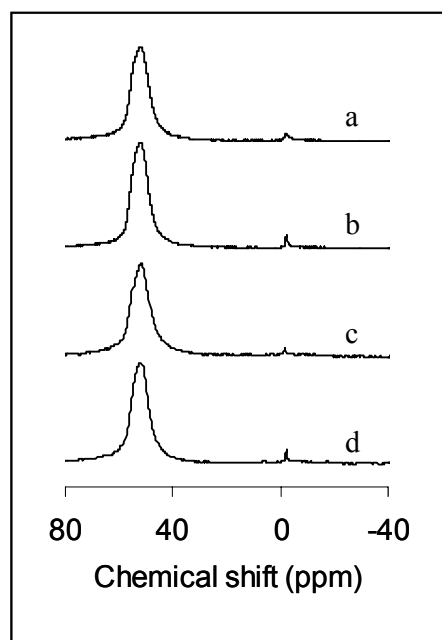


Figure 1: ^{27}Al MAS NMR spectra of (a) HZS, (b) HZS-3 \times 4%, (c) HZL and (d) HZL-4%

2.3.2. IR spectra of the zeolites

The IR spectra of the activated HZS, HZS-4% and HZS-3 \times 4% samples are compared in Figure 2. The band at 3745 cm^{-1} , 3606 cm^{-1} and 3665 cm^{-1} are characteristic for isolated silanol groups located on the external surface of the zeolite, for the bridging hydroxyl groups (Brønsted acid sites) and extra-framework alumina

species, respectively.³¹ For HZL, the apparent transmittance at the region between 4000 cm^{-1} and 2400 cm^{-1} was too low to obtain usable spectra.

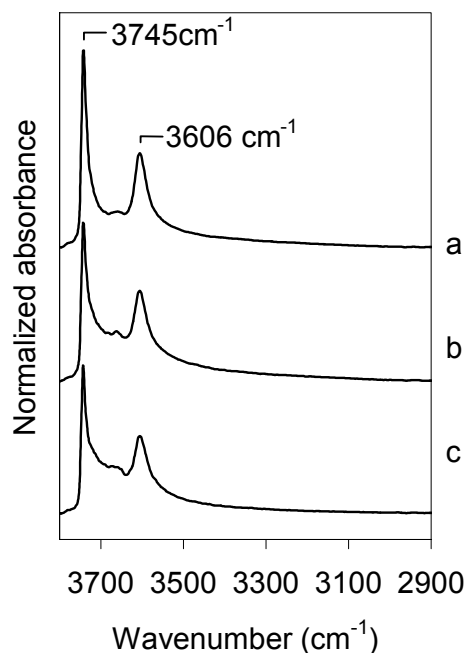


Figure 2: IR spectra of (a) HZS, (b) HZS-4% and (c) HZS-3x4%

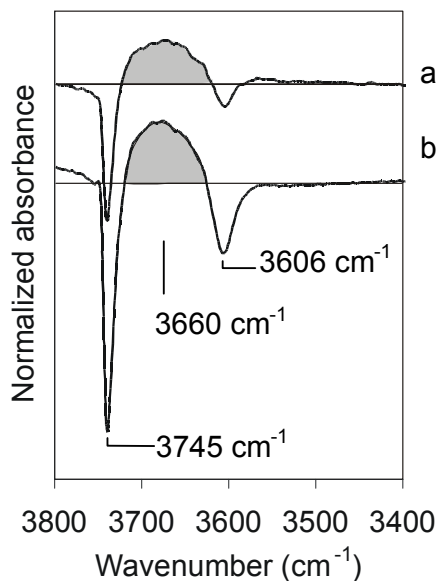


Figure 3: Changes in the IR spectra of activated (a) HZS-4% and (b) HZS-3x4% compared to HZS

To clearly visualize the changes in the hydroxyl group region of the spectra after modification, the differences of the IR spectra of HZS-4% and HZS-3x4% with that of HZS are shown in Figure 3. Two negative bands at 3745 cm^{-1} and 3606 cm^{-1} and a

new broad band with a maximum around 3660 cm^{-1} (indicated in grey) were observed. The presence of two negative bands at 3745 cm^{-1} and 3606 cm^{-1} indicated that the concentration of the bridging hydroxyl and silanol groups decreased after silylation. The three-cycle silylation led to a further decrease in the concentration of the hydroxyl groups and to a further increase in the broad band (3660 cm^{-1}), which was assigned by Shaikh *et al.*³² to hydrogen bonded silanol groups. In order to confirm this assignment, deuterium exchange was performed for HZS before and after silylation. The IR spectra of activated HZS, HZS-3×4%, deuterium exchanged HZS and deuterium exchanged HZS-3×4% are shown in Figure 4.

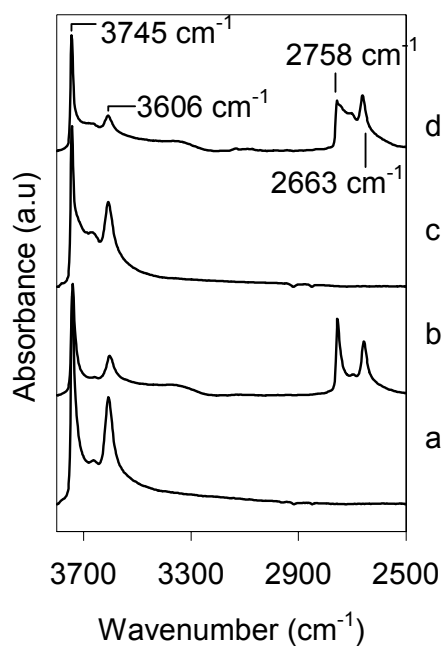


Figure 4: IR spectra of HZS after (a) activation and (b) deuterium exchange and HZS-3×4% after (c) activation and (d) deuterium exchange.

The bands partially remaining after deuteration of the zeolites at 3745 cm^{-1} and 3606 cm^{-1} revealed that the isotope exchange was not complete for these hydroxyl groups.³³ It can be clearly seen, however, that all three hydroxyl bands appeared at the corresponding -O-D region, which clearly indicates that the broad band observed at 3660 cm^{-1} results from hydroxyl groups that are accessible for D_2O .

The changes in the intensity of the hydroxyl groups before and after modification are listed in Table 1. Single cycle silylation for HZS led to a decrease in the concentration of the silanol and bridging hydroxyl groups by 6% and 9.5%, respectively. A further decrease in the concentration of these hydroxyl groups by 18% and 24% was observed after the three-cycle silylation, respectively. It is interesting to note that the ratios between the decrease in the concentration of the silanol and the bridging hydroxyl groups were almost the same after single and three-cycle silylation.

Table 1. Changes in the concentration of hydroxyl groups after silylation of HZS compared to the parent material

Sample	Decrease of acid site concentration after modification (%)		Ratio between 3745 cm ⁻¹ and 3610 cm ⁻¹
	3745 cm ⁻¹	3606 cm ⁻¹	
HZS-4%	6	9.5	0.67
HZS-3×4%	18	24	0.75

2.3.3. NH₃ adsorption and temperature programmed desorption

The NH₃-TPD and NH₃ uptakes of the parent and the silylated samples are shown in Figure 5 and summarized in Table 2, respectively.

Table 2. NH₃ sorption capacity of the samples investigated

Sample	Acid site density (mmol/g)	Decrease of acid site concentration after modification (%)
HZS	0.304	-
HZS-4%	0.275	9.5
HZS-3×4%	0.231	24
HZL	0.398	-
HZL-4%	0.364	8.5

Only one desorption peak was observed in the NH₃-TPD of the parent and the modified zeolites, which is attributed to NH₃ desorption from Brønsted and strong Lewis acid sites. Note that NH₃ uptake for HZL was 33% higher compared to HZS, although the nominal Si/Al ratios were the same for both zeolites. This indicates that

there is a larger amount of EFAl in HZS than in HZL. However, ^{27}Al MAS NMR did not indicate a markedly higher concentration of EFAl in the HZS sample, which is possibly due to the presence of NMR invisible EFAl resulting from the location of Al in non-symmetric environments.³⁴⁻³⁶ Single cycle silylation and three-cycle silylation for HZS led to a decrease in the concentration of acid sites by 9.5% and 24.0%, respectively. For HZL, silylation resulted in a decrease in the concentration of the acid sites by 8.5%.

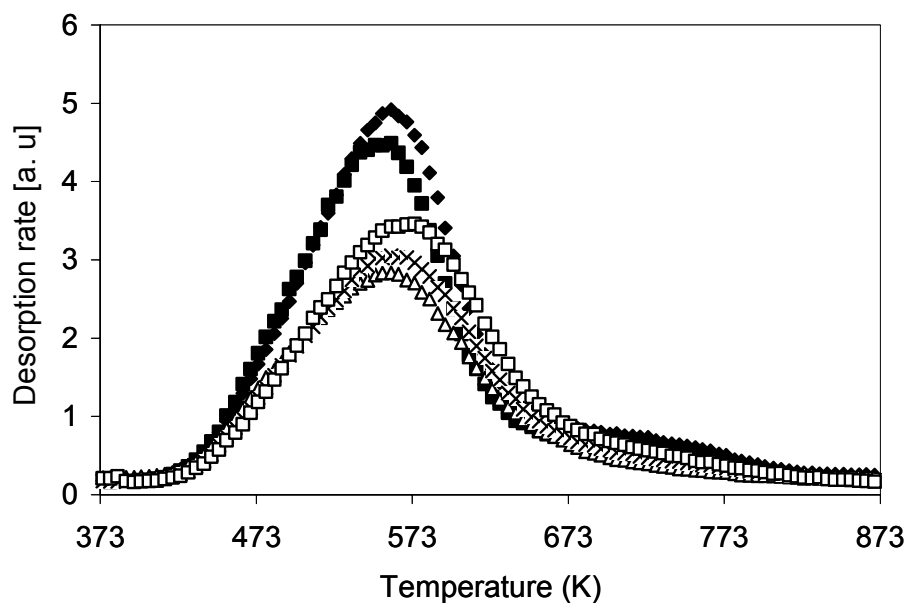


Figure 5: NH_3 -TPD of (\blacklozenge) HZL, (\blacksquare) HZL-4%, (Δ) HZS-3 \times 4%, (\times) HZS-4% and (\square) HZS

2.3.4. Adsorption of pyridine

The changes in the IR spectra after adsorption of pyridine on the zeolites before and after modification are compared in Figure 6. All samples investigated showed bands at 1636, 1491 and 1546 cm^{-1} , characteristic of pyridinium ions, and bands at 1623, 1490 and 1455 cm^{-1} , characteristic of coordinatively bound pyridine.³⁷ For the parent and silylated samples, the band at 3606 cm^{-1} completely disappeared after pyridine adsorption, which indicates that on all samples the acid sites are fully

accessible for pyridine, and, furthermore, that silylation of the zeolites does not lead to a blockage of acid sites.

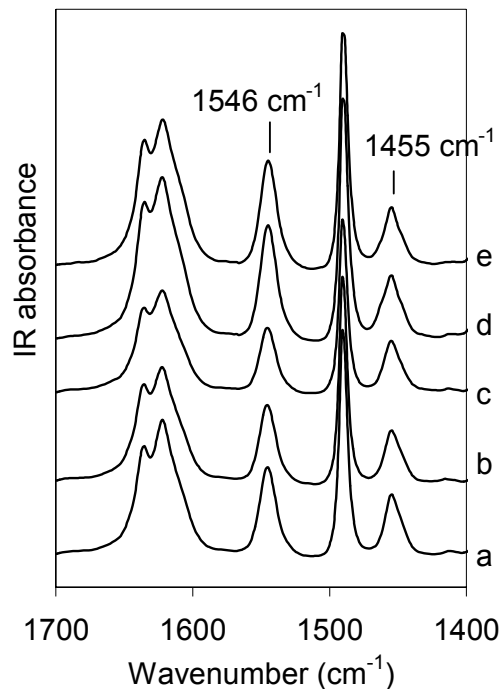


Figure 6: Changes in the IR spectra after adsorption of pyridine on (a) HZS, (b) HZS-4%, (c) HZS-3×4%, (d) HZL and (e) HZL-4%

Table 3. Concentration of Brønsted and Lewis acid sites determined by pyridine adsorption

Sample	$c_{\text{Brønsted}}$ (mmol/g)	c_{Lewis} (mmol/g)	Decrease of acid sites concentration after modification (%)	
			Brønsted	Lewis
HZS*	0.213	0.091	-	-
HZS-4%	0.187	0.079	12	14
HZS-3×4%	0.154	0.079	28	14
HZL	0.280	0.107	-	-
HZL-4%	0.261	0.095	6.7	13

*: Concentration of the acid sites obtained from NH_3 adsorption

In order to quantify the acid sites of the parent and the silylated zeolites, the integral intensities of the bands at 1546 cm^{-1} (Brønsted acid sites) and 1455 cm^{-1} (Lewis acid sites), in combination with the total concentration of acid sites determined for HZS by NH_3 -TPD, were used. The ratio between the molar extinction coefficients of the bands at 1455 cm^{-1} and 1546 cm^{-1} was reported to be 1.5.³⁸ The concentration of Brønsted and Lewis acid sites is compiled in Table 3.

Pyridine adsorption showed that single cycle silylation of HZS and HZL led to a decrease in the concentration of Brønsted acid sites by 6.7% and 12.1%, respectively. Three-cycle silylation of HZS resulted in a decrease in the concentration of Brønsted acid sites by 27.5%. In addition, silylation also led to a decrease in the concentration of Lewis acid sites of HZS and HZL. It is interesting to note that single cycle silylation for HZS deactivated the same amount of Lewis acid sites as three-cycle silylation.

2.3.5. Adsorption of di-*tert*-butyl-pyridine

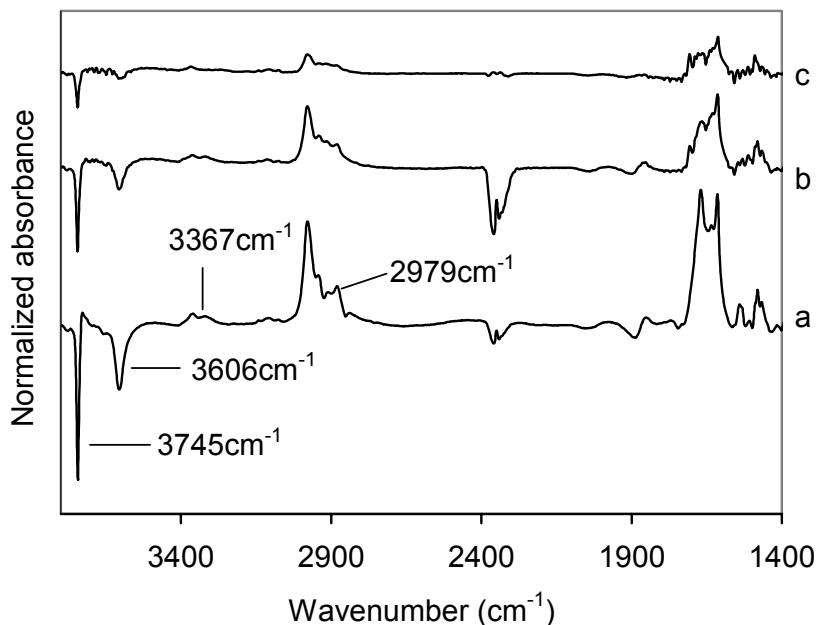


Figure 7: Changes in the IR spectra after adsorption of DTBPy on (a) HZS, (b) HZS-4% and (c) HZS-3x4%

DTBPy was used as probe molecule to characterize acid sites located on the external surface and in the pore mouth region of the zeolites. As the kinetic diameter of DTBPy (10.5 Å) is larger than the pore openings of HZSM-5 zeolites, DTBPy can not penetrate into the pores of HZSM-5 zeolites and, therefore, DTBPy molecules can only interact with the hydroxyl groups on the external surface and in the pore mouth region of the zeolites.

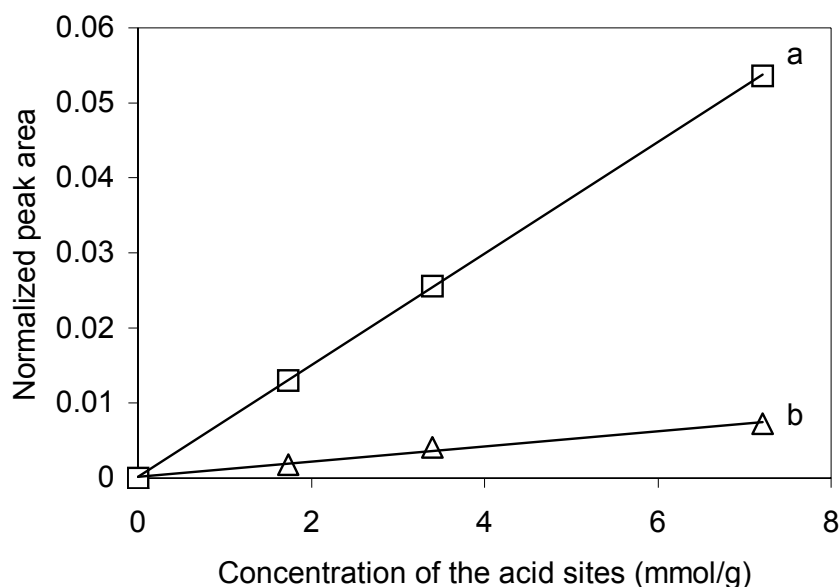


Figure 8: Correlation between concentration of acid sites interacting with DTBPy and area of the IR bands at (a) 3367 cm^{-1} and (b) 1616 cm^{-1} .

The differences in the IR spectra after DTBPy adsorption on HZS, HZS-4% and HZS-3×4% and the activated samples are shown in Figure 7. IR bands were observed at 3367, 2979, 2943, 2912, 2882, 1670, 1636, 1616, 1541, 1481 and 1468 cm^{-1} . The presence of two negative bands at 3745 cm^{-1} and 3606 cm^{-1} indicate that DTBPy molecules interacted with silanol and bridging hydroxyl groups. The bands at 3367 cm^{-1} and 1616 cm^{-1} were assigned to the N-H vibration and to the ring vibration of DTBPyH⁺, respectively, and can be used to quantitatively assess the concentration of the externally accessible Brønsted acid sites.^{29,39} The correlation between the concentration of Brønsted acid sites and the peak area of the bands at 3367 cm^{-1} and 1616 cm^{-1} is shown in Figure 8. The linear relation indicates that the amount of

DTBPy adsorbed on the surface of the zeolites is proportional to the concentration of the bridging hydroxyl groups interacting with DTBPy.

The concentration of accessible hydroxyl groups is compiled in Table 4. Approximately 28% of the bridging hydroxyl groups of HZS interacted with DTBPy. After single and three-cycle silylation of HZS, 13% and 6.7% of the bridging hydroxyl groups remained accessible for DTBPy. For HZL, 7% of the acid sites interacted with DTBPy, while after silylation, only 2% of the acid sites were accessible for DTBPy. It is interesting to note that the ratios between the silanol groups and the bridging hydroxyl groups interacting with DTBPy remained almost constant after the different silylation cycles for HZS.

Table 4. Quantitative results of DTBPy adsorption

Sample	Bridging hydroxyl groups interacting with DTBPy (%)	Ratio between silanol and bridging hydroxyl groups interacting with DTBPy	Removal of acid sites (%)	Removal of external acid sites (%)
HZS	28	0.78	-	-
HZS-4%	13	0.83	15	53%
HZS-3×4%	6.7	0.75	22	76%
HZL	7.0	-	-	-
HZL-4%	1.9	-	5.1	73%

2.4. Discussion

2.4.1. Surface hydroxyl groups

Three types of hydroxyl groups, i.e., silanol, bridging hydroxyl groups and hydroxyl groups on non-framework aluminum oxide species, were observed for HZS. The silanol groups and some of the non-framework aluminum oxide species are located at or close to the external surface of the particles, while the location of the bridging hydroxyl groups remains still controversial. Frequently, it is argued that a fraction of the bridging hydroxyl groups is located on the external surface of HZSM-5 zeolites, which is attributed to the non shape-selective behavior of the zeolites. On the other hand, Armaroli et al.⁴⁰ concluded that the bridging hydroxyl groups were only

confined to internal pores of HZSM-5. In general, the zeolite surface is ill-defined and, therefore, the assignment whether acid sites are located on the external surface or not remains ambiguous. Note, that probe molecules can also interact with acid sites located at the pore mouth of the zeolites, even if their dynamic diameter is larger than the pore openings.³⁰

For the enhancement of the shape-selectivity by CVD or CLD, knowledge about the distribution of the bridging hydroxyl groups on the external surface and in the pore mouth of HZSM-5 zeolites is essential. The first step of silylation is assumed to be initiated on the bridging hydroxyl groups accessible for the silylating agent.¹⁹ Conceptually, the enhancement of the shape selectivity by silylation results from the passivation of non-selective acid sites and, in parallel, from the narrowing of the pore openings of the zeolites.²⁰⁻²² Note that the narrowing of the pore openings would be most effectively achieved if the bridging hydroxyl groups were located in the pore mouth, while only a minor narrowing of the pore openings would be expected if silylation occurs on the external surface of the zeolite crystals only. We have observed that a more effective pore mouth narrowing has been achieved by CLD of tetramethoxysilane (TMOS) compared to TEOS.⁴¹ As the critical diameter of TMOS (8.9 Å) is smaller than that of TEOS (10.3 Å), TMOS molecules could reach deeper into the pores of the zeolite. These results indicate that the silylation mainly occurs at the pore mouth of the zeolite and that most of the bridging hydroxyl groups are located in the pores of zeolites, which is in agreement with the results of Armaroli et al..⁴⁰

After silylation by CLD, the formation of new hydroxyl groups was observed. The shift of the O-H stretching frequency to a lower wave number and the broadening of the band indicate that location and geometric environment of these hydroxyl groups is different from silanol groups on the external surface. As silylation is expected to occur in the pore mouth region, we would like to speculate that the newly formed silanol groups are also located in the pore mouth region and, furthermore, that the geometry of the pores leads to the formation of hydrogen bonding interactions between these silanol groups. The increase in the intensity of this broad band and the simultaneous narrowing of the pores of the zeolite also confirms that the newly

formed silanol groups are located in a sterically constrained region, i.e., the pore mouth region of the zeolites.⁴¹

2.4.2. Acid sites on the external surface and in the pore mouth of the zeolites

As the diameter of TEOS is larger than that of the pores of HZSM-5 zeolite, silylation by CLD of TEOS only modifies the external surface and the pore mouth of HZSM-5 zeolites.⁴² The decrease in the concentration of the hydroxyl groups of the zeolites after silylation by CLD was unequivocally determined using different characterization methods. Approximately 7.0% and 28% of the bridging hydroxyl groups were accessible for DTBPy in HZL and HZS, respectively, which is attributed to the different particle size of the two parent materials. As the specific surface area of spherical particles is reciprocally proportional to their radius, the specific surface area of the outer surface should be approximately 6 times larger for HZS compared to HZL. However, the fraction of acid sites located on the external surface and in the pore mouth region of HZS was found to be only 4 times higher than that of HZL. The difference can be tentatively attributed to (i) a lower concentration of the acid sites on the external surface and in the pore mouth region of HZS, or (ii) to a narrowing of the pore entrance of HZS by EFAl. One should note that there is a larger amount of EFAl present in HZS compared to HZL, which might narrow the pores of HZS and, thus, constraints the DTBPy sorption on accessible Brønsted acid sites.

For both samples, silylation also led to a decrease in the concentration of Lewis acid sites as already described by Shaikh et al.³². For HZS, single cycle and three-cycle silylation led almost to the same decrease in the concentration of Lewis acid sites, which indicates that all Lewis acid sites accessible for TEOS are already completely silylated after first cycle. This points to an easier accessibility of the Lewis acid sites located on aluminum oxide species and suggests that the silylation of Lewis acid sites proceeds more rapidly than that of Brønsted acid sites.

For single cycle silylation, pyridine adsorption showed that 0.038 mmol/g of the acid sites (Brønsted acid sites + Lewis acid sites) of HZS and 0.031 mmol/g of the acid sites of HZL were passivated. Considering the significantly higher concentration

of acid sites accessible for TEOS on HZS and that an excess of TEOS was used in each cycle, we conclude that a higher efficiency for silylation was achieved for the sample with the larger particle size. In contrast multiple silylation cycles were necessary for HZS, however, they did not lead to the same fractional decrease in the concentration of acid sites for each cycle. Note that the first silylation cycle of HZS led to a removal of 53% of the acid sites on the external surface and in the pore mouth region, while during the subsequent cycles only 76% of the acid sites were passivated, although a significant amount of acid sites remained in the pore mouth region. This might indicate that the acid sites on the external surface and in the pore mouth region were not homogeneously distributed.

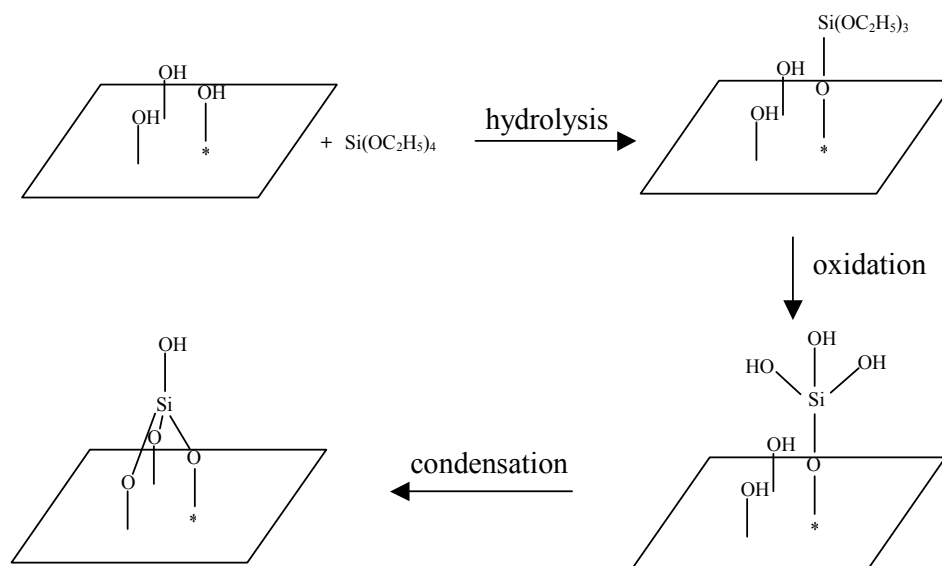
During the first silylation cycle, we conclude that TEOS molecules react with accessible acid sites and attach to the surface of the zeolite. This may hinder other TEOS molecules to access vicinal acid sites, if the concentration of the acid sites is high. The acid sites, however, may become accessible during subsequent silylation cycles, because the bulky ethoxyl groups on TEOS are removed during the calcination. Thus the density of the acid sites strongly affects the extent of the silylation reaction. As the Si/Al ratios of the zeolites used were relatively high (i.e., 45), the distribution of the acid sites should have only a minor influence on the passivation effects. Therefore, we would like to assign the different silylation effects to acid sites located at different depths in the pores of the zeolite. During the first silylation cycle, TEOS molecules preferentially interact with acid sites that are easily accessible and, therefore, high passivation effects are achieved. In the second and third cycle, the concentration of accessible acid sites is strongly reduced and the narrowing of the pore openings further hinders TEOS molecules from penetrating into zeolite pores. Therefore, a decreasing extent of passivation can be expected in subsequent modification cycles.

2.4.3. Silylation mechanism of CLD

The concentration of silanol groups, bridging hydroxyl groups and Lewis acid sites was reduced after silylation by TEOS. Niwa et al.^{19,32,43} proposed, based on the

acid strength of different hydroxyl groups, that the reactivity of the bridging hydroxyl groups was higher than that of the silanol groups. In addition, CVD modification of aluminum oxide indicated that at first a homogeneous monolayer of silica was generated before the first Si-O-Si bonds were formed. It was also found that silylation of silicalite and NaZSM-5 zeolites is less effective compared to acidic zeolites^{44,45} Combining these results, the reactivity of the three sites should be:

Lewis acid sites ~ bridging hydroxyl groups > silanol groups.



*: Bronsted or Lewis acid site

Scheme 1: Scheme of silylation reaction between TEOS and the surface hydroxyl groups of HZSM-5

For HZS, all accessible Lewis acid sites for TEOS were removed by silylation, while in contrast, multi-cycle silylation led to a further decrease in the concentration of the silanol and the bridging hydroxyl groups. This suggests that the reaction of TEOS with Lewis acid sites occurs prior to the silanol and the bridging hydroxyl groups, because a fraction of Lewis acid sites is located at the external surface, thus, having a higher accessibility for TEOS compared to the bridging hydroxyl groups and additionally, Lewis acid sites are probably stronger acidic than Brønsted acid sites. For each silylation cycle, a decrease in the concentration of the silanol groups was

observed before the complete deactivation of the accessible bridging hydroxyl groups, although the reactivity of the bridging hydroxyl groups with TEOS is higher than the silanol groups. This suggests that TEOS molecules react with the bridging hydroxyl groups and subsequently condense with vicinal silanol groups during calcination. The similar ratio of the decrease in the concentration of the silanol and bridging hydroxyl groups for single and multi-cycle silylation confirms this.

The CLD mechanism of the silylation process is shown in Scheme 1. Silylation of the zeolites includes two stages (i) the liquid phase reaction and (ii) the calcination process. The hydrolysis of TEOS only occurs on Brønsted and Lewis acid sites during liquid phase reaction, which leads to the formation of Si-O-Al bonds. During calcination, the residual ethoxyl groups are oxidized into hydroxyl groups, which partially condense with vicinal silanol groups to form Si-O-Si bands. Therefore, modification of zeolites by CLD of TEOS leads to a simultaneous decrease in the concentration of Brønsted sites, Lewis acid sites and silanol groups.

In general, modification of zeolites with different crystal sizes will lead to different silylation effects. Zeolites with small crystals as well as a high specific surface area require a comparatively high amount of silylating agent and in most cases multi-cycle silylation to achieve an effective passivation of unselective acid sites. The presence of EFAl also lowers the silylation efficiency. Typically, zeolites with small crystal size contain a relatively high amount of EFAl because of the fast crystallization. Therefore, pretreatment of zeolites, such as pre-dealumination of the external surface of zeolites,⁴¹ can be used to enhance the modification effects.

2.5. Conclusions

Silylation of HZSM-5 with CLD of TEOS leads to the passivation of Brønsted and Lewis acid sites on the external surface and in the pore mouth region of the zeolites. For samples with small crystal sizes, single cycle silylation deactivates all Lewis acid sites accessible for TEOS, however, a multi-cycle silylation is advantageous to further deactivate Brønsted acid sites. In contrast, for samples with large crystals, effective silylation can be achieved with a single cycle silylation step.

The deactivation of Lewis acid sites occurs prior to the passivation of Brønsted acid sites and silanol groups, which results from the easier accessibility and higher acid strength of Lewis acid sites. The deactivation of the Brønsted acid sites is attributed to a hydrolysis reaction with TEOS, while the reaction with the silanol groups occurs during the subsequent calcination by a condensation of the hydroxyl groups.

Silylation preferentially occurs in the pore mouth region. New hydrogen bonded hydroxyl groups are formed by CLD modification in the pore mouth region of the zeolite.

Acknowledgments

The authors thank J.-O. Barth for the measurements of the ^{27}Al MAS NMR. Financial support from the Bayerische Forschungsverbund Katalyse (FORKAT II) and Süd-Chemie AG is gratefully acknowledged.

References

1. Weitkamp, J. *Solid State Ionics*, **131**, 175 (2000).
2. Kaeding, W. W.; Barile, G. C.; Wu, M. M. *Catal. Rev.-Sci. Eng.* **26**, 597 (1984).
3. Olson, D. H.; Haag, W. O. *Catalytic Materials*, ACS Symposium Series, Vol. 248, ACS, Washington, DC, 1984.
4. Kaeding, W. W.; Chu, C.; Young, L. B.; Weinstein, B.; Butter, S. A. *J. Catal.* **67**, 159 (1981).
5. Das, J.; Bhat, Y. S.; Halgeri, A. B. *Ind. Eng. Chem. Res.* **33**, 246 (1994).
6. Röger, H. P.; Krämer, M.; Möller, K. P.; O'Connor, C. T. *Microporous Mesoporous Mater.* **21**, 607 (1998).
7. Mirth, G.; Lercher, J. A. *J. Catal.* **95**, 3736 (1991).
8. Mirth, G.; Cejka, J.; Lercher, J.A. *J. Catal.* **139**, 24 (1993).
9. Mirth, G.; Lercher, J.A. *J. Catal.* **147**, 199 (1994).
10. Hibino, T.; Niwa, M.; Murakami, Y. *J. Catal.* **128**, 551 (1991).
11. Kürschner, U.; Jerschke, H. G.; Schreier, E; Völter, J. *Appl. Catal.* **57**, 167 (1990).

12. Wang, I.; Ay, C. L.; Lee, B. J.; Chen, M. H. *Appl. Catal.* **54**, 257 (1989).
13. Bhat, Y. S.; Das, J.; Rao, K. V.; Halgeri, A. B. *J. Catal.* **159**, 368 (1996).
14. Fraenkel, D. *Ind. Eng. Chem. Res.* **29**, 1814 (1990).
15. Csicsery, S. M. *Zeolites* **4**, 202 (1984).
16. Kaeding, W. W.; Chu, C.; Young, L. B.; Butter, S. A. *J. Catal.* **69**, 392 (1981).
17. Tynjala, P.; Pakkanen, T. T. *J. Mol. Catal. A* **122**, 159 (1997).
18. Fang, L. Y.; Liu, S. B.; Wang, I. *J. Catal.* **185**, 33 (1999).
19. Niwa, M.; Katada, N.; Murakami, T. *J. Phys. Chem.* **94**, 6441 (1990).
20. Niwa, M.; Katada, N.; Murakami, Y. *J. Catal.* **134**, 340 (1992).
21. Niwa, M.; Kato, S.; Hattori, T.; Murakami, Y. *J. Chem. Soc., Faraday Trans. 1*, **80**, 3135 (1984).
22. Yue, Y. H.; Tang, Y.; Liu, Y.; Gao, Z. *Ind. Eng. Chem. Res.* **35**, 430 (1996).
23. Gründling, C.; Eder-Mirth, G.; Lercher, J. A. *J. Catal.* **160**, 299 (1996).
24. Weber, R. W.; Möller, K. P.; Unger, M.; O'Conner, C. T. *Microporous Mesoporous Mater.* **23**, 179 (1998).
25. Weber, R. W.; Möller, K. P.; O'Conner, C. T. *Microporous Mesoporous Mater.* **35**, 533 (2000).
26. Kim, J. H.; Ishida, A.; Okajima, M.; Niwa, M. *J. Catal.* **161**, 387 (1996).
27. Weber, R. W.; Fletcher, J. C. Q.; Möller, K. P.; O'Conner, C. T. *Micropor. Mater.* **7**, 15 (1996).
28. Melson, S.; Schüth, F. *J. Catal.* **170**, 46 (1997).
29. Coma, A.; Fornes, V.; Forni, L.; Marquez, F.; Martinez-Triguero, J.; Moscotti, D. *J. Catal.* **179**, 451 (1998).
30. Pieterse, J. A. Z.; Veefkind-Reyes, S.; Seshan, K.; Lercher, J. A. *J. Phys. Chem. B* **104**, 5715 (2000).
31. Sayed, M. B.; Kydd, R. A.; Cooney, R. P. *J. Catal.* **88**, 137 (1984).
32. Shaikh, R. A.; Hegde, S. G.; Behlekar, A. A.; Rao, B. S. *Catal. Today* **49**, 201 (1999).
33. Vimont, A.; Thibault-Starzyk, F.; Lavalley, J. C. *J. Phys. Chem. B* **104**, 286 (2000).

34. Man, P. P.; Klinowski, J. *Chem. Phys. Lett.* **147**, 581 (1988).
35. Brunner, E.; Ernst, H.; Freude, D.; Frohlich, T.; Hunger, M.; Pfeifer, H. *Stud. Surf. Sci. Catal.* **49A**, 623 (1989).
36. Grobet, P. J.; Geerts, H.; Tielen, M.; Martens, J. A.; Jacobs, P. A. *Stud. Surf. Sci. Catal.* **46**, 721 (1989).
37. Glazunov, V. P.; Odinkov, S. E. *Spectrochim. Acta* **38A**, 399 (1982).
38. Emeis, C. A. *J. Catal.* **141**, 347 (1993).
39. Knözinger, H.; Krietenbrink, H.; Ratnasamy, P. *J. Catal.* **48**, 436 (1977).
40. Armaroli, T.; Trombetta, M.; Alejandre, A. G.; Solis, J. R.; Busca, G. *Phys. Chem. Chem. Phys.* **2**, 3341 (2000).
41. Zheng, S.; Heydenrych, H. R.; Jentys, A.; Lercher, J. A. submitted to *Topics in Catalysis*.
42. Zheng, S.; Heydenrych, H.; Röger, P.; Jentys, A.; Lercher, J. A. *Stud. Surf. Sci. Catal.* **135**, 214 (2001).
43. Hibino, T.; Niwa, M.; Murakami, Y. *Zeolites* **13**, 519 (1993).
44. Begum, H. A.; Katada, N.; Niwa, M. *Microporous Mesoporous Mater.* **46**, 13 (2001).
45. Chun, Y.; XU, Q.; Yan, A.; Ye, X. *Stud. Surf. Sci. Catal.* **105**, 2075 (1997).

Chapter 3

On the influence of modification by chemical liquid deposition on toluene diffusion in HZSM-5

Abstract

HZSM zeolite was modified by chemical liquid deposition of *tetra*-ethoxysilane and the diffusivities of toluene in HZSM-5 zeolites before and after silylation were studied using the frequency response method. Toluene molecules preferentially occupied the intersections with acid sites and silylation did not lead to change in toluene adsorption in the zeolite. Two diffusion processes were identified on both zeolites which were assigned to the diffusion of toluene in the straight and sinusoidal channels of the zeolite. The difference in toluene diffusivities was related to the marked tortuosity of the diffusion pathways in the sinusoidal channels. Toluene diffusivities in both channels were found to be dependent on toluene loading which was related to the interaction of toluene with the acid sites of the zeolite. Silylation of the zeolite led to a decrease in toluene diffusivities in both the straight and sinusoidal channels of the zeolites. In addition the amount of toluene molecules accessing the sorption sites through the sinusoidal channels increased after the modification, while the total uptake remained unaffected by the modification. Based on the data presented a partial blocking of about 75 % of the pore opening during the modification is proposed.

3.1. Introduction

HZSM-5 zeolites have attracted great interest in industrial and academic researches because of their high *para*-selectivity in isomerization, disproportionation and alkylation reactions of methyl and ethyl substituted benzene molecules^{1, 2, 3}. As the diffusivities of products and reactants are crucial parameters for the control of the shape selectivity of zeolites, numerous papers addressing sorption and transport processes of aromatic molecules such as benzene, toluene and xylenes in ZSM-5 zeolites were published^{4, 5}. The kinetic diameters of these molecules and the dimensions of the pores of ZSM-5 zeolites are in the same range, therefore, this combination is a challenging example to verify the potential of novel experiments and theories developed to study diffusion processes including pulsed-field gradient NMR (PFG NMR)^{4, 5}, quasi elastic neutron scattering (QENS)^{6, 7}, tracer exchange⁸, zero-length column^{9, 10}, uptake-rate measurement followed by FT-IR^{11, 12} and gravimetry^{13, 14}, the frequency response (FR) method^{15, 16} and simulation^{17, 18}. Typically, with PFG-NMR and QENS self-diffusivity is determined, while uptake measurements are used to observe transport diffusivity. Conceptually, the difference between both is that transport diffusivity is determined under non-equilibrium conditions, while self-diffusivity is obtained under equilibrium conditions. Transport diffusivity can be related to the intracrystalline-diffusivity applying the Darken equation¹⁹. Significant discrepancies, however, have been reported for the same diffusion processes determined by different techniques⁴.

Typically, as-synthesized HZSM-5 zeolites show only a low shape-selectivity in reactions of substituted benzene molecules, which is generally attributed to the presence of unselective acid sites located on the external surface and in the pore mouth region of zeolites as well as to slightly large pore openings of HZSM-5 zeolites^{20, 21}. To achieve an enhanced *para*-selectivity, post-synthesis modification of zeolites is necessary. The deposition of an inert silica layer on the external surface of zeolites applying chemical vapor deposition (CVD)^{22, 23} or chemical liquid deposition (CLD)^{24, 25} has been proven to be one of the most effective approaches to tailor the external surface of zeolites in order to obtain stable and shape-selective catalysts. This type of modification leads to a combination of two beneficial effects, i.e., a passivation of the unselective acid sites located on the external surface and in the pore mouth region and, at the same time, a

narrowing of the pore mouth openings of the zeolites. In principle, silylation effects of HZSM-5 zeolites can be assessed by studying the diffusion of molecules with kinetic diameters comparable to the size of the pores. A successful narrowing of pore openings of zeolites will result in a significant hindrance for the diffusion of aromatic molecules with relatively larger diameters, such as *o*-xylene.²⁶ The influence of the modification of the external surface on the diffusivities of aromatic molecules with relatively small diameters, such benzene, toluene and *p*-xylene, has been seldom addressed in detail²⁷.

In this chapter, the sorption and diffusion of toluene in HZSM-5, modified by chemical liquid deposition of tetra-ethoxysilane (TEOS) was studied by the frequency response method. The influence of silylation on the diffusivities of toluene was related to the structural properties of the zeolites before and after silylation in order to explain the enhanced shape selectivity of the modified zeolite.

3.2. Experimental

3.2.1. Materials

HZSM-5 zeolite with a silica-alumina ratio of 45 and a particle size of 3 μm was used as the parent material. The modification was carried out applying chemical liquid deposition of TEOS according to the following procedure. 2 g of zeolite was suspended in 50 ml hexane and heated to reflux under stirring. 0.3 ml of TEOS (equal to 4 wt% SiO_2) was added into the mixture and the silylation process was carried out for 1 h under reflux. Hexane was removed by evaporation and the sample was calcined at 773 K in dry air for 4 h. The parent and modified zeolites are referred to as HZ and HZM, respectively. The effects of the modification on the concentration of the acid site distribution in the zeolite were described previously²⁸.

3.2.2. Adsorption of toluene

The adsorption isotherms and the differential heats of adsorption of toluene in the zeolite samples were measured in a modified SETARAM TG-DSC 111 instrument. Approximately 15 mg of sample was pressed into wafers, broken into small platelets

and charged into the quartz crucible used in the TG-DSC system. The sample was activated by heating to 823 K with an increment of 10 K/min for 1 h in vacuum ($p < 10^{-6}$ mbar). After activation, the temperature of the sample was stabilized at 373 K or 403 K. Toluene vapour was introduced into the closed system in small doses and allowed to equilibrate with the zeolite until further pressure decrease and mass increase were not observed. The toluene pulses were repeated until toluene pressure reached 14 mbar. The increase in the mass of the sample and the heat flux during the adsorption process were collected simultaneously.

3.2.3. Diffusion measurements by the frequency-response method

The diffusivities of toluene in the parent and silylated zeolites were measured using the frequency response method^{16,29}. Approximately 30 mg of zeolite was carefully dispersed on several layers of glass wool in a quartz tube in order to avoid the bed-depth effects³⁰. The sample was activated at 823 K under vacuum (pressure below 10^{-7} mbar) for 1 h. Toluene with partial pressures between 0.05 and 1.5 mbar was introduced into the system at 373 or 403 K. After the sorption equilibrium was established, the volume of the system was modulated by magnetically driven bellows, which resulted in a square-wave perturbation of the volume ($\pm 1\%$) in a frequency range between 0.001 and 1 Hz. The response of the pressure to the volume perturbation was recorded with a Baratron pressure transducer (MKS 16A11TCC).

The measurement of diffusion coefficients by the frequency response method is based on a perturbation of the sorption equilibrium by a modulation of the pressure resulting from the periodic change (square wave) of the volume of the closed chamber. The characteristic parameters of the frequency response experiment, i.e., the phase lag and amplitude, are obtained experimentally from the pressure response during the volume perturbations at different frequencies using a Fourier transformation³¹. Typically the characteristic functions of the frequency response method are described by the following equations:

$$\text{in-phase: } (P_B/P_Z) \cos\Phi_{Z-B} - 1 = K \delta_c \quad 1$$

$$\text{out-of-phase: } (P_B/P_Z) \sin\Phi_{Z-B} = K \delta_s \quad 2$$

$$\delta_c = (1/\eta)[(\sinh\eta + \sin\eta)/(\cosh\eta + \cos\eta)] \quad 3$$

$$\delta_s = (1/\eta)[(\sinh\eta - \sin\eta)/(\cosh\eta - \cos\eta)] \quad 4$$

$$\eta = (\omega L^2/2D)^{1/2} \quad 5$$

where Φ_{Z-B} is the difference between the phase lags in the presence and absence of the zeolite, P_B and P_Z the relative amplitudes of the pressure during the volume change in the absence and in the presence of the zeolite, ω the angular frequency of the volume modulation, D the diffusion coefficient and L the diameter of zeolite crystals. δ_c and δ_s , which are functions of the diffusion coefficient, are known as the in-phase and out-of-phase characteristic functions, respectively. K is a constant related to the gradient of the sorption isotherm at the equilibrium pressure p_e ¹⁵:

$$K = (RT_0/V_e)(dQ_e/dp_e) \quad 6$$

where T_0 is the temperature, V_e the system volume, Q_e the equilibrium amount sorbed and p_e the equilibrium partial pressure. The in-phase and out-of-phase functions obtained from the experimental measurements over the frequency range studied were fitted to obtain the diffusion coefficients using a model with two individual diffusion processes under isothermal conditions given in Equation 7 and 8³².

$$\text{in-phase: } (P_B/P_Z) \cos\Phi_{Z-B} - 1 = K_H \delta_{cH} + K_L \delta_{cL} \quad 7$$

$$\text{out-of-phase: } (P_B/P_Z) \sin\Phi_{Z-B} = K_H \delta_{sH} + K_L \delta_{sL} \quad 8$$

where H and L denotes the fast and slow diffusion processes, respectively. In principle, the diffusion process with the maximum of out-of-phase characteristic function at higher frequency is indicative to a higher diffusion coefficient.

3.3. Results

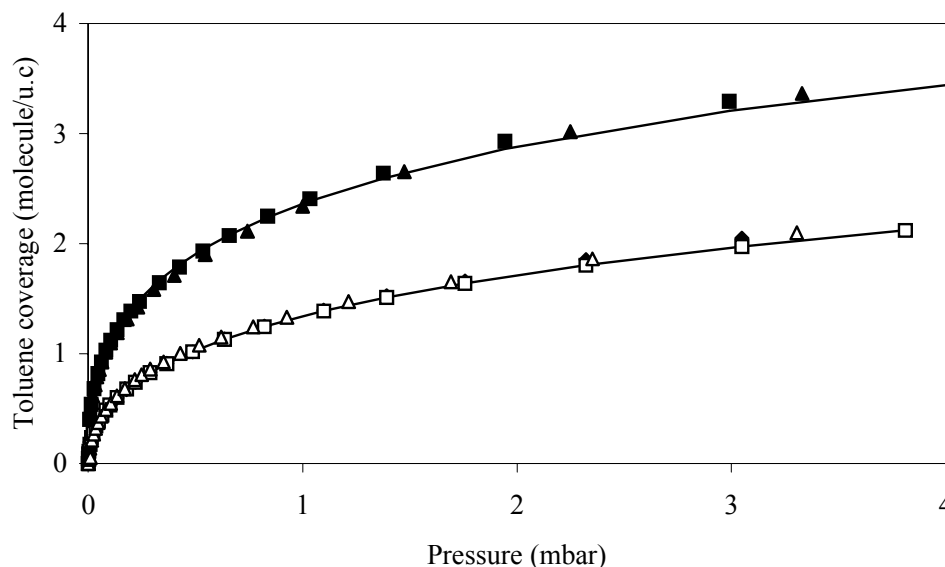
The sorption isotherms of toluene in the parent and silylated zeolites, shown in Figure 1, could be well described by Langmuir-Freundlich model:¹³

$$Q = \frac{Q_0 \times b \times p^m}{1 + b \times p^m} \quad 9$$

where Q denotes the amount of toluene adsorbed at a pressure p , Q_0 the maximum amount of toluene adsorbed. The constants Q_0 , b and m were obtained by fitting the experimental data and listed in Table 1.

Table 1. The parameters of isotherms obtained by fitting

	HZ		HZM	
	373 K	403 K	373 K	403 K
Q_0	13.6	6.5	13.3	6.3
b	0.21	0.26	0.22	0.30
m	0.38	0.47	0.39	0.51

**Figure 1.** Isotherms of (■,□) HZ and (▲,△) HZM at 373 K (filled symbols) and 403 K (open symbols).

The intracrystalline-diffusion coefficients of toluene in the parent and silylated zeolites at different toluene loading were obtained by correcting the transport diffusion coefficients, determined by the frequency response method, using Darken equation:¹⁹

$$D_0 = D \times \frac{\partial \ln Q}{\partial \ln p} \quad 10$$

Where D_0 denotes the intracrystalline-diffusion coefficient of toluene, D the transport diffusion coefficient and Q the amount of toluene adsorbed at a partial pressure p .

The differential heats of adsorption as a function of the toluene coverage determined at 373 K for the parent and silylated zeolites are compared in Figure 2. For both samples the heats of adsorption showed a similar dependence on the coverage of toluene. In the region of toluene loadings below 0.5 molecules per unit cell (mol./u.c.), the differential

heats of adsorption decreased from 100 KJ/mol to 80 KJ/mol. At toluene loadings between 0.5 and 1.6 and between 2 and 4 mol./u.c. constant heats of adsorption of 80 and 70 kJ/mol, respectively, were observed for both zeolite samples. At toluene loadings above 4 mol./u.c. a sharp decrease in the heats of adsorption was observed.

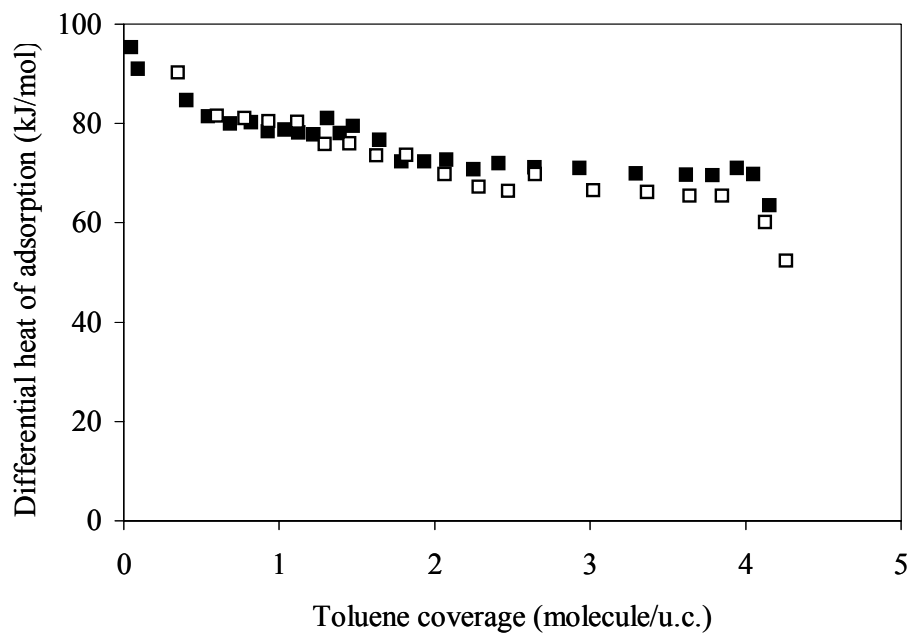


Figure 2. Heats of adsorption of toluene in HZ (□) and HZM (■) at 373 K.

The characteristic functions of the frequency response experiment during toluene adsorption with an equilibrium partial pressure of 0.6 mbar in the parent and silylated zeolites are shown in Figure 3 and 4.

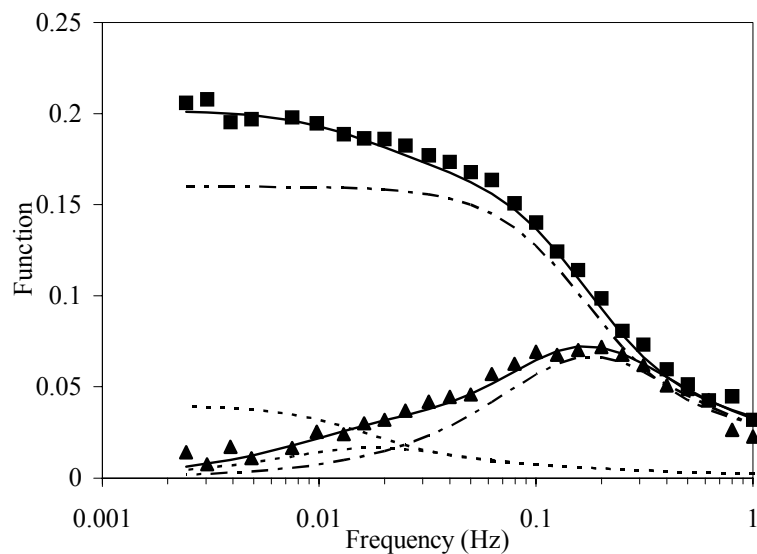


Figure 3: FR spectra of toluene diffusion in HZ at 373 K and toluene pressure of 0.6 mbar. (■) denotes the experimental data of in-phase and (▲) out-of-phase characteristic functions. Solid lines are theoretical fitting curves using two-process model, (· · ·) fitting curves of slow diffusion process and (- · -) fitting curves of fast diffusion process.

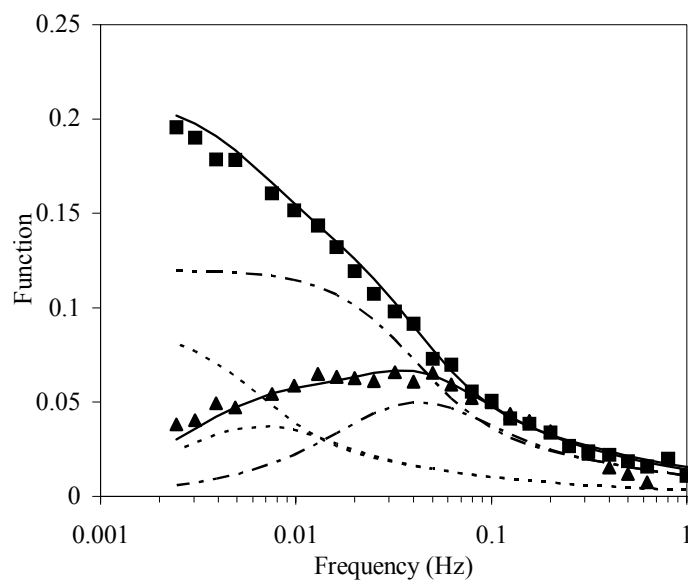


Figure 4: FR spectra of toluene diffusion in HZM at 373 K and toluene pressure of 0.6 mbar. (■) denotes the experimental data of in-phase and (▲) out-of-phase characteristic functions. Solid lines are theoretical fitting curves using two-process model, (· · ·) fitting curve of slow diffusion process and (- · -) fitting curve of fast diffusion process.

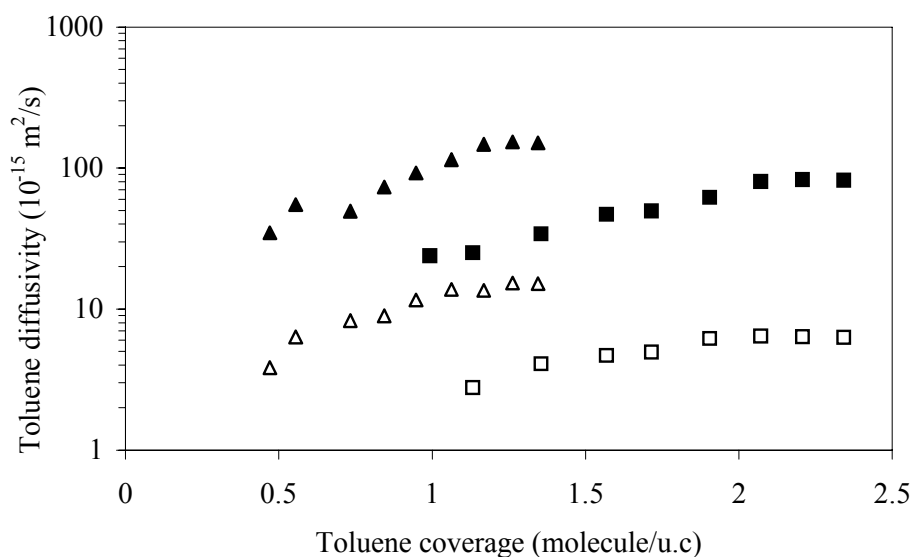


Figure 5. Dependence of diffusivities of toluene in HZ on molecule loading at (■,□) 373 K, and (▲,△) 403 K. Filled symbols denote the fast diffusion process and open symbols the slow diffusion process.

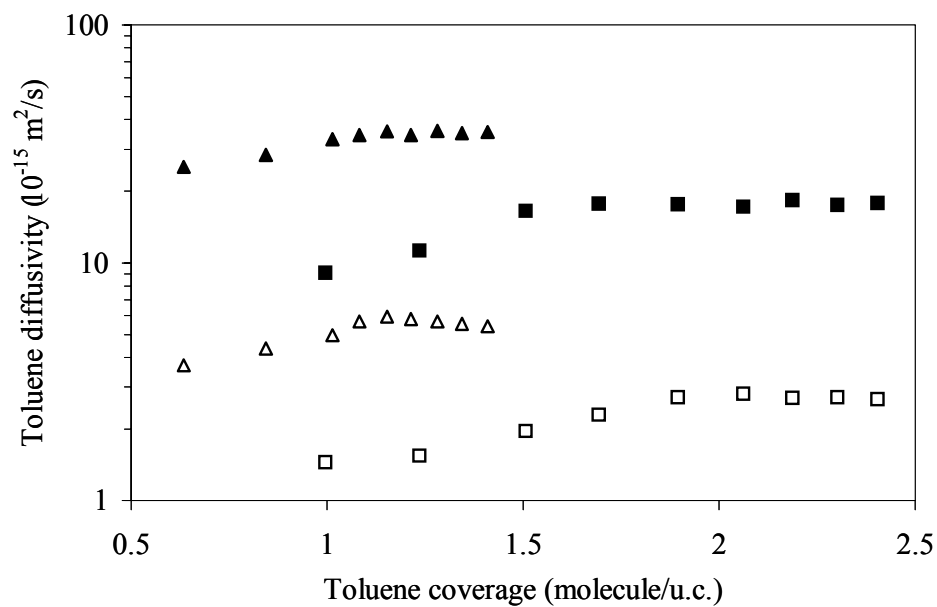


Figure 6. Dependence of diffusivities of toluene in HZM on molecule loading at (■,□) 373 K, and (▲,△) 403 K. Filled symbols denote the fast diffusion process and open symbols the slow diffusion process.

After fitting the experimental data, two maxima were obtained in the out-of-phase characteristic function, indicating the presence of two independent diffusion processes for toluene in both samples³³. Conceptually, the amount of molecules diffusing through the pores of the sample during the pressure modulation in the frequency response experiments is characterized by K value. For toluene diffusion studied at a partial pressure of 0.6 mbar, the K values for the diffusion process with high (K_H) and low diffusivity (K_L) were 0.32 and 0.11 for HZ and 0.225 and 0.225 for HZM, respectively. This indicates that for the parent material a larger number of molecules were involved in the transport process with the higher diffusivity, while after the modification an equal number of molecules were involved in both diffusion processes. The dependencies of the intracrystalline-diffusion coefficients for the two diffusion processes D_H and D_L at 373 K and 403 K on the toluene loading are shown in Figure 5 for HZ and in Figure 6 for HZM. Silylation led to a decrease in the diffusivities by a factor of 4 for D_H and 2 for D_L at all temperatures. In both samples the intracrystalline-diffusivity determined at 373 K and 403 K increased with increasing toluene loading in the zeolites and remained approximately constant at toluene loadings higher than 2 and 1.2 mol./u.c., respectively, while the ratios of K_H to K_L were independent on toluene loading for both zeolites.

3.4. Discussion

3.4.1 Toluene adsorption in the zeolites

For toluene adsorption in MFI type zeolites three possible locations were reported: (i) intersections between the straight and sinusoidal channels, (ii) straight channels and (iii) sinusoidal channels. For both zeolite samples the heat of adsorption sharply decreased from 100 to 80 kJ/mol at loadings below 0.5 mol./u.c., revealing the presence of a minor fraction of strongly (Lewis) acidic sorption sites. These sites are most probably related to extra framework Al-oxide species³⁴. For both zeolite samples the heats of adsorption at toluene loadings below 1.6 mol./u.c. were found to be 10 kJ/mol higher compared to toluene loadings between 2 and 4 mol./u.c.. The concentration of Brønsted acid sites, calculated from the density of acid sites of the zeolites is 1.6 sites

per unit cell²⁸, therefore, the additional contribution of 10 kJ/mol observed in the heat of adsorption at low loadings can be directly related to the hydrogen bonding interaction of toluene with the SiOHAl groups, which were in good agreement with the results of Thamm *et al.*³⁵ Toluene molecules preferentially occupy the intersections of the zeolite channels³⁶ at toluene loadings below 2 mol./u.c. and interact with the bridging hydroxyl groups via hydrogen bonding interaction at toluene loadings below 1.6 molecules/u.c., which also implies that most of acid sites are located in the intersections of the zeolites. Also at toluene loadings between 2 and 4 mol./u.c. constant heats of adsorption were observed, which indicates that in this range toluene molecules are adsorbed at intersections without direct interaction with the bridging hydroxyl groups (Brønsted acid sites). The number of intersections per unit cell in ZSM-5 type zeolites is 4 and, therefore, at toluene loadings above 4 mol./u.c. all available sorption sites at intersections were occupied, which is reflected in a sharp decrease in the heats of adsorption. The dimensions of the straight channels, the sinusoidal channels and the intersections are 5.6×5.3 , 5.5×5.1 and 8.9 \AA , respectively⁵. As the kinetic diameter of toluene molecules (5.8 \AA) is close to the dimensions of the straight or sinusoidal channels, the repulsive forces between toluene molecules and the pore walls are more dominant compared to positions in the intersections. Simulation results^{37,38} also showed that the potential energy of toluene molecules located in the straight or sinusoidal channels is higher compared to that in the intersections of HZSM-5 zeolite.

3.4.2. Toluene diffusion in the zeolites

Two independent processes for toluene diffusion in ZSM-5 were already observed by Rees *et al.*³⁹ and were explained by toluene diffusion in the straight and sinusoidal channels of ZSM-5. Alternatively, the diffusion of toluene molecules with the methyl group oriented in front or to the back was proposed for the two processes³⁹. However, the diffusivities of toluene usually observed are only 2-3 times higher compared to those of benzene⁴⁰, which cannot exhibit an orientation effect^{41,42}. Based on the large difference between the diffusivities of the two processes (about 10 times for the parent material), we favor the assignment of the two diffusion processes to toluene diffusion in the straight and sinusoidal channels. For toluene diffusion in HZ at 373 K, the corrected

diffusion coefficient for the fast process is $8 \times 10^{-14} \text{ m}^2/\text{s}$, which is in agreement with the results reported in the literatures^{40,43}, while for the slow diffusion process the corrected diffusion coefficient was $6.5 \times 10^{-15} \text{ m}^2/\text{s}$. Note that both diffusion coefficients were not dependent on the toluene loading at loadings above 2 mol./u.c.. In principle toluene can access the adsorption sites at the intersections of the zeolite by diffusing through the straight or the sinusoidal channels. As the diameter of sinusoidal channels is slightly smaller than that of the straight channels, a lower diffusivity for toluene in the sinusoidal channels compared to the straight channels is expected. However, the difference between the diffusion coefficients of the two processes is about an order of magnitude, which appears to be too large to result from the difference in the pore diameter only. Therefore, we would like to speculate that the difference in the diffusion coefficients mainly results from the tortuosity of the sinusoidal channels. During the diffusion of toluene molecules through the sinusoidal channels the molecules have to change their direction in each intersection, while in the other channels a straight diffusion path is possible. This results in an additional hindrance to toluene diffusion in the sinusoidal channels, which leads to lower diffusivities in the sinusoidal channels compared to the straight channels of the zeolite.

For the dependence of the diffusivity on the loading of toluene different trends were reported in the literature. Choudhary *et al.*⁴⁴ and Tsikoyiannis⁴⁵ observed, in accordance with the results reported here, increasing diffusivities with the loading in the pores. However, a constant¹⁴ and a decreasing diffusivity³⁹ with increasing toluene concentration were also observed. In the range of toluene loadings studied by the Frequency Response method, the toluene diffusivities increased in the both materials and remained constant at toluene loadings above 2 mol./u.c.. This trend can be described with a type III diffusion process assuming the decreased mobility of diffusion molecules due to the strong interaction with the adsorption sites of zeolite^{46,47}. Based on the diffusion mechanism of the random walk model, toluene molecules diffuse inside the pores by jumps between adsorption sites⁴⁸. Consequently, the residence time of toluene molecules adsorbed on intersections of the zeolite with Brønsted acid sites will be longer compared to sorption sites at intersections without Brønsted acid sites due to the additional energetic contribution of 10 kJ/mol resulting from the hydrogen bonding interaction of the toluene molecules with the SiOHAl groups. In agreement with the

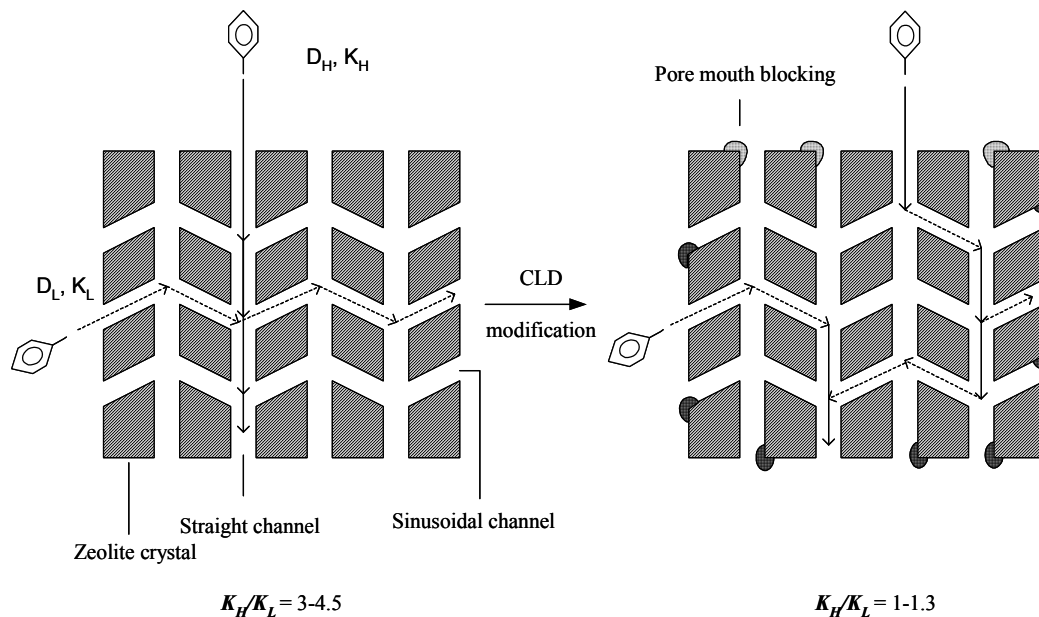
heats of adsorption measured for both samples, the diffusivity increases with the loading as long as Brønsted acid sites are available for adsorption (coverage lower than 2 mol./u.c. at 373 K). At toluene loadings above 2 mol./u.c., all Brønsted acid sites were occupied by toluene molecules and, therefore, a higher diffusivity was observed, which did not depend on the toluene loading of the sample. In agreement with other authors^{49,50} we would like to speculate that the presence of Brønsted acid sites retards the toluene diffusion. In addition, Hufton *et al.*⁵¹ also observed lower diffusivities of isobutene in silicalite at coverage below one molecule per seven channel intersections due to the presence of defect sites acting as strong adsorption sites. Note that the diffusivities of toluene observed at 403 K keep constant at lower toluene loadings (1.2 mol./u.c.) compared to that at 373 K for the parent and silylated zeolites (see Figure 5 and 6). This indicates that the influence of the direct interaction of the bridging hydroxyl groups with toluene molecules on the diffusivity generally decreases with increasing temperature. Masuda *et al.*⁵² also observed the same diffusivities of aromatic molecules in HZSM-5 zeolite as in silicalite (i.e., non acidic ZSM-5) at high temperatures although at lower temperatures markedly lower diffusivities were observed in HZSM-5 compared to silicalite.

Due to its larger kinetic diameter of 10.3 Å TEOS was found to modify only the external surface of ZSM-5 zeolites²⁸ by a reaction of TEOS with the bridging hydroxyl groups located in the pore mouth region and silanol groups located on the external surface of the crystals. Brønsted acid sites accessible for TEOS molecules are effectively passivated by the deposition of an amorphous oxide layer. In addition silylation leads to the narrowing or blocking of the pore entrance²⁶, which may directly influence the transport of the molecules to the sites inside the pores. Two independent diffusion processes, assigned to the transport through the straight (described by K_H and D_H) and sinusoidal channels (described by K_L and D_L), were observed in the frequency response experiments. After silylation, toluene diffusivities in both channels decreased. Moreover, the ratio between the diffusivities of toluene in the straight and sinusoidal channels (i.e., D_H/D_L) decreased from 10 to 6 after the modification. In addition, after silylation the ratio K_H/K_L , which is indicative for the amount of molecules involved in the diffusion process, decreased from 3 and 4.5 to 1 and 1.3 at 373 K and 403 K, respectively. Note that K is proportional to the gradient of the sorption isotherm (see

equation 6) and indicates the change in the number of molecules adsorbed (dQ) during the pressure step (dp) in the frequency response experiment. Therefore, the increase in the ratio K_H/K_L clearly points out that after the silylation a larger fraction of molecules diffused into the pores of the zeolite via the sinusoidal channels compared to the parent material.

In general, the modification of HZSM-5 by TEOS could either lead to a narrowing of the pore entrances or to a complete blocking of the pore openings. Note that the degree of pore blocking depends on the kinetic diameter of the molecules diffusing into the channels of the zeolite. For a given amount of TEOS deposited on HZSM-5 molecules with a small kinetic diameter (e.g. alkanes) might still enter into the zeolite pores through the modified pore openings, but the narrowed aperture leads to a lower diffusivity. However, for the same material the pores might be too narrow for molecules with a slightly larger kinetic diameter (e.g. Toluene) and, therefore, the blockage of the pore openings would be detected for this material. For the transport of toluene into the modified HZSM-5 zeolite a decrease in the diffusivities for the transport through the straight and sinusoidal channels and a lower amount of toluene molecules entering through the straight channels compared to the sinusoidal channels were observed. The lower diffusivities after the modification point to either a narrowing of the pores, or a partial blocking of the pores. The first situation can be straightforwardly explained by the dependence of the diffusion coefficient on the pore diameter⁵³, which reflects the hindered mobility of molecules diffusing inside the channels of a molecule sieve in the configurational regime. However, in the case of a partial blocking of the pores a lower diffusivity of toluene could be also observed. For the parent and modified zeolites identical sorption isotherms of toluene were observed (see Figure 1), which indicates that the toluene uptakes under equilibrium conditions were not affected by the modification. Note that we have previously shown that the modification resulted in a deposition of SiO_2 on the outer surface, while intra-pores were not affected. Consequently, in both materials the same number of molecules was transported between the gas phase and the sorption sites at the intersections during the pressure modulation in the frequency response experiments. If a fraction of pore entrances is blocked after the modification the average length of the diffusion path from the remaining accessible pore entrances to the sorption sites inside the zeolite particle becomes longer compared

to the unmodified zeolite. A schematic comparison of the diffusion pathways in the parent and modified zeolites is given in scheme 1.



Scheme 1: Influence of CLD modification on toluene diffusion in the zeolites

----- : slow diffusion process; ——— : fast diffusion process

Conceptually, the longer diffusion path can be understood as a virtual enlargement of the zeolite crystals, which results in a lower diffusivity. In addition, the increased tortuosity of the diffusion path inside the modified material will lead to a lower diffusivity compared to the parent material. Note that we observed a 10 times higher diffusion coefficient for toluene in the straight channels compared to the sinusoidal channels for the parent material. Based on the model of an apparent enlargement of the zeolite crystals the tortuosity of the diffusion pathway in the straight channels is enhanced and, therefore, the ration between the diffusivities in the straight and sinusoidal channels becomes smaller. Therefore, we would like to speculate that the modification led to a partial blocking of the pore entrances. In addition, this model also perfectly agrees with the enhanced *para*-selectivity of the modified HZSM-5 catalysts for the toluene disproportionation²⁶, as catalysts with a larger primary crystal size typically show enhanced shape selectivity and only minor effects on the activity. Furthermore, based on the decrease in D_H by 4 times after the modification we would

like to speculate that about 75% of the pore entrances were blocked after the modification. Note that this is in perfect agreement with the decrease in the concentration of SiOHAl groups located on the external surface and in pore mouth region by 73% resulted from the modification²⁸. As the silylation does not affect the toluene isotherm, an identical number of molecules have to enter through the pores and, therefore, the sum of K_H and K_L remains the same for both materials. However, the change in the ratio between K_H and K_L does not indicate a preferential blocking of the straight channels. Modification leads to a more marked decrease in the diffusivity for the fast transport process (i.e. thorough the straight channels) compared to slow diffusion process (i.e. thorough the sinusoidal channels), therefore, more toluene molecules diffuse through the sinusoidal channels of the silylated zeolite.

3.5. Conclusions

The diffusivities of toluene in HZSM-5 zeolites before and after silylation by chemical liquid deposition of *tetra*-ethoxysilane were studied using the frequency response method. Two diffusion processes were identified on both materials. The faster process was assigned to the transport of toluene in the straight channels, the slower process was assigned to the transport in the sinusoidal channels of the zeolite. The main reason for the differences in the diffusivity was related to the tortuosity of the diffusion pathways of the sinusoidal channels. The diffusivities in both channels were found to be a function of the toluene loading and related to the interaction of toluene with the acid sites of the zeolite. Silylation of the zeolite led to a decrease in toluene diffusivities in both the straight and sinusoidal channels of the zeolites. In addition the amount of toluene molecules accessing the sorption sites through the sinusoidal channels increased after the modification, while the total uptake remained unaffected by the modification. The decrease in the amount of toluene diffusion in the straight channels of the silylated zeolite resulted from a partial blocking of about 75 % of the pore openings after the silylation.

Acknowledgments

The financial support of the Bayerische Forschungsverbund Katalyse (FORKAT II) and Süd-chemie AG are gratefully acknowledged.

References

1. Weitkamp, J. *Solid State Ionics* **2000**, *131*, 175.
2. Kaeding, W. W.; Barile, G. C.; Wu, M. M. *Catal. Rev.-Sci. Eng.* **1984**, *26*, 597.
3. Olson, D. H.; Haag, W. O. *ACS Symp. Ser.* **1984**, *248*, 275.
4. Kärger, J.; Ruthven, D. M. *Zeolites* **1989**, *9*, 267.
5. Karger, J.; Ruthven, D. M. *Diffusion in Zeolites and Other Microporous Solids*, Wiley, New York, **1992**.
6. Cohen, L. E.; Kahn, R.; Mezei, F. *J. Chem. Soc., Faraday Trans. 1* **1983**, *79*, 1911.
Jobic, H.; Bée, M.; Pouget, S. *J. Phys. Chem. B* **2000**, *104*, 7130.
7. Jobic, H.; Bee, M.; Caro, J.; Bülow, M.; Kärger, J.; Pfeifer, H. *Stud. Surf. Sci. Catal.* **1991**, *65*, 445.
8. Förste, C.; Kärger, J.; Pfeifer, H.; Riekert, L.; Bülow, M. *J. Chem. Soc., Faraday Trans. 1* **1990**, *86*, 881.
9. Brandani, S.; Jama, M.; Ruthven, D. M. *Micropor. Mesopor. Mater.* **2000**, *35*, 283.
10. Ruthven, D. M.; Brandani, S. *Membr. Sci.* **2000**, *6*, 187.
11. Kärge, H. G.; Nießen, W. *Catalysis Today* **1991**, *8*, 451.
12. Mirth, G.; Lercher, J. A. *J. Catal.* **1993**, *139*, 24.
13. Schumacher, R.; Karge, H. G. *J. Phys. Chem.* **1999**, *103*, 1477.
14. Zikanova, A.; Bulow, M.; Schlodder, H. *Zeolites* **1987**, *7*, 115.
15. Yasuda, Y. *Heter. Chem. Rev.* **1994**, *1*, 103.
16. Rees, L. V. C. *Stud. Surf. Sci. Catal.* **1994**, *84*, 1133.
17. Sastre, G.; Raj, N.; Catlow, C. R. A.; Roque-Malherbe, R.; Corma, A. *J. Phys. Chem. B* **1998**, *102*, 3198.
18. Smit, B.; Daniel, L.; Loyens, J. C.; Verbist, G. L. M. *Faraday Discuss.* **1997**, *106*, 93.
19. Ash, R.; Barrer, R. M. *Surf. Sci.* **1967**, *8*, 461.

20. Wang, I.; Ay, C. L.; Lee, B. J.; Chen, M. H. *Appl. Catal.* **1989**, *54*, 257.
21. Csicsery, S. M. *Zeolites* **1984**, *4*, 202.
22. Niwa, M.; Katada, N.; Murakami, T. *J. Phys. Chem.* **1990**, *94*, 6441.
23. Hibino, T.; Niwa, M.; Murakami, Y. *J. Catal.* **1991**, *128*, 551.
24. Gründling, C.; Eder-Mirth, G.; Lercher, J. A. *J. Catal.* **1996**, *160*, 299.
25. Yue, Y. H.; Tang, Y.; Liu, Y.; Gao, Z. *Ind. Eng. Chem. Res.* **1996**, *35*, 430.
26. Zheng, S.; Heydenrych, H.; Röger, P.; Jentys, A.; Lercher, J. A. *Stud. Surf. Sci. Catal.* **2001**, *135*, 214.
27. Kärge, H. G.; Niessen, W.; Bludau, H. *Appl. Catal. A: General* **1996**, *146*, 339.
28. Zheng, S.; Heydenrych, H. R.; Jentys, A.; Lercher, J. A. *J. Phys. Chem. B* **2002**, *106*, 9552.
29. Song, L. J.; Sun, Z. L.; Rees, L. V. C. *Micropor. Mesopor. Mater.* **2002**, *55*, 31.
30. Onyestak, G.; Shen, D.; Rees, L. V. C. *Micropor. Mater.* **1996**, *5*, 279.
31. Goodyear, C. C. *Singles and information*, Butterworth, London, **1971**.
32. Yasuda, Y. *J. Phys. Chem.* **1982**, *86*, 1913.
33. Rees, L. V. C.; Shen, D. *Stud. Surf. Sci. Catal.* **1994**, *87*, 563.
34. Narayanan, S.; Sultana, A.; Le, Q. T.; Auroux, A. *Appl. Catal. A: General* **1998**, *168*, 193.
35. Thamm, H. *J. Phys. Chem.* **1987**, *91*, 8.
36. Huang, Y.; Havenga, E. A. *Chem. Mater.* **2001**, *13*, 738.
37. Klemm, E.; Wang, J.; Emig, G. *Micropor. Mesopor. Mater.* **1998**, *26*, 11.
38. Nakazaki, Y.; Goto, N.; Inui, T. *J. Catal.* **1992**, *136*, 141.
39. Song, L.; Rees, L. V. C. *Micropor. Mesopor. Mater.* **2000**, *35-36*, 301.
40. Qureshi, W. R.; Wei, J. *J. Catal.* **1990**, *126*, 147.
41. Cavalcante, C. L.; Ruthven, D. M. *Ind. Eng. Chem. Res.* **1995**, *34*, 185.
42. Chon, H.; Park, D. H. *J. Catal.* **1988**, *114*, 1.
43. Xiao, J.; Wei, J. *Chem. Eng. Sci.* **1992**, *47*, 1143.
44. Choudhary, V. R.; Srinivasan, K. R. *J. Catal.* **1986**, *102*, 316; **1986**, *102*, 329.
45. Tsikoyiannis, J. G., 1986, Ph.D. thesis, Department of Chemical Engineering, MIT, Cambridge, MA.

46. Kärger, J.; Pfeifer, H. *Zeolites*, **1987**, 7, 90.
47. Kärger, J.; Ruthven, D. M. *Stud. Surf. Sci. Catal.* **1997**, 105, 1843.
48. Xiao, J.; Wei, J. *Chem. Eng. Sci.* **1992**, 47, 1123.
49. Shen, D.; Rees, L. V. C. *Zeolites* **1991**, 11, 666.
50. Koriabkina, A. O.; De Jong, A. M.; Schuring, D.; Van Grondelle, J.; Van Santen, R. A. *J. Phys. Chem. B* **2002**, 106, 9559.
51. Hufton, J. R.; Ruthven, D. M.; Danner, R. P. *Micropor. Mater.* **1995**, 5, 39.
52. Masuda, T.; Fujikata, Y.; Nishida, K.; Hashimoto, K. *Micropor. Mesopor. Mater.* **1998**, 23, 157.
53. Chen, N. Y. *Stud. Surf. Sci. Catal.* **1988**, 38, 153.

Chapter 4

On the enhanced selectivity of HZSM-5 modified by chemical liquid deposition

Abstract

The external surfaces and pore mouth regions of HZSM-5 samples with different crystal sizes were modified by chemical liquid deposition (CLD) with *tetra*-ethoxysilane (TEOS), which led to the passivation of unselective acid sites. The modification was found to be more effective for zeolite samples with larger crystals. The diffusivity of *o*-xylene was substantially lowered after silylation, while the pore volume hardly changed. Dealumination of the external surface of the zeolite crystals enhanced the silylation effects, which was related primarily to the removal of acid sites associated to extra framework alumina. For the modified catalysts, a significant increase in the selectivity to *p*-xylene in the disproportionation of toluene was achieved.

4.1. Introduction

As a shape-selective catalyst, HZSM-5 zeolite has attracted both academic and industrial interest^{1,2}. Processes catalyzed by HZSM-5 to selectively produce *para*-alkylbenzenes have been well documented, such as toluene disproportionation, in which the well-defined ten-membered channel (5.3Å × 5.6Å) renders HZSM-5 *p*-selective. Although the mechanisms of the generation of *p*-selectivity are still controversial, it is generally accepted that product shape selectivity (diffusion selectivity) or/and transition-state selectivity contributes to the shape selectivity of HZSM-5^{3,4}.

Product shape selectivity is based on the fact that the intra-crystalline diffusivity of the *p*-isomer is larger than those of the other isomers in the channels of HZSM-5 and *p*-selectivity can be achieved even though a less favorable isomer mixture exists in the pores. On the other hand, according to transition-state theory⁵, only the *p*-isomer is generated in the pores of HZSM-5 because of hindrances to these transition states that lead to the *o*- or *m*-isomers. These isomers can thus only be produced by isomerization of the primary *p*-isomer over non-selective acid sites of the zeolite. Therefore, the narrowing of the pore mouth and the deactivation of non-selective acid sites that were located on the external surface or in the pore mouth region could enhance the *p*-selectivity of HZSM-5.

Various modification techniques have been suggested or adopted to improve the shape selectivity of HZSM-5^{3,6,7,8,9}. Chemical vapor deposition (CVD) is one of the most effective ways to deactivate the non-selective acid sites and, at the same time, narrow the pore openings of HZSM-5. High selectivity has been observed after CVD modification^{10,11}.

CLD has been recently developed to modify HZSM-5 zeolite because of its adaptability to large scale in certain applications, and an enhancement in the shape selectivity of HZSM-5 has been also achieved after CLD modification^{12, 13}. In comparison with CVD, less attention, however, has been paid to CLD. Therefore, the mechanism and effects of CLD modification are still unclear.

In this chapter, *tetra*-ethoxysilane (TEOS) was used to modify the outer surface of zeolites with different crystal sizes. The effects of CLD modification on the structure of

the zeolite, the diffusivities of the products and the selectivity of toluene disproportionation catalyzed by the parent and modified zeolites were investigated.

4.2. Experimental

4.2.1. Materials

Two HZSM-5 zeolite samples with identical silica-alumina ratio of 45, and particle sizes of 0.5 μm and 3 μm , designated as HZS and HZL, respectively, were used as the parent materials.

4.2.2. Silylation

2 g of zeolite was suspended in 50 ml of hexane and heated to reflux under stirring. TEOS (0.3 ml) (equal to 4 wt% SiO_2) was added into the mixture and the silylation was carried out for 1 h under reflux. Hexane was removed by evaporation and the sample was calcined at 773 K in dry air for 4 h. The samples are referred to as HZS-4% and HZL-4%. The HZS-3 \times 4% sample was obtained by repeating the above-described procedure three times for HZS.

4.2.3. Pore volume measurements

The pore volume measurements of the parent and modified zeolites were carried out on a PMI automated BET-sorptometer at 77.3 K using nitrogen as the analysis gas.

4.2.4. Adsorption isotherm of toluene

The toluene sorption isotherm was measured in a modified SETARAM TG-DSC 111 instrument. Approximately 15mg of sample was pressed into wafers and cut into small platelets that were charged into a quartz crucible. The sample was activated by heating to 823 K at a rate of 10 K/min and holding at this temperature for 1 h under vacuum ($p < 10^{-6}$ mbar). After activation, toluene vapour was introduced into the system at 403 K in small doses and allowed to equilibrate with the zeolite until a further pressure decrease and mass increase was not observed. The mass uptake of the zeolite was recorded.

4.2.5. Dealumination of the external surface

10 g of HZS was mixed with 200 ml oxalic-acid solution (2 M) under stirring and the mixture was heated under reflux for 10 h. Subsequently, the sample was filtered and washed repeatedly with de-ionized water. After drying at 393 K for 2 h, the sample was calcined in dry air at 773 K for 4 h. The sample is designated as DeAl-HZS

4.2.6. Alumination of the external surface of silylated zeolite

Alumina deposition on HZL-4% was carried out using aluminum isopropoxide as the reaction reagent. 7 mg of aluminium isopropoxide was dissolved in 50 ml n-hexane and 1 g of HZL-4% was added. Then the slurry was heated under reflux for 24 h. The sample was recovered by filtration and washed three times with n-hexane. The zeolite was calcined at 773 K for 4 h in pure oxygen atmosphere to remove hydrocarbon residues. The sample is designated as Al-HZL-4%.

4.2.7. Infrared spectroscopy and diffusion measurement

IR spectra were measured in the transmission absorption mode using a Bruker IFS 88 FTIR spectrometer at a resolution of 4 cm⁻¹. Pyridine and di-*tert*-butyl-pyridine (DTBPy) adsorption was carried out in vacuum. The time-resolved *o*-xylene uptakes were measured in a flow system. Experimental details were described elsewhere^{14,15,16}. Prior to the measurement, the samples were activated at 823 K for 1h in vacuum. Adsorption of DTBPy or pyridine was carried out at a partial pressure of 2×10⁻² mbar at 373 K for 15 min. Weakly adsorbed probe molecules were removed by evacuating the sample at 423 K for 1 h before the collection of the IR spectra.

The diffusion of *o*-xylene was studied at 1 mbar partial pressure in helium carrier gas. IR spectra were collected at 373 K at time intervals of 15 s. The diffusion coefficients were calculated using the square root law^{14,15,16}:

$$Q_t/Q_\infty = 6/r_0(Dt/\pi)^{1/2}$$

where Q_t denotes the amount of sorbate adsorbed after the time t [s], Q_∞ is the amount adsorbed at equilibrium coverage, r_0 the radius of zeolite crystals and D the diffusion coefficient.

The IR spectra were normalized using the intensity of the structural vibrations at 1990 cm^{-1} and 1870 cm^{-1} and the relative amount of *o*-xylene adsorbed was determined from the intensity of the IR bands of *o*-xylene at 1497 cm^{-1} and 1468 cm^{-1} .

4.2.8. Toluene disproportionation

Toluene disproportionation was carried out in a fixed-bed reactor at 773 K. 0.06g of sample was activated at 773 K for 1 h in 20 ml/min of He stream prior to experiments. Toluene with a partial pressure of 22.5 mbar was injected into 20 ml/min of He stream using a syringe pump. An on-line GC equipped with a FID detector was used to analyze the composition of the products from the toluene disproportionation reaction.

4.3. Results and discussion

4.3.1. Pore volume

The pore volume, corrected for the mass of SiO_2 added during the CLD process, is shown in Table 1.

Table 1. Micro-pore volume of parent and modified zeolites

Sample	SiO_2 coating amount (%)	Micropore volume ml/g corrected
HZS	-	0.0703
HZS-4%	4%	0.0686
HZS-3×4%	12%	0.0667
HZL	-	0.0776
HZL-4%	4%	0.0779

Silylation of the zeolites by CLD did not result in a significant change in the micropore volumes of the silylated zeolites compared to the parent zeolite. This indicates that the silylation occurred only on the external surface of the zeolite crystals, without influencing the internal pores and the acid sites located in the pores of the zeolite.

4.3.2. Toluene isotherm

The change in the pore volume of HZSM-5 before and after silylation was also probed by the adsorption of toluene. Toluene isotherms over the parent and modified zeolites, corrected for the weight increase by the silylation, are shown in Figure 1.

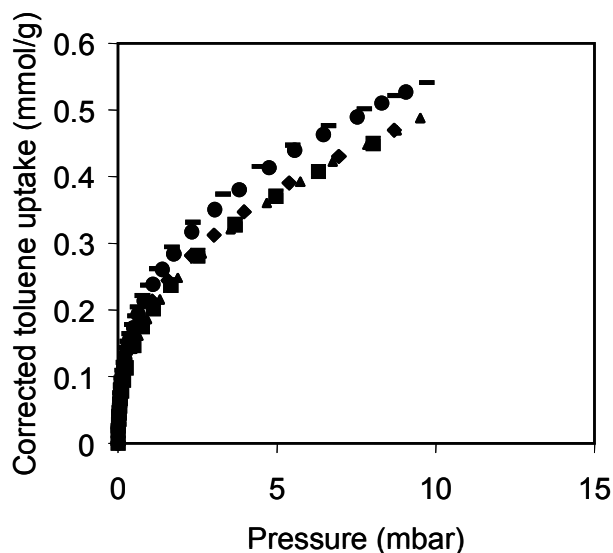


Figure 1. The isotherms of toluene over (◆)HZS;(■)HZS-4%; (▲)HZS-3×4%;(●)HZL and (—)HZL-4% at 403K

In agreement with the pore volume measurements, the uptake of toluene on HZL was slightly larger than on HZS. After silylation the corrected uptakes of toluene over the silylated zeolites did not showed an insignificant change.

4.3.3. Structural IR

The changes in the hydroxyl groups of HZS before and after modification (difference spectra) are compared in Figure 2. Two types of hydroxyl groups were observed. The band at 3745 cm^{-1} is characteristic of the silanol groups located on the external surface of HZSM-5; the band at 3606 cm^{-1} is characteristic of the bridging hydroxyl groups (Brønsted acid sites). The transmittance of the HZL sample in the hydroxide region was too low to allow quantitative comparison of IR bands in this region. Previous IR studies showed that the intensities of the hydroxyl groups were not affected by CVD modification, although the deactivation of external acid sites was

detected^{17,18}. In contrast, the present study clearly indicated changes in concentration of the hydroxyl groups after CLD modification.

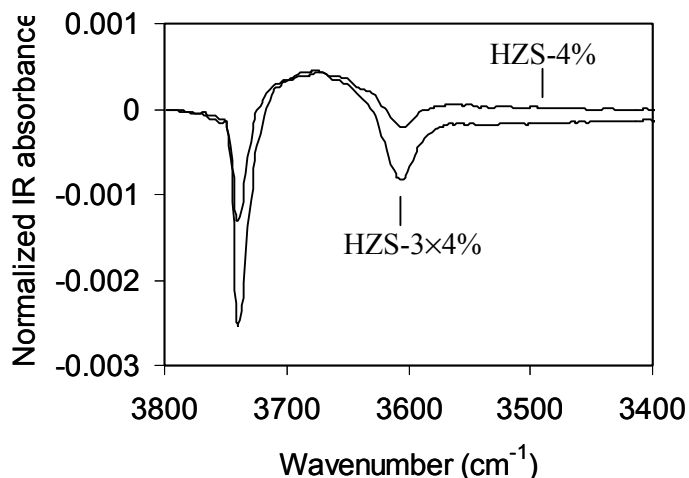


Figure 2. The difference spectra of HZS-4% and HZS-3x4% with HZS

Silylation led to a marked decrease in the concentration of both the silanol and bridging hydroxyl groups. For HZS-4%, the fractional removal of the silanol and bridging hydroxyl groups was 6% and 9% of the total concentration, respectively, while after the three-cycle silylation the fractional removal of the silanol and bridging hydroxyl groups increased to 18% and 21%, respectively.

The removal of hydroxyl groups resulted from the reaction between TEOS and the hydroxyl groups during the silylation. This also resulted in a decrease in the acid site concentration of the modified zeolites with different crystal sizes, as observed by NH₃-TPD and pyridine adsorption¹⁹. Pore volume and toluene uptake measurements indicated that the silylation occurred only on the outer surface of the zeolite. Therefore, this suggests that CLD modification only led to the deactivation of the hydroxyl groups located on the external surface and in the pore-mouth region of the zeolites.

4.3.4. DTBPy adsorption

Figure 3 shows the changes in the IR spectra after adsorption of DTBPy on HZS, HZS-4% and HZS-3×4%. The bands at 3745 cm^{-1} and 3606 cm^{-1} are characteristic of the silanol and bridging hydroxyl groups of the zeolites. The bands at 3367 cm^{-1} and 1616 cm^{-1} are assigned to the N-H vibration and to a ring vibration of the DTBPyH⁺ ion, respectively^{20,21}.

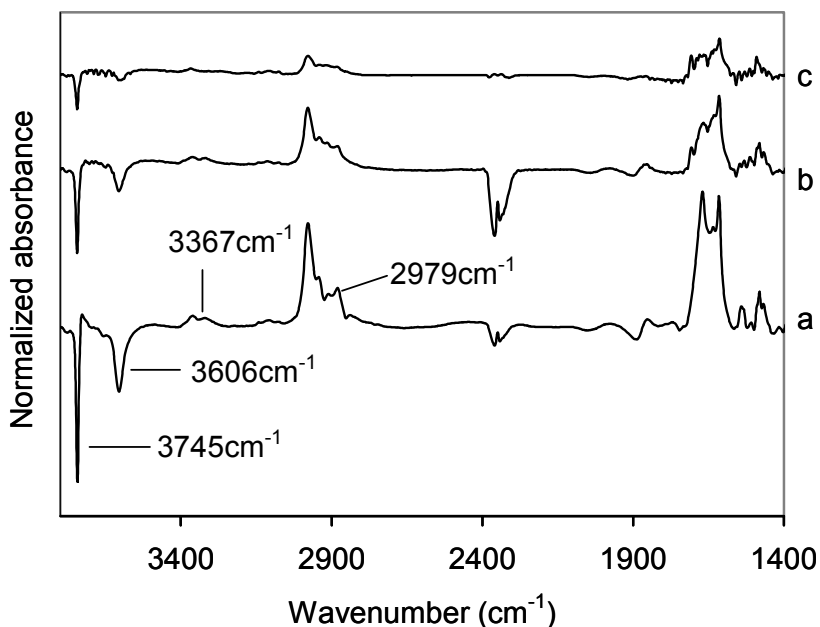


Figure 3. Differences in the IR spectra after DTBPy adsorption on (a) HZS, (b) HZS-4% and (c) HZS-3×4%.

After adsorption of DTBPy on HZS, the asymmetric stretching vibration of the $-\text{CH}_3$ groups in DTBPy was shifted to 2979 cm^{-1} , indicating a hydrogen bonding interaction between the $-\text{CH}_3$ groups and the hydroxyl groups of the zeolite²¹. The presence of two negative bands at 3606 cm^{-1} and 3745 cm^{-1} shows that the DTBPy molecules interacted with the silanol and with bridging hydroxyl groups of the zeolites.

As the minimum kinetic diameter of DTBPy (10.5 \AA) is larger than that of the pore openings of HZSM-5, DTBPy molecules cannot penetrate into the interior pores of HZSM-5 zeolite and are thus expected to interact only with the hydroxyl groups located on the external surface and in the pore mouth region of the zeolite. The amounts of the hydroxyl groups interacting with DTBPy are compiled in Table 2. With HZS, 28 % of the bridging hydroxyl groups were accessible for DTBPy, while with HZL only 7 % of

the bridging hydroxyl groups interacted with DTBPy. This indicates that a higher amount of the acid sites exists on the external surface and in pore mouth region of HZS compared to HZL; this result is attributed to the small crystal size of HZS. After silylation, the amounts of the silanol and bridging hydroxyl groups accessible for DTBPy were significantly lowered for both zeolites. We attribute it to the reaction of the silylation agent with the hydroxyl groups located on the external surface and in the pore mouth region of the zeolite. Single-cycle silylation of HZS led to a decrease of 53% in the concentration of Brønsted acid sites in the outer region of the zeolite. Three-cycle silylation of HZS and single-cycle silylation of HZL led to a similar degree of removal of the bridging hydroxyl groups, i.e., 76% and 73 %, respectively, indicating that the modification by CLD was more effective for the HZSM-5 sample with larger crystal size.

Table 2. Concentration of externally accessible Brønsted acid sites determined by adsorption of DTBPy.

Sample	Fraction of externally accessible bridging hydroxyl groups (%)	Removal of acid sites (%)
HZS	28	
HZS-4%	13	53
HZS-3×4%	6.7	76
HZL	7.0	
HZL-4%	1.9	73

4.3.5. Diffusivities of aromatic molecules

The uptakes and the diffusion coefficients for *o*-xylene in the parent and modified samples are compared in Figure 4 and Table 3, respectively.

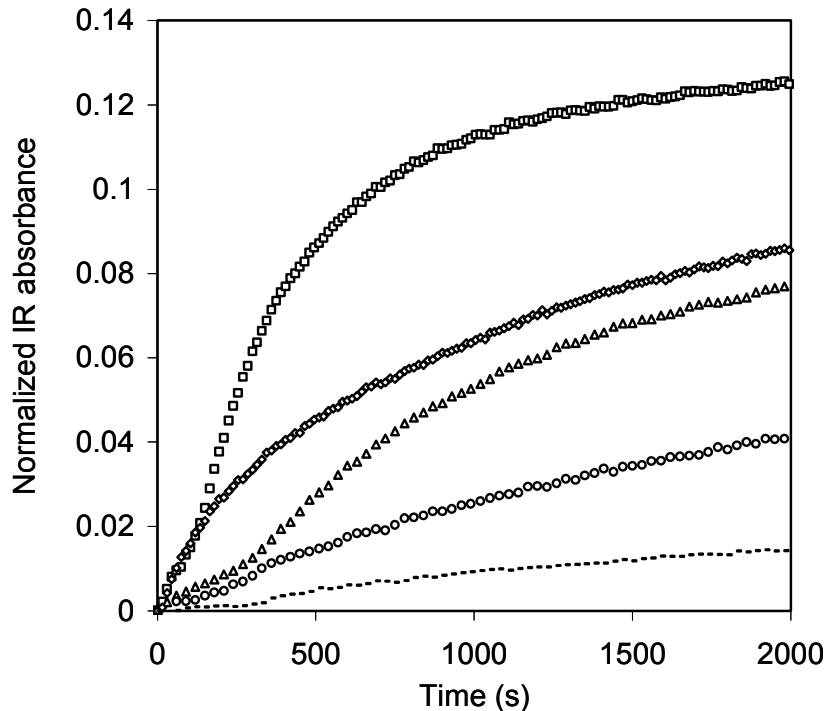


Figure 4. *o*-Xylene uptake of () HZS, (Δ) HZS-4%, (o) HZS-3 \times 4%, (\diamond) HZL and (-) HZL-4%

Table 3. Diffusivities of *o*-xylene in parent and modified zeolites at 373 K and 10^{-2} mbar.

Sample	Diffusion coefficient ($\times 10^{-17}$ m ² /s)
HZS	0.6
HZS-4%	0.2
HZS-3 \times 4%	0.07
DeAl-HZS	0.9
DeAl-HZS-3 \times 4%	0.04
HZL	5.15
HZL-4%	0.1

The diffusivities of *o*-xylene were found to depend on the crystal size of the zeolite and on the modification procedure. Note that the effect of the crystal size on the

diffusivity is typically explained using the concept of “surface barrier”^{22, 23}. Silylation led to a decrease of the diffusivity of *o*-xylene and this effect was enhanced for HZS by multiple cycles of silylation.

A decrease in the diffusion coefficients for *o*-xylene in the silylated zeolites was found to result from the narrowing or blocking of the zeolite pore openings, which indicates that CLD is an effective method to modify zeolites. In agreement with the characterization of the surface properties, these results indicate that, at the same silylation level, a more effective pore mouth narrowing/blocking was achieved for HZL than for HZS.

4.3.6. Toluene disproportionation

Table 4. Activity and selectivity of parent and modified zeolites for toluene disproportionation.

Catalyst	Conversion (%)	Composition of xylenes (%)		
		<i>Para</i>	<i>Meta</i>	<i>ortho</i>
HZS	1.24	22.5	54.4	23.2
HZS-4%	1.15	25.8	53.6	20.6
HZS-3×4%	1.04	42.3	44.3	12.3
DeAl-HZS	1.50	22.0	55.0	23.0
DeAl-HZS-4%	1.32	26.8	53.0	20.2
DeAl-HZS-3×4%	1.10	52.6	37.4	14.0
HZL	0.86	28.6	53.4	18.0
HZL-4%	0.83	71.0	24.7	4.3
Al-HZL-4%	1.13	61.3	31.5	7.2

Note. Temperature = 773 K. WHSV: 1.44 h⁻¹.

The activity and selectivity of the zeolites for toluene disproportionation are compared in Table 4. For HZL a higher *p*-selectivity and a lower reaction rate was observed compared to the values for HZS. This points to a lower concentration of unselective acid sites in HZL compared to that in HZS and to the existence of intra-particle diffusion limitations. After silylation, the activity decreased and the selectivity

to *p*-xylene increased for both samples, which indicates the passivation of unselective acid sites located on the external surface and in the pore mouth region of the zeolite and a further enhancement of the intra particle diffusion constraints.

In general, the increase in *p*-selectivity can result from the narrowing or blocking of the pore openings, which could enlarge the differences between *p*-xylene and *o*-xylene diffusivities, and/or from the passivation of unselective acid sites, typically located in the pore mouth region. Note that silylation of HZL with 4% of TEOS led to the most pronounced enhancement in the *p*-selectivity within the series of catalysts studied, while HZS showed only a slight increase in the *p*-selectivity at the same level of silylation. Even after three-cycle silylation, the *p*-selectivity of HZS-3×4% was lower than that of HZL-4%. The observation agrees well with the variations of the *o*-xylene diffusion, for which the same level of inhibition of *o*-xylene over HZS was not achieved even after three silylation cycles.

4.3.7. Influence of pre-dealumination on the modification effects

In order to explore whether or not differences in the surface chemical composition could account for the differences in modification observed for the samples with the large and small crystal sizes, the external surface of HZS was dealuminated prior to the silylation. It was observed that a markedly higher concentration of extra-framework aluminium oxides is present in HZS compared to that in HZL. The presence of extra-framework aluminium oxides could hinder the access of the silylation agent to the pore mouth and, hence, dealumination of the external surface could facilitate the silylation of the zeolite with small crystal size.

In principle, oxalic acid only dealuminates the external surface of HZSM-5 because its diameter is larger than the pore openings of HZSM-5 zeolite. The IR spectra after adsorption of pyridine on HZS and on DeAl-HZS are compared in Figure 5. The IR bands observed at 1546 cm^{-1} and 1454 cm^{-1} indicate the presence of Brønsted and Lewis acid sites on both samples²⁴. De-alumination of HZS led to a decrease in the concentration of Brønsted acid sites by 10% and in that of Lewis acid sites by 50%.

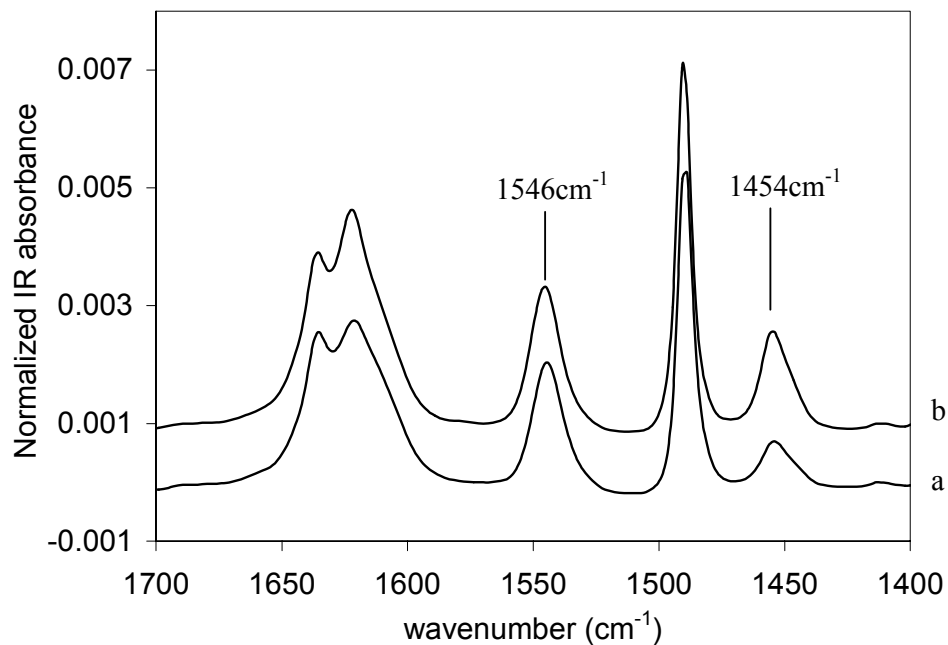


Figure 5: Differences in the IR spectra after pyridine adsorption on (a) HMF190-0.1 and (b) DeAl-HMF190-0.1.

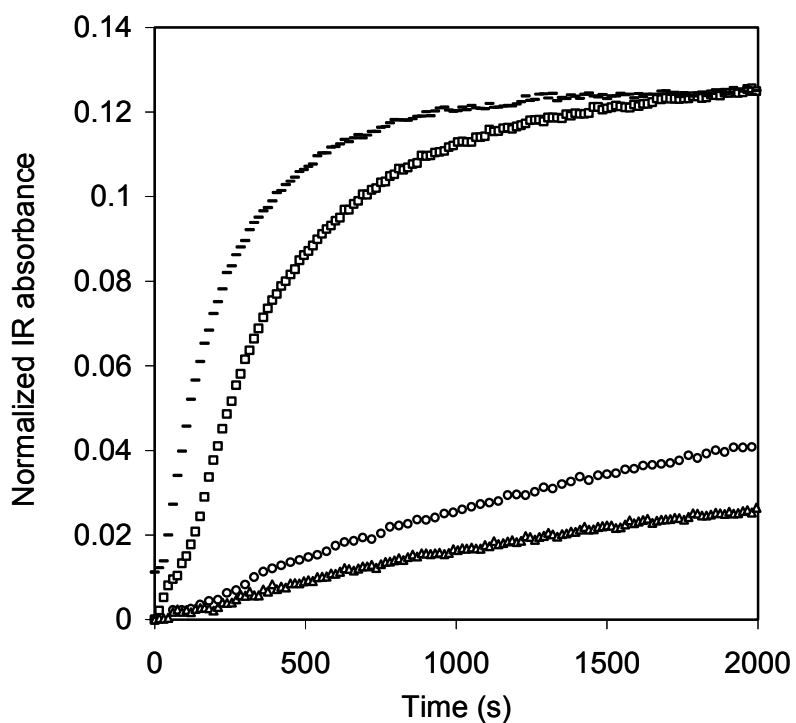


Figure 6. *o*-Xylene uptake of (■) HZS, (○) HZS-3×4%; (●) DeAl-HZS and (△) DeAl-HZS-3×4%.

DTBPy adsorption indicated that approximately 28% of the Brønsted acid sites are located in the pore mouth region of HZS. From this we conclude that the dealumination did not completely remove all unselective acid sites. The diffusion coefficient for *o*-xylene (see Figure 6 and Table 3), however, slightly increased after dealumination, which implies that the extra-framework aluminum oxide somewhat narrowed the pore openings of HZS. Note that the presence of extra-framework aluminum oxide might lead to a part of the unselective acid sites inaccessible for the silylation agent. The lower diffusion coefficient of *o*-xylene and the improved *p*-selectivity for DeAl-HZS-3×4% (52.6%) compared to that for HZS-3×4% (42.3 %) indicated that, under the same silylation conditions, pre-treatment of the zeolite by dealumination enhanced the silylation effects.

4.3.8. Influence of unselective acid sites

The reasons for the enhanced *p*-selectivity of zeolites are shown above to be related to diffusion constraints processes and/or the passivation of unselective acid sites. While the enhancement of the *p*-selectivity by controlling their diffusion processes (at the pore openings) has been generally accepted²⁵, specific information on the role of acid sites at the outside of the particles is scarce. Among other factors, this lack of information is related to the fact that the modification of the external surface of a zeolite simultaneously affects the width of pore openings and the concentration of acid sites located on the external surface and in the pore mouth region of the zeolite. Therefore, we generated unselective acid sites on the surface of HZL-4% by alumina deposition with aluminum isopropoxide²⁶. As aluminum isopropoxide is too large to penetrate into the pores of HZL-4%, sites generated are assumed to be confined to the external surface of the modified zeolite.

Indeed, the *p*-selectivity of Al-HZL-4% for toluene disproportionation was lowered to 61.3 %, compared to 71.0 % of HZL-4% (see Table 4), which is in line with expectations that easily accessible aluminum has a negative influence on secondary isomerization of xylenes. As alumina deposition on the external surface of the zeolite should lead to a further narrowing of the pore openings of the zeolite (improvement of shape selectivity), the observed lower *p*-selectivity is only attributed to the generation of unselective acid sites on the external surface of HZL-4%.

4.4. Conclusions

CLD of zeolite by TEOS proved to be an effective way to enhance the *p*-selectivity for toluene disproportionation. After single-cycle silylation and three-cycle silylation, 9% and 21%, respectively, of the bridging hydroxyl groups of the zeolite with small crystals were passivated by TEOS. Additionally, CLD led to a narrowing of the pore openings of the zeolite and, thus, to a restricted *o*-xylene diffusion into the pores of HZSM-5. More effective modification of HZL was achieved compared to HZS at the same silylation level. Therefore, multi-cycle silylation was necessary to further narrow the pore mouth and, simultaneously, to deactivate the unselective acid sites of the small crystals to enhance *p*-selectivity. For the zeolite with small crystal size, dealumination of the external surface led to a slight enlargement of the pore opening; this allowed a further narrowing of the pore opening of zeolite by silylation. Thus, an enhanced *p*-selectivity for toluene disproportionation was achieved. Unselective acid sites located on the external surface and in the pore mouth regions of the zeolites lower the *p*-selectivity during toluene disproportionation.

References

1. Kaeding, W. W.; Barile, G. C.; Wu, M. M. *Catal. Rev.-Sci. Eng.* **26**, 597 (1984).
2. Chen, N. Y.; Garwood, W. E.; Dwyer F. G. *Shape Selective Catalysis in Industrial Application*, 2nd ed., revised and expanded Marcel Dekker, New York, 1996.
3. Kaeding, W. W. *J. Catal.* **95**, 512 (1985)
4. Paparatto, G.; Moretti, E.; Leofanti, G.; Gatti, F. *J. Catal.* **105**, 227 (1987)
5. Csicsery, S. M. *zeolites* **4**, 203 (1984).
6. Kürschner, U.; Jerschke, H. G.; Schreier E.; Völter, J. *Appl. Catal.*, **57**, 167 (1990).
7. Niwa, M.; Kalo, M.; Tattori, T.; Mewakami, Y. *J. Phys. Chem.* **90**, 6233 (1986).
8. Fang, L.; Liu, S.; Wang, I. *J. Catal.* **185**, 33 (1999).

9. Kim, J.; Namba, S.; Yashima, T. *Zeolites* **11**, 59 (1991).
10. Kim, J.; Ishida, A.; Okajima, M.; Niwa, M. *J. Catal.* **161**, 387 (1996).
11. Röger, P.; Krämer, M.; Möller, K. P.; O'Connor, C. *Micropor. Mesopor. Mater.* **21**, 607 (1998).
12. Yue, Y.; Tang, Y.; Liu Y.; Gao, Z. *Ind. Eng. Chem. Res.* **35**, 430 (1996).
13. Webber, R.; Möller, K.; Unger M.; O'Connor, C. *Micropor. Mesopor. Mater.* **23** 179 (1998).
14. Mirth, G.; Lercher, J. A. *J. Catal.*, **95**, 3736 (1991).
15. Mirth, G.; Cejka, J.; Lercher, J. A. *J. Catal.* **139**, 24 (1993).
16. Mirth, G.; Lercher, J. A. *J. Catal.* **147**, 199 (1994).
17. Tynijälä P.; Pakkanen, T. T. *J. Mol. Catal., A: Chem.* **122**, 159 (1997).
18. Niwa, M.; Kato, S.; Hattori, T.; Murakami, Y. *J. Chem. Soc. Faraday Trans. I*, **80** 3135 (1984).
19. Zheng, S.; Heydenrych, H. R.; Jentys, A.; Lercher, J. A. *J. Phys. Chem. B* **106**, 9552 (2002).
20. Coma, A.; Fornes, V.; Forni, L.; Marquez, F.; Martinez-Triguero, J.; Moscotti, D. *J. Catal.* **179**, 451 (1998).
21. Knözinger, H.; Krietenbrink, H.; Ratnasamy, P. *J. Catal.* **48**, 436 (1977)
22. Bülow, M. *Z. Z. Chem.* **25**, 81 (1985).
23. Kärger, J.; Bülow, M.; Millward, G. R.; Thomas, J. M. *Zeolites*, **6**, 146 (1986).
24. Emeis, C. A. *J. Catal.* **141**, 347 (1993).
25. Kim, J.; Kunieda, T; Niwa, M. *J. Catal.* **173**, 433 (1998).
26. Mokaya, R. *Angew. Chem. Int. Ed.* **38**, 2930 (1999).

Chapter 5

On the enhanced *para*-selectivity of HZSM-5 modified by antimony oxide

Abstract

The dispersion of antimony oxide on HZSM-5 zeolites was carried out by solid state reaction at 773 K. Crystalline phases of antimony oxide were not detected at Sb_2O_3 loadings up to 10.2 wt%. Antimony oxide was found to strongly interact with the hydroxyl groups of the zeolite, i.e. silanol and bridging hydroxyl groups, and with extra-framework aluminium oxide. Only a small amount of Sb_2O_3 penetrated into the pores of the zeolite, while the main fraction of Sb_2O_3 was deposited on the external surface of the zeolite crystals. With increasing antimony oxide loading a pronounced pore narrowing of the zeolite was observed, which suppressed the further penetration of antimony oxide into the pores of the zeolite. The dispersion of antimony oxide on the surface of the zeolite led to a complete removal of unselective Brønsted acid sites and to a narrowing of the pore mouth openings of the zeolite. Both effects led to an enhanced *para*-selectivity and to a lower activity of antimony oxide modified HZSM-5 zeolites for toluene disproportionation.

5.1. Introduction

Due to their unique structure HZSM-5 zeolites show an enhanced *para*-selectivity in the toluene disproportionation, methylation of toluene and xylene isomerization^{1,2}. A further enhancement of the shape selectivity can be achieved by post synthetic modification, which leads to a removal of unselective acid sites located in the pore mouth regions and/or to a narrowing of the pore openings, which enlarges the differences in the diffusivities between the undesired *o*- or *m*-isomers and the *p*-isomers^{3,4,5,6}.

The aim of the post synthetic modification is to deposit metal and non-metal oxides on the external surface of zeolite crystals. Niwa *et al.*^{7,8} systematically studied the modification of zeolites by chemical vapor deposition (CVD) and found that amorphous SiO₂ layers were only formed on the external surface of the zeolite if bulky molecules, such as Si(OCH₃)₄ or Si(OC₂H₅)₄, were used as silylation agents. Tynjala *et al.*⁹ found that the deposition of SiO₂ and Ge₂O₃ by CVD on the surface of zeolites effectively enhanced the selectivity to small olefins and linear aliphatic products in the conversion of methanol to hydrocarbons. Kaeding *et al.*^{10, 11} observed an enhanced *para*-selectivity for the alkylation of toluene with methanol on phosphorus modified HZSM-5 zeolites and suggested that the phosphorus reagent interacted with the acid sites of the zeolite and attached to the zeolite via framework oxygen atoms, which partially blocked the pore openings and, therefore, restricted the diffusion of *m*- and *o*-xylenes. Kaeding *et al.*^{12,13} further studied the modification of HZSM-5 with Ca, Mg, B and Mn oxides and achieved an enhanced *para*-selectivity in toluene methylation and toluene disproportionation.

The deposition of oxides onto the surface of zeolites can be carried out by impregnation¹⁴, ion exchange¹⁵, chemical deposition^{7,8, 16, 17} and solid state reactions^{18,19}. Karge *et al.*¹⁸ used solid state reactions to achieve a markedly higher exchange degree of La ions in zeolite Y compared to ion exchange in liquid phase. The ion exchange of Ni and Co into HZSM-5 and zeolite Y was studied by Jentys *et al.*^{20,21}, who also achieved a significantly higher exchange degree by a solid state reaction compared to ion exchange in liquid phase due to the absence of a hydration

of the cations in the solid reaction. MoO₃ modified HZSM-5 zeolite obtained by solid state reaction showed a similar benzene selectivity for the conversion of methane to aromatics compared to that prepared by impregnation method^{22, 23}. Xiao *et al.*²⁴ observed an enhanced conversion over CuCl₂/HZSM-5 catalysts prepared by solid state reaction for the selective reduction of NO by propylene compared to CuZSM-5 obtained using ion-exchange in aqueous phase. The modification of HZSM-5 with antimony oxide by solid state reaction was studied by Lee *et al.*²⁵, who reported an enhanced *para*-selectivity of antimony oxide modified HZSM-5 zeolites for toluene methylation by methanol. Systematical and quantitative studies on the dispersion of oxides and salts on the surface of different supports were comprehensively reviewed by Xie *et al.*¹⁹.

In this chapter we described the interaction between antimony oxide and HZSM-5, the location of antimony oxide and the modification effects using IR spectroscopy, Raman spectroscopy, XRD and sorption of probe molecules and related the structural properties of the modified materials to their activity and shape-selectivity in the toluene disproportionation reaction.

5.2. Experimental

5.2.1. Materials

HZSM-5 zeolite with Si/Al ratio of 45 and particle size of 0.5 μm, determined by SEM, was used as the parent material. A series of antimony oxide modified samples were prepared by heating a physical mixture of antimony oxide and the zeolite under N₂ atmosphere to 773 K at a rate of 10 K/min followed by calcination at this temperature for 2 h. The content of antimony oxide in the modified zeolites after calcination was determined by chemical analysis (AAS). The pore volumes of the parent and modified zeolites were measured by N₂ adsorption with a Micrometrics ASAP 2000 apparatus at 77.3 K. The XRD patterns of the parent and antimony oxide modified zeolites were collected in a Philips XRD powder diffraction-meter using Cu Kα radiation and a 2θ scan rate of 10 degree/min.

5.2.2. ^{27}Al MAS NMR

^{27}Al MAS NMR spectra of the parent and modified zeolites were recorded on a Bruker AVANCE MSL-300 NMR spectrometer at a field strength of 7.5 T and 15 kHz spinning speed using 4 mm ZrO_2 -rotors. Spectra were collected at a frequency of 78.205 MHz with 1.0 μs excitation pulses and 0.1 s recycle times. The ^{27}Al chemical shifts were referenced to 1 molar aqueous solution of $\text{Al}(\text{NO}_3)_3$.

5.2.3. *In-situ* Raman and IR spectroscopy

For *in-situ* Raman measurements, the physical mixture of antimony oxide (20 wt%) and the zeolite was pressed into a self-supporting wafer and placed in a sample holder consisting of a gold plate attached to a heating wire. The sample holder was mounted in the center of a Raman cell connected to a flow system. The sample was heated to 873K (rate of 5 K/min) under a N_2 flow of 20 ml/min. Raman spectra were collected every 2 min with a Renishaw Raman spectrometer (Type 1000) equipped with a CCD detector using a 785 nm diode laser for excitation.

The dispersion of antimony oxide over the zeolite as a function of the calcination temperature was followed using IR spectroscopy. A self-supporting wafer of the physical mixture of antimony oxide (5 wt%) with the zeolite was placed in a gold sample holder in the center of a furnace, which was connected to a vacuum system. The sample was heated in vacuum ($<10^{-6}$ mbar) to 823 K (rate of 5 K/min) and IR spectra were collected in a time interval of 1 min with 4 cm^{-1} resolution using a Bruker IFS 88 FTIR spectrometer.

5.2.4. Pyridine and *tert*-butyl-pyridine (DTBPy) adsorption

A self-supporting wafer of the sample was placed in a gold sample holder in the center of a furnace, which was connected to a vacuum system. During activation the sample was heated in vacuum ($<10^{-6}$ mbar) to 773 K with a rate of 10 K/min and kept at this temperature for 1 h. The adsorption of pyridine or DTBPy was carried out at a partial pressure of 2×10^{-2} mbar using an equilibration time of 15 min. After removing physically adsorbed molecules by degassing at 423 K for 1 h, IR spectra were

collected at 423 K with 4 cm^{-1} resolution using a Bruker IFS 88 FTIR spectrometer. In order to allow quantitative comparisons of the intensities of IR bands, all IR spectra were normalized using the area of the overtone lattice vibration bands of the zeolites at 1990 cm^{-1} and 1870 cm^{-1} .

5.2.5. Diffusion measurements

The diffusivities of *o*-xylene in the parent and antimony oxide modified zeolites were determined using IR spectroscopy in a flow system, which was described previously^{26, 27}.

The zeolite was pressed into a self-supported wafer and placed inside a gold sample holder and mounted in the center of an *in-situ* cell connected to a flow system. The sample was activated in helium flow by heating to 773 K with a rate of 10 K/min and holding at this temperature for 1 h. After the sample temperature was stabilized at 373 K, *o*-xylene with a partial pressure of 1 mbar was injected into carrier gas using a syringe pump. IR spectra were collected in a time interval of 30 sec. The diffusion coefficients were calculated using the square root law^{28,29}:

$$Q_t/Q_\infty = 6/r_0(D.t/\pi)^{1/2}$$

where Q_t denotes the amount adsorbed at time t [s], Q_∞ is the amount adsorbed at equilibrium coverage, r_0 the radius of zeolite crystal and D the diffusion coefficient.

The area of the IR bands at 1497 and 1468 cm^{-1} was used to quantify the relative amount of *o*-xylene adsorbed in the zeolites. To compare different samples the spectra were normalized to the intensity of the overtone vibration of HZSM-5 at 1990 cm^{-1} and 1870 cm^{-1} .

5.2.6. Toluene disproportionation

Toluene disproportionation was carried out in a fixed-bed reactor at 773 K. Prior to the experiments 0.06 g of sample was activated at 773 K for 1 h in a He stream of 20 ml/min. Toluene was injected into the He stream using a syringe pump. The partial pressure of toluene in the He stream of 20 ml/min was 22.5 mbar. The composition of the products from the toluene disproportionation reaction was analyzed with an on-line GC equipped with a FID detector.

5.3. Results

The content of antimony oxide before and after calcination at 773 K and the pore volumes of the parent and modified zeolites are listed in Table 1.

Table 1. Antimony oxide content and pore volume of the samples

Code	Sb ₂ O ₃ content before calcination (wt%)	Sb ₂ O ₃ content after calcination (wt%)	Pore volume (cm ³ /g)	Corrected pore volume (cm ³ /g)*
HZ	-	-	0.088	0.088
SbZ1	5	3.3	0.078	0.081
SbZ2	10	6.5	0.07	0.075
SbZ3	15	7.7	0.07	0.076
SbZ4	20	10.2	0.069	0.077

* Corrected based on the content of antimony oxide after calcination.

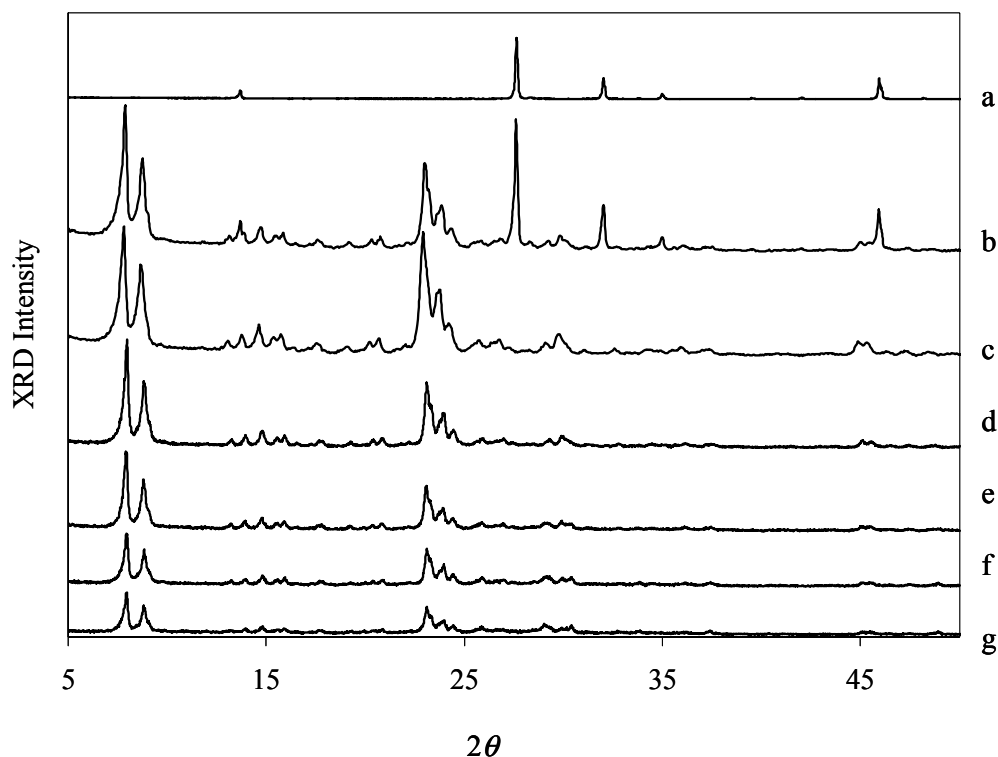


Figure 1. XRD patterns of (a) antimony oxide, (b) physical mixture of antimony oxide and zeolite, (c) HZ, (d) SbZ1, (e) SbZ2, (f) SbZ3 and (g) SbZ4

Chemical analysis of the modified zeolites showed that the content of antimony oxide substantially decreased for all modified samples after calcination at 773 K, which suggests that a marked amount of antimony oxide was lost during the

calcination process. In addition, modification of the zeolite with 3.3 wt% of antimony oxide led to a decrease of the pore volume by 10.2 wt%, which can be tentatively assigned to the pore filling of the zeolite with Sb_2O_3 or a partial collapse of the zeolite structure. Further increase in the Sb_2O_3 loading did not lead to a decrease in the pore volumes of the zeolites.

The XRD patterns of the parent and antimony oxide modified zeolites are compared in Figure 1. In the XRD pattern of the parent zeolite only diffraction peaks typical for HZSM-5 were present. In the physical mixture of 5 wt% antimony oxide and HZSM-5 the diffraction peaks of antimony oxide were clearly observed, while after calcination of the mixture at 773 K diffraction peaks assigned to antimony oxide disappeared. Note that crystalline phases of antimony oxide were not detected in any of the modified zeolites after calcination.

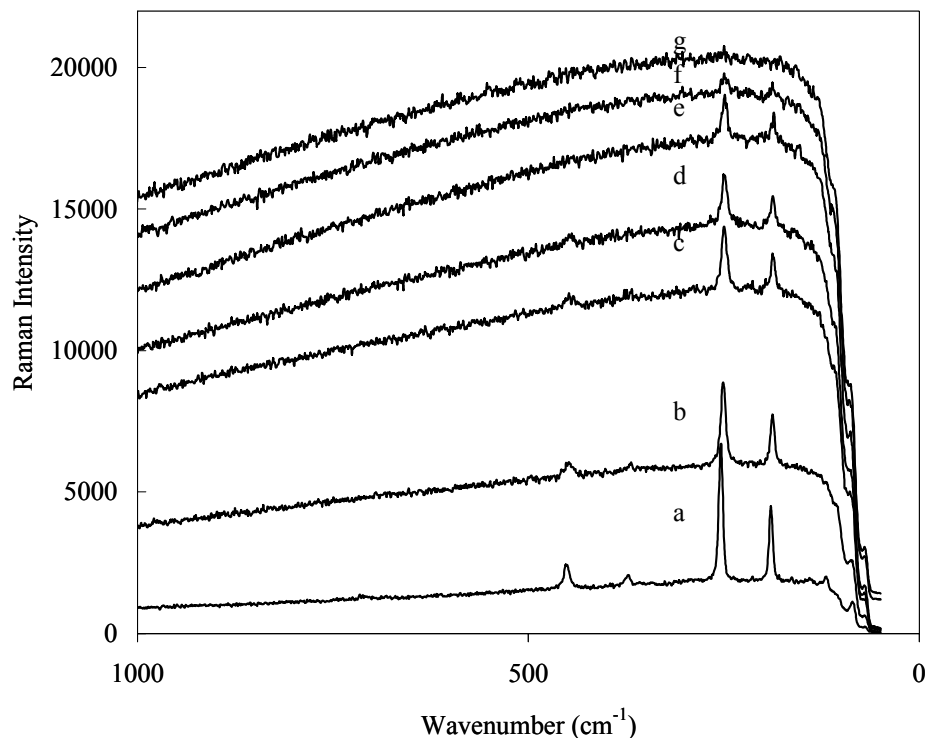


Figure 2. Raman spectra of the physical mixture of antimony oxide with zeolite calcined at (a) 323 K, (b) 473 K, (c) 573 K, (d) 623 K, (e) 683 K, (f) 703 K and (g) 723 K

In situ Raman spectroscopy was used to study the changes in the crystalline phases of antimony oxide during the solid state reaction of Sb_2O_3 with the zeolite. The Raman spectra of the physical mixture of the parent zeolite and antimony oxide (20 wt%) calcined at different temperatures are shown in Figure 2. At ambient temperature, bands assigned to antimony oxide were clearly observed at 450, 373, 253 and 189 cm^{-1} . In addition a broad band at low wave-number resulting from fluorescence effects was observed. With increasing calcination temperature, the intensity of the broad band increased, which resulted from the enhanced fluorescence effects of the dehydrated zeolite due to the formation of surface hydroxyl groups³⁰. The intensity of Raman bands assigned to antimony oxide started to decrease at a calcination temperature of 623 K and all bands completely disappeared at a calcination temperature of 723 K, also indicating the absence of crystalline antimony oxide in the mixture after the solid state reaction.

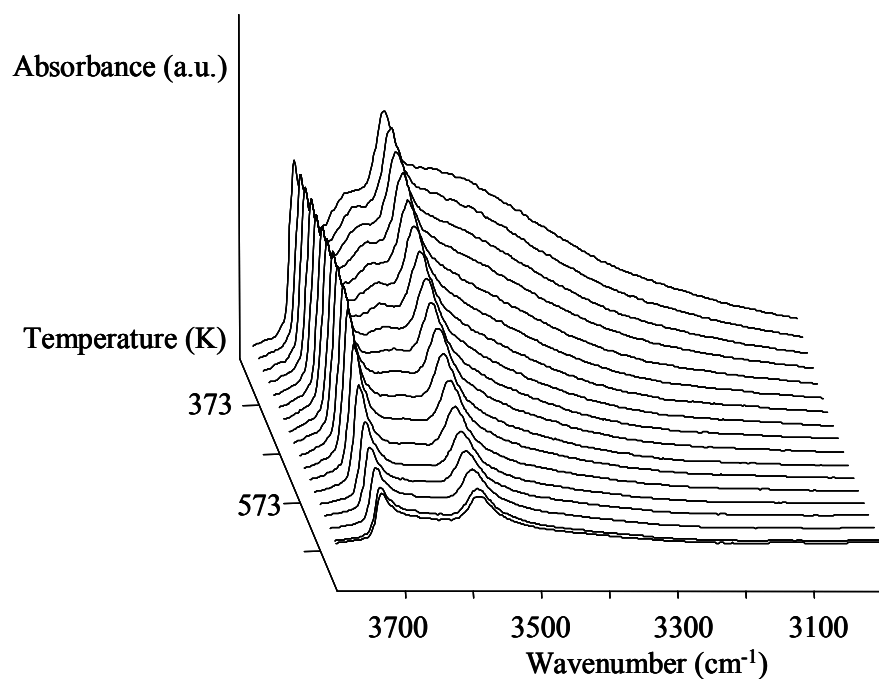


Figure 3. *In-situ* IR spectra during the solid state reaction of Sb_2O_3 and HZSM-5.

The changes in the concentration of the silanol and bridging hydroxyl groups of

the zeolite, followed by *in-situ* IR spectroscopy, showed a similar trend. The IR spectra recorded during the solid state reaction of a physical mixture of the zeolite and Sb_2O_3 (5 wt%) are shown in Figure 3. At ambient temperature, a broad band around 3000 cm^{-1} and two bands at 3745 cm^{-1} and 3606 cm^{-1} , characteristic of the silanol and bridging hydroxyl groups of the zeolite, were observed in the hydroxyl group region. With increasing the calcination temperature, the intensity of the broad band continuously decreased, which resulted from the desorption of H_2O of the zeolite. At temperature above 643 K a continuous decrease in the intensity of the hydroxyl groups was observed, which is an indication of the solid state reaction between Sb_2O_3 and the zeolite. At temperatures higher than 713 K a further decrease in the intensity of the bands characteristic of the hydroxyl groups was not observed.

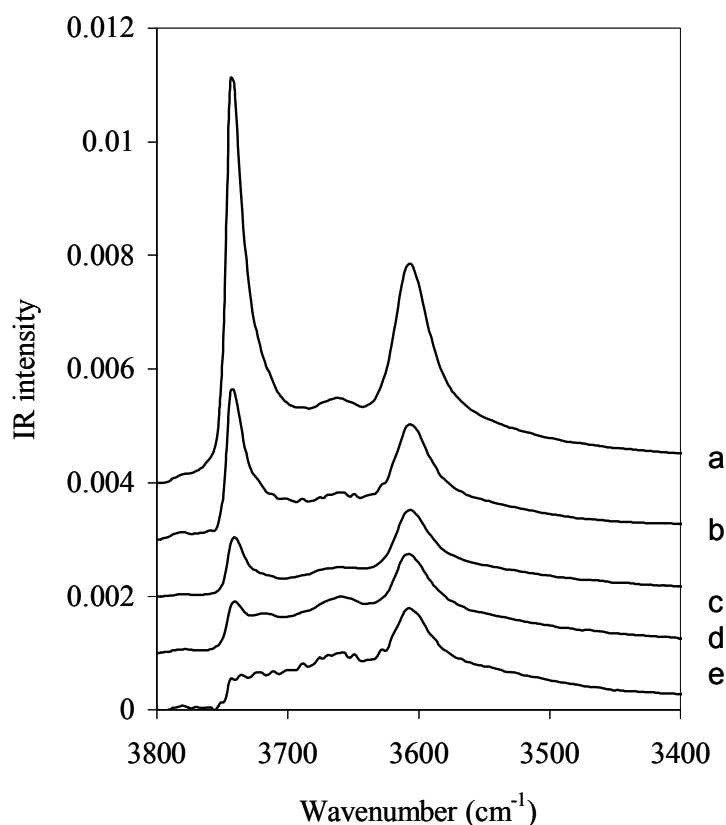


Figure 4. IR spectra of activated (a) HZ, (b) SbZ1, (c) SbZ2, (d) SbZ3 and (e) SbZ4

The IR spectra of the hydroxyl groups of the zeolites after Sb_2O_3 modification are

shown in Figure 4. Three IR bands at 3745, 3680 and 3606 cm^{-1} were observed in the hydroxyl group region, which can be assigned to the non-acidic silanol groups, hydroxyl groups of extra-framework aluminum-oxide and bridging hydroxyl groups, respectively³¹. The relative changes in the concentration of the hydroxyl groups are summarized in Table 2.

Table 2. Changes in the concentration of hydroxyl groups after modification with Sb_2O_3

Samples	Decrease in the concentration of Silanol groups (%)	Decrease in the concentration of bridging hydroxyl groups (%)
SbZ1	60	48
SbZ2	87	48
SbZ3	93	50
SbZ4	98	48

Modification with 3.3 wt% antimony oxide led to a decrease in the intensity of the silanol groups by 60 % and of the bridging hydroxyl groups by 48 %, respectively. A slight decrease in the intensity of the hydroxyl groups of the extra-framework aluminum was also observed. A further increase in antimony oxide loading to 6.5 wt% led to a decrease in the intensity of the silanol groups by 87 %, while a further decrease in the intensity of the bridging hydroxyl groups was not observed. At 10.2 wt% antimony oxide loading, the silanol groups almost completely disappeared, while the decrease in the intensity of the bridging hydroxyl groups was similar to all other Sb_2O_3 modified samples.

The IR spectra after adsorption of Pyridine on the Sb_2O_3 modified samples are shown in Figure 5. IR bands at 1636, 1490 and 1545 cm^{-1} , characteristic of pyridinium ions (pyridine interacting with Brønsted acid sites), and at 1623, 1490 and 1454 cm^{-1} , characteristic of coordinatively bound pyridine (pyridine interacting with Lewis acid sites) were observed^{32,33}. The intensity of the bands at 1545 cm^{-1} and 1454 cm^{-1} were used to calculate the relative changes in the concentration of acid sites after the modification (summarized in Table 3). Note that for all samples investigated the band characteristic of the bridging hydroxyl groups at 3606 cm^{-1} completely

disappeared after pyridine adsorption (spectra not shown), which indicates that all bridging hydroxyl groups (Brønsted acid sites) were accessible for pyridine and, therefore, a partial blocking of the pores after the modification of the zeolites can be excluded. The changes in the concentration of Lewis and Brønsted acid sites clearly revealed that the modification led to a decrease in the concentration of Lewis and Brønsted acid sites on all modified samples by about 20% and 50%, respectively, which is in perfect agreement with the density of the hydroxyl groups present after the Sb_2O_3 modification.

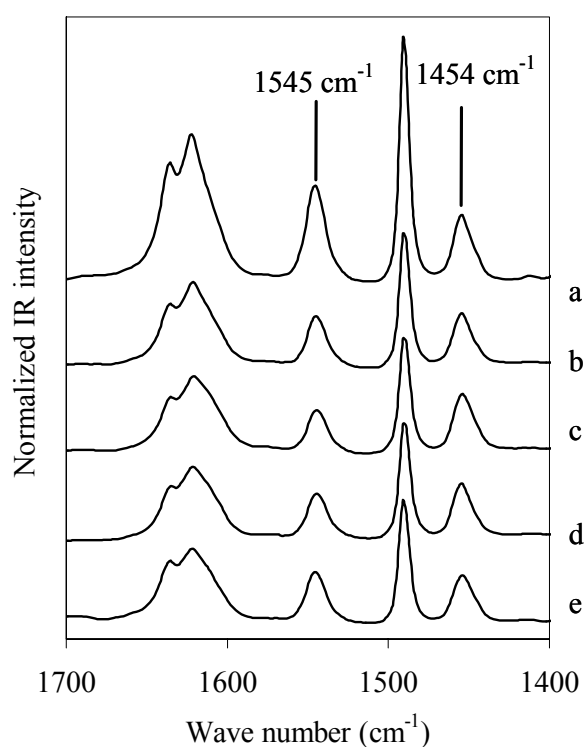


Figure 5. IR spectra during adsorption of 10^{-2} mbar Pyridine at 423K on (a) HZ, (b)SbZ1, (c) SbZ2, (d) SbZ3 and (e) SbZ4

Table 3. Changes in the concentration of acid sites after modification with Sb_2O_3

Samples	Decrease in the concentration of Lewis acid site (%)	Decrease in the concentration of Brønsted acid sites (%)
SbZ1	21	51
SbZ2	22	50
SbZ3	18	54
SbZ4	21	48

Sorption of DTBPy was used to quantify the concentration of the externally accessible acid sites. The kinetic diameter of DTBPy (10.5 Å) is significantly larger compared to the pore openings of HZSM-5^{34,35,36} and, therefore, this probe molecule can only interact with hydroxyl groups located on the external surface or in the pore mouth region of the zeolite. IR spectra of DTBPy adsorption on the parent and modified zeolites are compared in Figure 6.

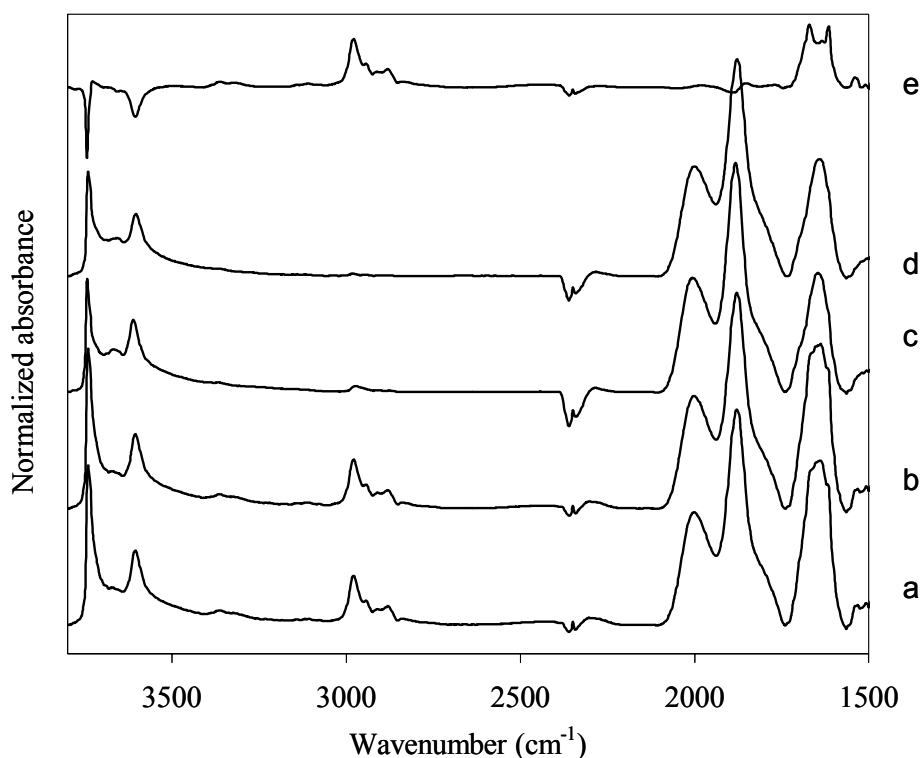


Figure 6. IR spectra during adsorption of 2×10^{-2} mbar of DTBPy (a) HZ at room temperature, (b) HZ after outgassing at 423 K for 1 h, (c) SbHZ1 at room temperature, (d) SbHZ1 after outgassing at 423 K for 1 h and (e) difference spectra of HZ between after desorption and before adsorption of DTBPy

For the unmodified zeolite, adsorption of DTBPy led to a marked decrease in the intensity of the bands at 3745 cm^{-1} and 3606 cm^{-1} resulting from the interaction between the hydroxyl groups with DTBPy molecules. Other bands at 2979, 2943, 2912, 2882 cm^{-1} , characteristic of interaction of CH_3 groups with hydroxyl groups of the zeolite, 3367 and 1616 cm^{-1} , characteristic of interaction of DTBPy molecules with Brønsted acid sites, 1541 , 1481 and 1468 cm^{-1} , characteristic of physically adsorbed DTBPy, were also observed. The bands at 3367 cm^{-1} and 1616 cm^{-1} ,

assigned to the N-H vibration and to the ring vibration of DTBPyH⁺, respectively^{35,36}, were used to determine the concentration of the externally accessible Brønsted acid sites³⁶. Approximately 28% of the bridging hydroxyl groups of the parent zeolite are accessible for DTBPy molecules. After the modification of HZSM-5 with 3.3 wt% Sb₂O₃ the sorption of DTBPy at room temperature was almost completely suppressed. Only small bands in the C-H stretching vibration region around 2979 cm⁻¹ were observed³⁷, while the bands at 3367 cm⁻¹ and 1616 cm⁻¹, characteristic of the interaction of DTBPy molecules with Brønsted acid sites, were absent. After evacuation of the antimony oxide modified sample at 423 K for 1 h DTBPy were completely removed from the surface, indicating that DTBPy molecules were only physically absorbed. The adsorption of DTBPy on the samples with higher Sb₂O₃ loading gave similar results, which indicates that after the modification all externally accessible Brønsted acid sites of the zeolite were passivated.

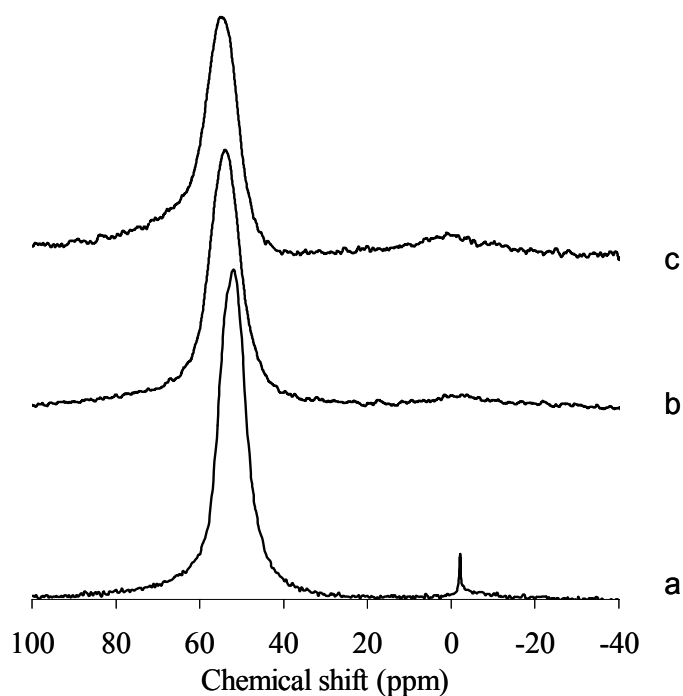


Figure 7. ²⁷Al MAS NMR spectra of (a) HZ, (b) SbZ1 and (c) SbZ4.

²⁷Al MAS NMR spectra of HZ, SbZ1 and SbZ4 are compared in Figure 7. Two

peaks with the chemical shifts at 53 ppm and -5 ppm are typically observed for HZSM-5, which are assigned to the framework Al (FAL) and extra-framework Al-oxide species (EFAL), respectively. Integration of these peaks in the NMR spectra of HZ revealed that about 2.5% of the Al was present as EFAL. For both Sb₂O₃ modified samples the intensity of the peak at -5 ppm decreased and became significantly broadened compared to the parent material, which resulted from the change in the coordination environment of EFAL. This confirms that the decrease in the concentration of the bridging hydroxyl groups observed after the solid state reactions did not result from a partial dealumination, i.e. the removal of Al from the T-atom positions of the zeolite. In addition, the marked broadening of the peak of EFAL, e.g. the change of the coordination environment of EFAL, suggested a strong interaction of Sb₂O₃ with EFAL.

The diffusion of *o*-xylene (kinetic diameter of 6.3 Å³⁸) was used to study the effects of the modification on the pore openings of the HZSM-5 zeolite. Typical IR spectra during the time-resolved uptake of *o*-xylene over HZ at 373 K are presented in Figure 8. With increasing adsorption time, the intensity of IR bands at 3745 and 3606 cm⁻¹ decreased, indicating the interaction of *o*-xylene with the hydroxyl groups via hydrogen bonding, and a broad band around 3168 cm⁻¹ characteristic of the perturbed bridging hydroxyl groups was observed. Simultaneously, the intensity of the IR bands assigned to *o*-xylene at 1497, 1468 and around 3000 cm⁻¹ increased. The changes in the intensity of the bands at 1497 and 1468 cm⁻¹ as a function of adsorption time over the parent and modified samples are compared in Figure 9. An equilibration time of 30 min was observed for *o*-xylene adsorption in the unmodified zeolite. After modification with 3.3 wt% Sb₂O₃ a decrease in *o*-xylene uptake by approximately 26% was observed, while the equilibration time of *o*-xylene adsorption was not affected, indicating the same diffusivity as the parent material. A further increase in the Sb₂O₃ loading resulted in a marked decrease in *o*-xylene diffusivity, however, the uptake of *o*-xylene remained the same for all modified samples. The diffusion coefficients of *o*-xylene in the parent and modified zeolites, calculated using the square root law, are listed in Table 4.

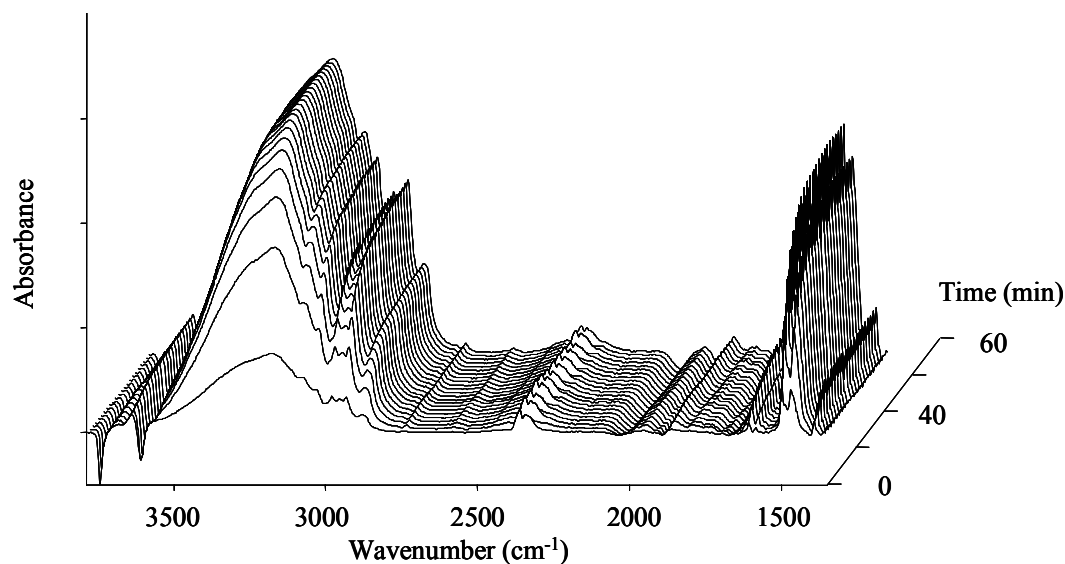


Figure 8. Time-resolved IR spectra during adsorption of 1 mbar *o*-xylene in HZ at 373 K.

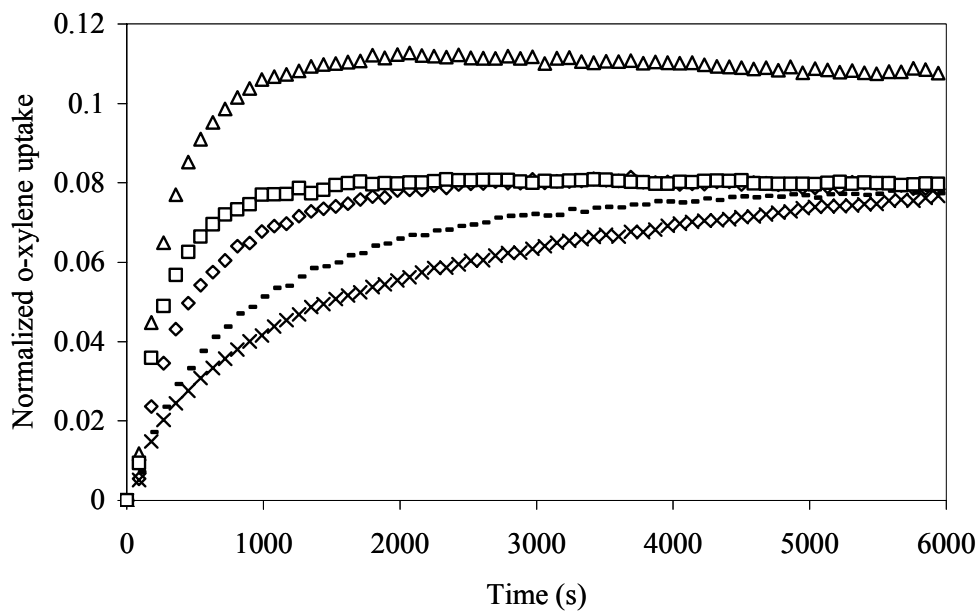


Figure 9. Intensity of the band at 1497 cm^{-1} and 1468 cm^{-1} during *o*-xylene adsorption with 1 mbar at 373 K on (Δ) HZ, (\square) SbZ1, (\diamond) SbZ2, ($-$) SbZ3 and (\times) SbZ4.

For the parent zeolite, the diffusion coefficient was $7.8 \times 10^{-18} \text{ m}^2/\text{s}$. Modification of the zeolite with 3.3 wt% Sb_2O_3 did not influence the diffusivity, which indicates that at this loading the modification with Sb_2O_3 did not influence the size of the pore openings. In contrast at antimony oxide loading between 6.5 wt% and 10.2 wt% a strong decrease in the diffusion coefficients from 3.9×10^{-18} to $6.6 \times 10^{-19} \text{ m}^2/\text{s}$ was observed, which clearly indicates a narrowing of the pore entrances of the zeolite.

Table 4. Diffusion coefficients of *o*-xylene in the parent and modified zeolites

Samples	Diffusion coefficient of <i>o</i> -xylene ($\times 10^{-18} \text{ m}^2/\text{s}$)
HZ	7.8
SbZ1	7.4
SbZ2	3.9
SbZ3	1.9
SbZ4	0.66

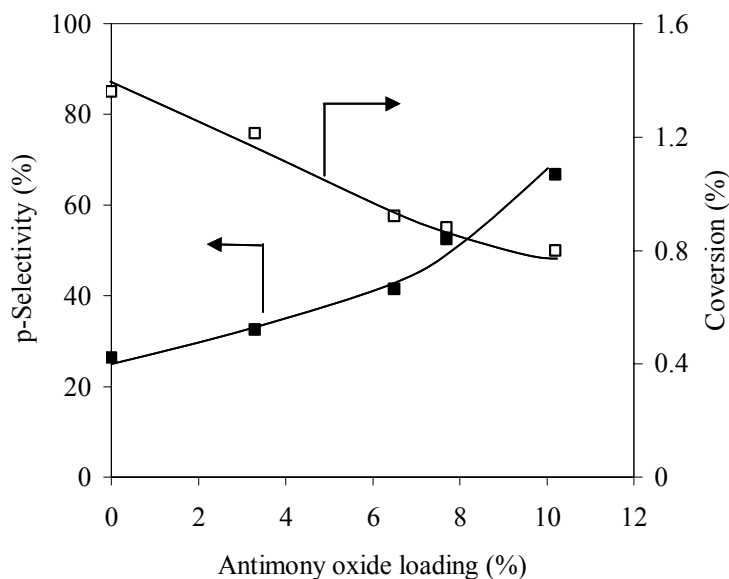


Figure 10. Activity and selectivity of the modified zeolites for toluene disproportionation at 773 K

The activities and selectivity of the parent and Sb_2O_3 modified zeolites for toluene disproportionation are compared in Figure 10. For the parent zeolite the ratio between the xylene isomers was close to the thermodynamic equilibrium. After

modification with Sb_2O_3 an increase in the *para*-selectivity from 33% (3.3 wt % Sb_2O_3) to 68% (10.2 wt% Sb_2O_3) was reached. The activity of the catalyst with the highest Sb_2O_3 loading (10.2 wt%), however, decreased by 41 % compared to the unmodified zeolite.

5.4. Discussion

5.4.1. Dispersion of antimony oxide on the zeolite

Metal-oxides and salts can be dispersed over different supports, such as Al_2O_3 , SiO_2 , TiO_2 , ZrO_2 and zeolites by solid state reactions¹⁹. This process essentially occurs at elevated temperatures in order to overcome the lattice energy of the crystalline species.

After the solid state reaction of Sb_2O_3 with HZSM-5 crystalline antimony oxide phases could not be detected by XRD even for catalysts with a Sb_2O_3 loading up to 10.2 wt%, which indicates an effective dispersion of Sb_2O_3 on the zeolite. Raman spectra of the physical mixture of antimony oxide and the zeolite calcined at different temperatures showed that the transformation of crystalline Sb_2O_3 into a highly dispersed phase was completed at 723 K. In agreement with Raman results *in-situ* IR spectroscopy revealed that the concentration of the hydroxyl groups started to decrease at temperatures above 643 K due to the solid state reaction between Sb_2O_3 and the zeolite. In principle, the dispersion of metal oxides/salts occurs via a surface diffusion mechanism. The dispersion of a metal-oxide typically starts at temperatures above the Tammann temperature^{39,40,41}, which is approximately equal to half of the melting point of the oxide in Kelvin. For Sb_2O_3 the dispersion by solid state reaction, however, started at temperatures above 643 K, which is substantially higher compared to the Tammann temperature of Sb_2O_3 (464 K). Note that during temperature programmed desorption of H_2O (shown for the parent zeolite in Figure 11) the dehydration of the zeolite occurred at approximately 600 K, which indicates that the solid state reaction of Sb_2O_3 proceeds with the hydroxyl groups of the zeolite. Therefore, the dehydration of the zeolite is necessary to generate active hydroxyl

groups, as the interaction between the oxide and the hydroxyl groups of the zeolite appears to be the driving force for the dispersion of Sb_2O_3 . In addition a significant loss of Sb_2O_3 occurred during the solid state reaction (see table 1), therefore, we would like to speculate that the transport of Sb_2O_3 via the vapor phase may also contribute to the dispersion of Sb_2O_3 over the zeolite, although the sublimation temperature of Sb_2O_3 is 1425 K.

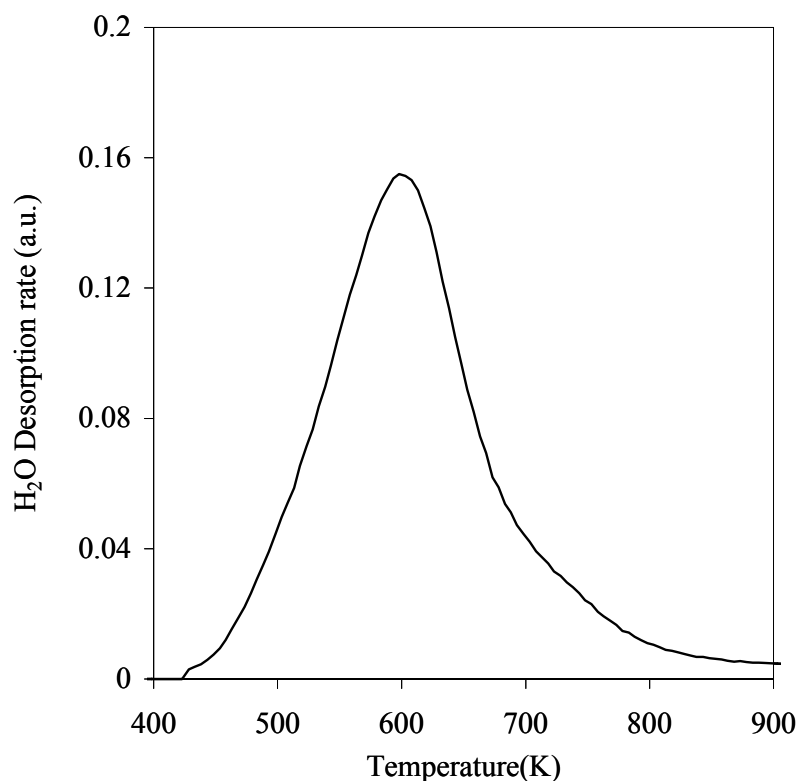
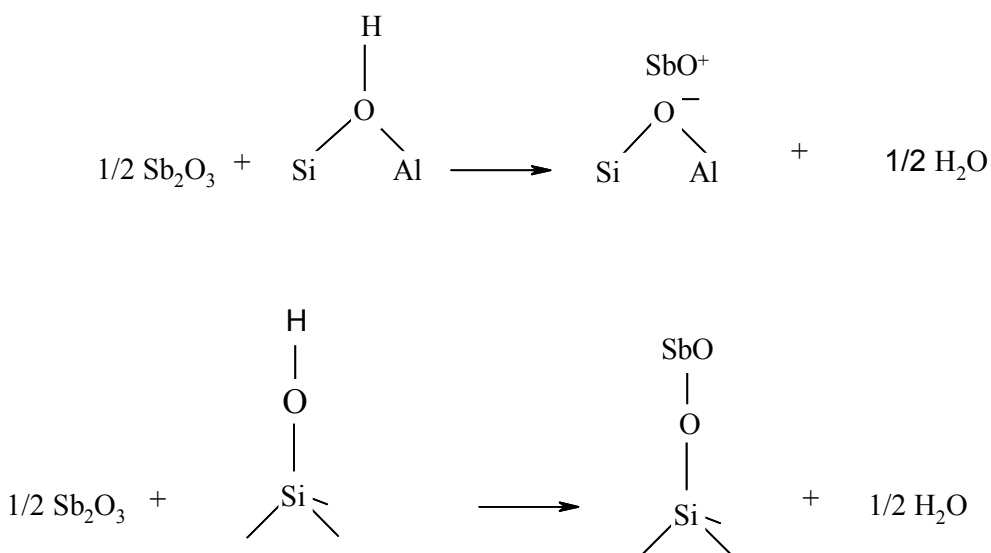


Figure 11. Temperature programmed desorption of H_2O on HZ

After the modification of the zeolites with antimony oxide, a marked decrease in the intensity of the silanol and bridging hydroxyl groups was observed by IR spectroscopy. This indicates that antimony oxide not only strongly interacts with the bridging hydroxyl groups, but also with the silanol groups. Due to the weak basic character of Sb_2O_3 , the interaction of Sb_2O_3 with the accessible bridging hydroxyl

groups (Brønsted acid sites) of the zeolite occurs via the formation of SbO^+ species, which act as charge compensating species and, therefore, leads to a partial removal of the acid sites. Due to the weakly acidic character of the SiOH groups the interaction of antimony oxide with the silanol groups is speculated to occur via covalent bonds. A scheme of the surface reactions is given in scheme 1. Note that the decrease in the concentration of SiOHAl groups after the modification was independent on the Sb_2O_3 loading. Moreover, with increasing Sb_2O_3 loading the accessible bridging hydroxyl groups were passivated before the reaction of Sb_2O_3 with the SiOH groups, which indicates that antimony oxide preferentially interacts with the bridging hydroxyl groups because of their stronger acidity. Additionally, the concentration of Lewis acid sites decreased after the modification, which revealed that antimony oxide also reacted with extra-framework aluminum-oxide (EFAL) species. Similar to the interaction of antimony oxide with Brønsted acid sites, the decrease in the concentration of Lewis acid sites was independent on the Sb_2O_3 loading and, moreover, it was observed that the accessible Lewis acid sites reacted with Sb_2O_3 before the removal of the silanol groups was completed.



Scheme 1. Solid state reaction of Sb_2O_3 with the hydroxyl groups of HZSM-5 zeolite

5.4.2. Influences of modification on the structural properties of the zeolite

The comparison of the pore volume before and after the modification showed that the pore volume of the zeolite decreased after the modification with 3.3 wt % Sb_2O_3 , (see Table 1), which resulted from the penetration of a small amount of antimony oxide into the pores of the zeolite. At higher Sb_2O_3 loading a further decrease in the pore volume was not observed, which indicates that the deposition of Sb_2O_3 occurs primarily on the external surface. Note, that a partial collapse of the zeolite framework structure after the modification can be excluded.

Adsorption of DTBPy indicates that after modification with 3.3 wt% Sb_2O_3 all externally accessible acid sites were removed by the reaction of Sb_2O_3 with the accessible bridging hydroxyl groups. The decrease in the concentration of Brønsted acid sites after modification (determined by IR spectroscopy and sorption of Pyridine) was 50%, while DTBPy adsorption indicated that only 28% of the Brønsted acid sites are located in the pore mouth region of the parent zeolite³⁶. Therefore, antimony oxide not only interacts with Brønsted acid sites located in the pore mouth region, but also penetrates into the zeolite pores. While the changes in the concentration of Lewis and Brønsted acid sites were not a function of the Sb_2O_3 loading, the concentration of the silanol groups continuously decreased with increasing the antimony oxide loading. This clearly indicates that Sb_2O_3 primarily interacts with the strongly acidic Brønsted and Lewis acid sites. After all strongly acidic sites accessible for Sb_2O_3 were passivated, antimony oxide is only dispersed on the external surface of the zeolite crystals. Considering the pore volume of SbZ4 remains identical to SbZ1, while the concentration of SiOH groups decreased only from 60% to 98 % we would like to speculate that antimony oxide is polymerized on the external surface and in the pore mouth region of the zeolite at high Sb_2O_3 loadings.

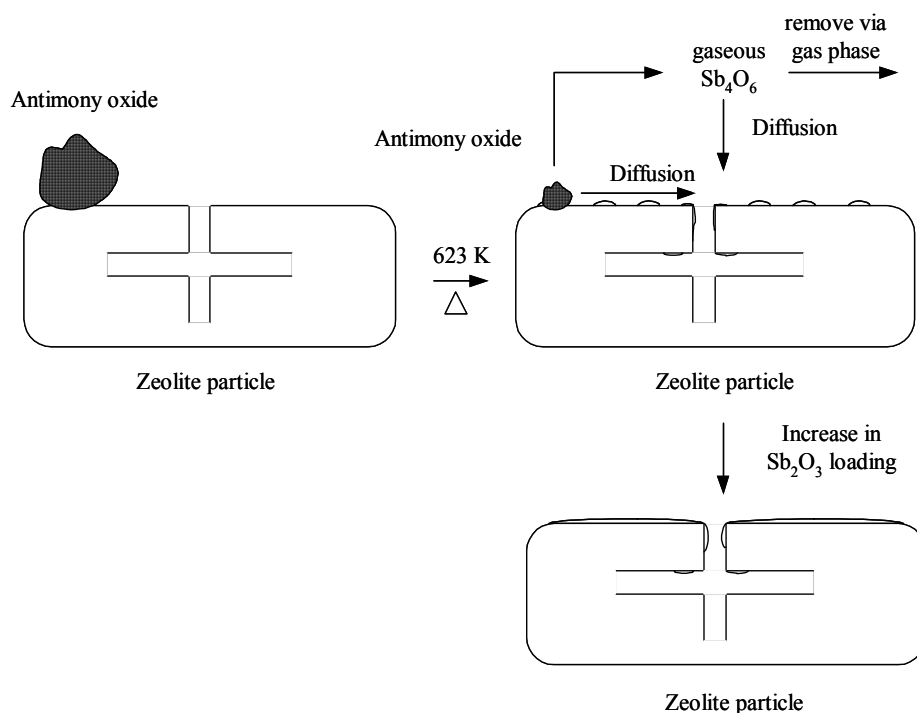
The results of *o*-xylene adsorption also support these conclusions. At low antimony oxide loading (3.3 wt%) the amount of *o*-xylene adsorbed markedly decreased compared to the parent zeolite, the diffusivity, however, remained unchanged. With increasing antimony oxide loading the amount of *o*-xylene uptake

did not further decrease, while the diffusivity of *o*-xylene into the pores was strongly suppressed. This indicates that at low Sb₂O₃ loading strong acid sites located in the pore mouth region and inside the pores are primarily passivated, which leads to a reduction of the pore volume. SbO⁺ species resulting from the reaction of Sb₂O₃ with the acid sites located in the pore mouth region are too small to influence the pore openings of the modified zeolite as well as the diffusivity of *o*-xylene. At higher Sb₂O₃ loading, Sb₂O₃ is polymerized on the external surface and in the pore mouth region which leads to a further narrowing of the pore openings and imposes a diffusion hindrance to the diffusion of molecules, i.e. antimony oxide or *o*-xylene, into the pores of the zeolite.

The solid state reaction of antimony oxide with the zeolite was shown to occur via a combined surface diffusion and vapor diffusion mechanism. Antimony oxide diffuses in Sb₄O₆ subunits with a kinetic diameter of approximately 7.6 Å^{42,43}. As the size of these subunits is larger than the pore diameter of HZSM-5 zeolite, the diffusion of antimony oxide into the pores of the zeolite is sterically hindered and, therefore, only SiOHAl groups located in the pore mouth region should be accessible. However, after the modification a significantly higher concentration of Brønsted acid sites was found to be passivated, which indicates that the acid sites located inside the pores of the zeolite also participate in the solid state reaction. This suggests that the Sb₄O₆ subunits are partially decomposed during the solid state reaction of antimony oxide with the hydroxyl groups located on the external surface and in the pore mouth region of the zeolite. The smaller antimony oxide clusters formed subsequently enter into the pores of the zeolite and react with the bridging hydroxyl groups located in the pores of the zeolite.

Based on the reactions described, the dispersion of antimony oxide during the solid state reaction on the zeolite is depicted in Scheme 2. At low Sb₂O₃ loading, antimony oxide reacts with the bridging hydroxyl groups, non framework Al-oxide species and silanol groups via a surface and vapor diffusion mechanism. This interaction results in the complete passivation of externally accessible acid sites and the removal of Brønsted and Lewis acid sites by 50% and 20%, respectively. Most

antimony oxide is located on the external surface and in the pore mouth region of the zeolite and only a minor amount of antimony oxide penetrates into the pores of the zeolite. Note that the reaction of antimony oxide with the bridging hydroxyl groups located in the pore mouth region of the zeolite slightly narrowed the pore openings of the zeolite, the modification, however, is not marked enough to influence the *o*-xylene diffusivity. At higher Sb_2O_3 loading, antimony oxide only reacts with the silanol groups located on the external surface and in the pore mouth region of the zeolite and simultaneously Sb_2O_3 is polymerized on the external surface and in the pore mouth region of the zeolite, which leads to the narrowing of the pore openings and the marked hindrance for *o*-xylene diffusion.



Scheme 2. Model of the dispersion of Sb_2O_3 over the pore and the external surface of the zeolite

5.4.3. Influences of modification on the activity and selectivity of the zeolites for toluene disproportionation

The activity and selectivity of HZSM-5 zeolites for toluene disproportionation is generally controlled by the concentration and location of Brønsted acid sites⁴⁴ and the

dimensions of the pores, which can be adjusted by post-synthetic modifications. Narrowing of the pore openings of the zeolite lowers the diffusivity of *o*- and *m*-xylene, which typically leads to a strongly enhanced shape selectivity to *para*-products in the toluene disproportionation^{2,36}. After modification with 3.3 wt% Sb₂O₃ the activity of toluene disproportionation decreased by 15% compared to the parent zeolite, which is directly related to the lower concentration of Brønsted acid sites of SbZ1. The enhanced *para*-selectivity of this catalyst primarily results from the passivation of the unselective Brønsted acid sites, as the modification only leads to a minor narrowing of the pore openings of SbZ1. Our previous study⁴⁵ showed that introducing acid sites onto the external surface of the zeolite decreased the *para*-selectivity for toluene disproportionation. Therefore, the passivation of unselective acid sites suppresses secondary isomerization reactions of *p*-xylene, generated inside the pores, to other isomers and thus enhances the *p*-selectivity. At higher antimony oxide loading, a marked increase in the *para*-selectivity up to 60% was observed in the expense of the activity compared to the unmodified HZSM-5. The enhanced *para*-selectivity for the samples with higher Sb₂O₃ loading could be attributed to a further pore narrowing, which constrains the diffusion of *o*- and *m*-xylene isomers, as the concentration of Brønsted acid sites remains constant at higher antimony oxide loading. Therefore, the decrease in the activity of the HZSM-5 catalysts modified with higher Sb₂O₃ loadings results from mass transfer limitations to the products in the narrowed pores of the modified zeolites.

5.5. Conclusions

Antimony oxide can be dispersed on the surface and inside the pores of zeolites by solid state reactions at elevated temperatures via a surface and vapor diffusion processes. Crystalline antimony oxide phases were not detected even at antimony oxide loadings up to 10.2 wt%. *In-situ* Raman and IR spectroscopy indicated that the solid state reaction commenced at 623 K and completed at 723 K. During the solid state reaction antimony oxide clusters reacted with the silanol and bridging hydroxyl

groups and with extra-framework Al-oxide species of the zeolite. A small amount of antimony oxide penetrated into the pores of the zeolite and reacted with the bridging hydroxyl groups. The large fraction of antimony oxide, however, was located on the external surface of the zeolite crystals and led to a narrowing of the pore openings of the zeolite, which suppressed the further penetration of antimony oxide into the pores of the zeolite. The modification of HZSM-5 zeolite with antimony oxide led to the complete passivation of the unselective Brønsted acid sites at low Sb₂O₃ loadings and to a narrowing of the pores at higher Sb₂O₃ loadings. Both effects resulted in an enhanced shape selectivity to *p*-xylene in the toluene disproportionation reaction, but also led to a lower activity due to the lower concentration of Brønsted acid site and the generation of mass transfer limitations in the Sb₂O₃ modified HZSM-5 samples

Acknowledgments

The authors thank M. Brandmair for the Raman measurements and J.-O. Barth and R. Su for the measurements of the ²⁷Al MAS NMR. Financial support from the Bayerische Forschungsverbund Katalyse (FORKAT II) and Süd-Chemie AG is gratefully acknowledged.

References

1. Csicsery, S. M. *Zeolites* **4**, 202 (1984).
2. Tsai, T.; Liu, S.; Wang, I. *Appl. Catal. A: general* **181**, 355 (1999).
3. Olson, D. H.; Haag, W. O. *Catalytic Materials*, ACS Symposium Series, Vol. 248, ACS, Washington, DC, 1984.
4. Kürschner, U.; Jerschke, H. G.; Schreier, E.; Völter, J. *Appl. Catal.* **57**, 167 (1990).
5. Cejka, J.; Wichterlova, B. *Catal. Rev.* **43**, 375 (2002).
6. Fang, L. Y.; Liu, S. B.; Wang, I. *J. Catal.* **185**, 33 (1999).
7. Kim, J.; Ishida, A.; Okajima, M.; Niwa, M. *J. Catal.*, **161**, 387 (1996).
8. Niwa, M.; Katada, N.; Murakami, Y. *J. Catal.* **134**, 340 (1992).

9. Tynjala, P.; Pakkanen, T. T. *J. Mol. Catal. A: Chem.* **122**, 159 (1997).
10. Kaeding, W. W.; Butter, S. A. *J. Catal.* **61**, 155 (1980).
11. Kaeding, W. W.; Chu, C.; Young, L. B.; Weinstein, B.; Butter, S. A. *J. Catal.* **67**, 159 (1981).
12. Kaeding, W. W.; Young, L. B.; Chu, C. C. *J. Catal.* **89**, 267 (1984).
13. Young, L. B.; Butter, S. A.; Kaeding, W. W. *J. Catal.* **76**, 418 (1982).
14. Delmon, B.; Jacobs, P. A.; Poncelet, G. *Preparation of catalyst*, Elsevier Science, Amsterdam, 1976.
15. Breck, D. W. *Zeolite Molecular Sieves*, Wiley, New York, 1974.
16. Zheng, S.; Heydenrych, H.; Röger, P.; Jentys, A.; Lercher, J. A. *Stud. Surf. Sci. Catal.* **135**, 214 (2001).
17. Yue, Y. H.; Tang, Y.; Liu, Y.; Gao, Z. *Ind. Eng. Chem. Res.* **35**, 430 (1996).
18. Karge, H. G.; Hermann, K. B. *Zeolite chemistry and catalysis*, P. A. Jacobs Eds. 43 (1991).
19. Xie, Y.; Tang, Y. *Adv. Catal.* **37**, 1 (1990).
20. Kingler, G.; Lugstein, A.; Swagera, R.; Ebel, M.; Jentys, A.; Vinek, H. *Micropor. Mater.* **39**, 307 (2000).
21. Lugstein, A.; Jentys, A.; Vinek, H. *Appl. Catal. A: general* **166**, 29 (1998).
22. Borry, R. W.; Lu, E. C.; Kim, Y. H.; Huffsmith, A.; Reimer, J. A.; Iglesia, E. *J. Phys. Chem. B* **103**, 5787 (1999).
23. Ding, W.; Meitzner, G. D.; Iglesia, E. *J. Catal.* **206**, 14 (2002).
24. Xiao, F.; Zheng, S.; Sun, J.; Yu, R.; Qiu, S.; Xu, R. *J. Catal.* **176**, 474 (1998).
25. Lee, G. Y.; Zhao, J. C. *Petrochem Technol. (chinese)* **16**, 266 (1987).
26. Mirth, G.; Cejka, J.; Lercher, J. A. *J. Catal.* **139**, 24 (1993).
27. Mirth, G.; Lercher, J. A. *J. Catal.* **147**, 199 (1994).
28. Kärger, J.; Ruthven, D. M. *Diffusion in zeolite and other micro-porous Solids*, JohnWiley & Sons: New York, 1992.
29. Cavalcante, C.; Ruthven, D. *Ind. Eng. Chem. Res.* **34**, 185 (1995).
30. Mestl, G. *J. Mol. Catal. A: Chem.* **158**, 45 (2000).
31. Sayed, M. B.; Kydd, R. A.; Cooney, R. P. *J. Catal.* **88**, 137 (1984).
32. Glazunov, V. P.; Odinokov, S. E. *Spectrochim. Acta* **38A**, 399 (1982).
33. Emeis, C. A. *J. Catal.* **141**, 371 (1993).
34. Knözinger, H.; Krietenbrink, H.; Ratnasamy, P. *J. Catal.* **48**, 436 (1977).

35. Coma, A.; Fornes, V.; Forni, L.; Marquez, F.; Martinez-Triguero, J.; Moscotti, D. *J. Catal.* **179**, 451 (1998).
36. Zheng, S.; Heydenrych, H. R.; Jentys, A.; Lercher, J. A. *J. Phys. Chem. B* **106**, 9552 (2002).
37. Knözinger, H.; Krietenbrink, H.; Ratnasamy, P. *J. Catal.* **48**, 436 (1977).
38. Giannetto, G. *Zeolites*; Edit: Caracas, 130 (1990)
39. Knözinger, H.; Taglauer, E. *Handbook of Heterogeneous Catalysis*: Ertl, G.; Knözinger, H.; Weitkamp, J. Eds.; Wiley-VCH: Weinheim, **1**. 216 (1997).
40. Knözinger, H.; Taglauer, E. In *catalysis*; Spivey, J. J., Ed.; The Royal Society of chemistry, Cambridge, U.K., **10**, 1 (1993).
41. Mestl, G.; Knözinger, H. *Langmuir* **14**, 3964 (1998).
42. Norman, N. C. Ed. *Chemistry of Arsenic, Antimony and Bismuth*, Blackie Academic & Professional; 1992
43. Spengler, J.; Anderle, F.; Bosch, E.; Grasselli, R. K.; Pillep, B.; Behrens, P.; Lapina, O. B.; Shubin, A. A.; Eberle, H. J.; Knözinger, H. *J. Phys. Chem. B* **105**, 10772 (2001).
44. Vinek, H.; Lercher, J. A. *J. Mol. Catal.* **64**, 23 (1991).
45. Zheng, S.; Heydenrych, H. R.; Röger, H. P.; Jentys, A.; Lercher, J. A. *Topics in Catalysis* **22**, 101 (2003).

Chapter 6

Summary and conclusions

6.1. Summary

HZSM-5 zeolites are extensively used as shape-selective catalysts in the acid catalyzed industrial processes. The shape selectivity of zeolites results from the similarity of the dimension of the channels and pores of the zeolites to the kinetic diameters of the reactants and products, which leads to the suppression of the diffusion of the undesired products or/and the generation of these products in the pores. A small difference of the diffusivities between the desirable products and the undesirable ones, especially in zeolites with small crystals, as well as the presence of the unselective acid sites in the external surface and in the pore mouth region of the zeolites lowers the shape-selectivity. These disadvantages can be overcome using post-synthesis modification of the external surface of the zeolites, by which the pore openings can be narrowed or blocked and the unselective acid sites can be passivated. Consequently, the diffusion of the undesirable products and the secondary isomerization can be effectively suppressed and an enhanced shape-selectivity is obtained.

For an acid catalyzed reaction, the activity of zeolite is directly related to the concentration of the acid sites. Unselective acid sites, usually located on the external surface and in the pore mouth region of the zeolite, have to be removed in order to achieve a high *p*-selectivity, while acid sites in the interior of the pores, which contribute to the activity of the zeolite, should be preserved. Therefore, the selection of the silylation agent is of crucial importance. The silylation agents with smaller or larger kinetic diameters can either penetrate into the interior pores of the zeolite and passivate the selective acid sites, which leads to the decrease in the catalytic activity, or incompletely remove the unselective acid sites, which results in a lower *p*-selectivity. For MFI type zeolite, *tetra*-ethoxysilane (TEOS) with a diameter of 10.3 Å was proved to be the appropriate silylation agent for the modification of the external surface of HZSM-5 zeolites. Applicability of the operation, i.e. investment and environmental impact, is also an important concern. Modification using solid state

reaction of the zeolite with antimony oxide, a feasible and environmentally benign modification method, was also studied.

The work presented in this thesis described the effects of the modification on the properties of HZSM-5 zeolites with different crystal sizes using two different modification methods, i.e. chemical liquid deposition (CLD) of *tetra*-ethoxysilane (TEOS) and solid state reaction with antimony oxide. After modification, the properties of the zeolites were related to their activity and selectivity for toluene disproportionation.

Chapter 2 described the influences of the modification using CLD of TEOS on the acidic properties of the zeolites and the silylation mechanism. Silylation led to the partial passivation of the unselective Brønsted and Lewis acid sites located on the external surface and in the pore mouth region of the zeolites, while the acid sites in the interior pores were preserved. A single cycle silylation for the zeolite with large crystals resulted in a marked passivation of the external accessible acid sites. Multi-cycle silylation of the zeolite with small crystals is necessary to achieve enhanced modification effects.

The diffusivity of the reactant for toluene disproportionation, i.e. toluene, was determined using the frequency response method, which was described in *Chapter 3*. Toluene was found to diffuse in the straight and sinusoidal channels of the zeolites. Silylation blocked approximately 75% of the pore entrances of the zeolite and led to a decrease in the diffusivities of toluene in both channels. In addition the diffusivities of toluene were dependent on toluene loadings, which was related to the interaction of toluene molecules with acid sites. It is worthy to note that silylation resulted in the blocking of the pore openings and in the enhanced tortuosity of the straight channels of the silylated zeolite. This also implied that a higher *p*-selectivity can be achieved as a larger amount of toluene molecules diffuse in narrow channels, i.e. the sinusoidal channels of the zeolite, after silylation.

Regulation of the pore openings of the zeolite may markedly influence the selectivity of the catalyst. The changes of the pore entrance of the zeolites and their influence on the activity and selectivity for toluene disproportionation was presented

in *Chapter 4*. Silylation of the zeolites led to the blocking of the pore openings of the zeolites, which markedly hindered the diffusion of *o*- and *m*-xylene in the zeolites. Single cycle silylation of the zeolite with large crystals led to a more effective pore blocking. For zeolite with small crystals, effective blocking of pore entrances can be only achieved applying a multi-cycle silylation process.

The enhanced *p*-selectivity of the silylated zeolites for toluene disproportionation was clearly related to the passivation of the unselective acid sites and the pore mouth blocking. A novel method was proposed in *Chapter 4* to elucidate the functions of the unselective acid sites, i.e. introducing unselective acid sites onto the external surface of the silylated zeolite using alumination, by which the influence from pore opening regulation can be excluded. The presence of the unselective acid sites on the external surface of the silylated zeolite led to a decrease in the *p*-selectivity for toluene disproportionation, which unambiguously proved that the unselective acid sites lowered the shape selectivity of the zeolite. Based on the silylation mechanism, an effective alternative to achieve an enhanced modification effects was described. Pre-treatment of the external surface of the zeolite by dealumination markedly removed the extra-frame alumina located on the external surface and in the pore mouth region of the zeolite. Compared to the untreated zeolite, silylation of the dealuminated zeolite led to a more effective pore mouth blocking and to a higher *p*-selectivity for toluene disproportionation.

A feasible modification method, i.e. solid state reaction of the zeolite with antimony oxide, was described in *Chapter 5*. Antimony oxide with a loading amount up to 10 wt% can be effectively dispersed on the surface and inside the pores of zeolites at elevated temperatures via a surface and vapor diffusion processes. An activated zeolite was required for the dispersion of antimony oxide. During the solid state reaction antimony oxide reacted with the silanol and bridging hydroxyl groups of the zeolite and with extra-framework Al-oxide species. Only a small amount of antimony oxide penetrated into the pores of the zeolite and reacted with the bridging hydroxyl groups. The majority of the antimony oxide was found to disperse on the external surface of the zeolite crystals and led to a blocking of the pore openings of

the zeolite, which suppressed the further penetration of antimony oxide into the pores of the zeolite. The modification of HZSM-5 with antimony oxide resulted in a complete passivation of the unselective Brønsted acid sites at low Sb_2O_3 loadings and in a blocking of the pore mouth at higher Sb_2O_3 loadings. Both effects resulted in the enhanced shape selectivity to *p*-xylene for toluene disproportionation in an expense of catalytic activity due to the lower concentration of Brønsted acid sites and the generation of mass transfer limitations in the Sb_2O_3 modified HZSM-5 samples.

6.2. Conclusions

(1). The modification of HZSM-5 zeolites using CLD of TEOS led to the passivation of externally accessible Brønsted and Lewis acid sites via the silylation reaction between TEOS and the acid sites.

(2). The pore openings were blocked by the silylation, which significantly hindered the diffusion of *o*-xylene out of the pores of the zeolites.

(3). The passivation of unselective acid sites and the diffusion hindrance of *o*-xylene and *m*-xylene led to the enhanced *para*-selectivity of the modified zeolites for toluene disproportionation.

(4). The blocking of the pore openings of the silylated zeolite led to an enhanced tortuosity of the diffusion pathways, which resulted in lower toluene diffusivities of toluene in the straight and sinusoidal channels and in a larger amount of toluene molecules diffusing via the sinusoidal channels of the silylated zeolite compared to the parent zeolite.

(5). The modification of the zeolite using solid state reaction with antimony oxide led to the complete passivation of unselective acid sites and to the pore narrowing or blocking of the pore openings of the zeolite, which resulted in the enhanced *para*-selectivity of the modified zeolites for toluene disproportionation.

Curriculum vitae

Shourong Zheng was born on December 5, 1968 in Jiangxi, P. R. China. After finishing high school in 1985, he started his study in Chemistry in Department of Chemistry, Nanjing University, China and received his bachelor degree in 1989. He went on to study physical chemistry in Department of Chemistry, Nanjing University under the supervision of Professor Qijie Yan and Professor Xiancai Fu. In 1992, he finished his thesis, entitled *Study on the Dispersion of Hetro-poly acid over $r\text{-Al}_2\text{O}_3$* , and obtained his master degree. He was employed as an assistant Lecturer in Department of Environmental Science and Engineering in Nanjing University and was promoted to lecturer in 1994. In 1998, he spent one year as a visiting scholar in Department of Civil Engineering, University of Newcastle upon Tyne, UK working on the advanced catalytic oxidation of organic pollutants in a joint project between UK government and China. He joined TCII catalysis and reaction engineering group of Professor J. A. Lercher at Technical University of Munich, Germany and started a research on surface modification of HZSM-5 zeolites in 1999. The results are described in this thesis.

List of publications

Structural properties and sieving effects of surface modified ZSM-5

S. Zheng, H. Heydenrych, P. Röger, A. Jentys and J.A. Lercher,
Stud. Surf. Sci. Catal. **135**, 214 (2001).

Kinetic processes during sorption and diffusion of aromatic molecules on medium pore zeolites studied by time resolved IR spectroscopy

H. Tanaka, S. Zheng, A. Jentys and J.A. Lercher,
Stud. Surf. Sci. Catal. **142**, 1619 (2002).

The effect of chemical modification on the acidity distribution of HZSM-5 zeolites

Shourong Zheng, Hilton Heydenrych, Andreas Jentys, Johannes A. Lercher,
J. Phys. Chem. B **106**, 9552 (2002).

On the enhanced selectivity of HZSM-5 modified by chemical liquid deposition

S. Zheng, H. R. Heydenrych, H. P. Röger, A. Jentys and J. A. Lercher,
Topics in catalysis **22**, 101 (2003)

Enhanced para-selectivity of isomerization of xylenes in HZSM-5 zeolites modified by chemical liquid deposition: an in situ IR observation

Shourong Zheng, Andreas Jentys, Johannes A. Lercher,
In preparation.

On the influence of CLD modification on toluene diffusion in HZSM-5 zeolite determined by frequency response methods

Shourong Zheng, Hiroaki Tanaka, Andreas Jentys, Johannes A. Lercher,
Submitted to J. Am. Chem. Soc.

On the enhanced para-selectivity of HZSM-5 modified by antimony oxide

Shourong Zheng, Andreas Jentys, Johannes A. Lercher,
Submitted to J. Catalysis.